KERNFORSCHUNGSANLAGE JÜLICH GmbH
Institut für Plasmaphysik
Association EURATOM-KFA

Calculation of Poloidal Rotation in the Edge Plasma of Limiter Tokamaks

by

Hartmut Gerhauser
Hans Arno Claaßen

Jül - 2125
May 1987
ISSN 0366-0885

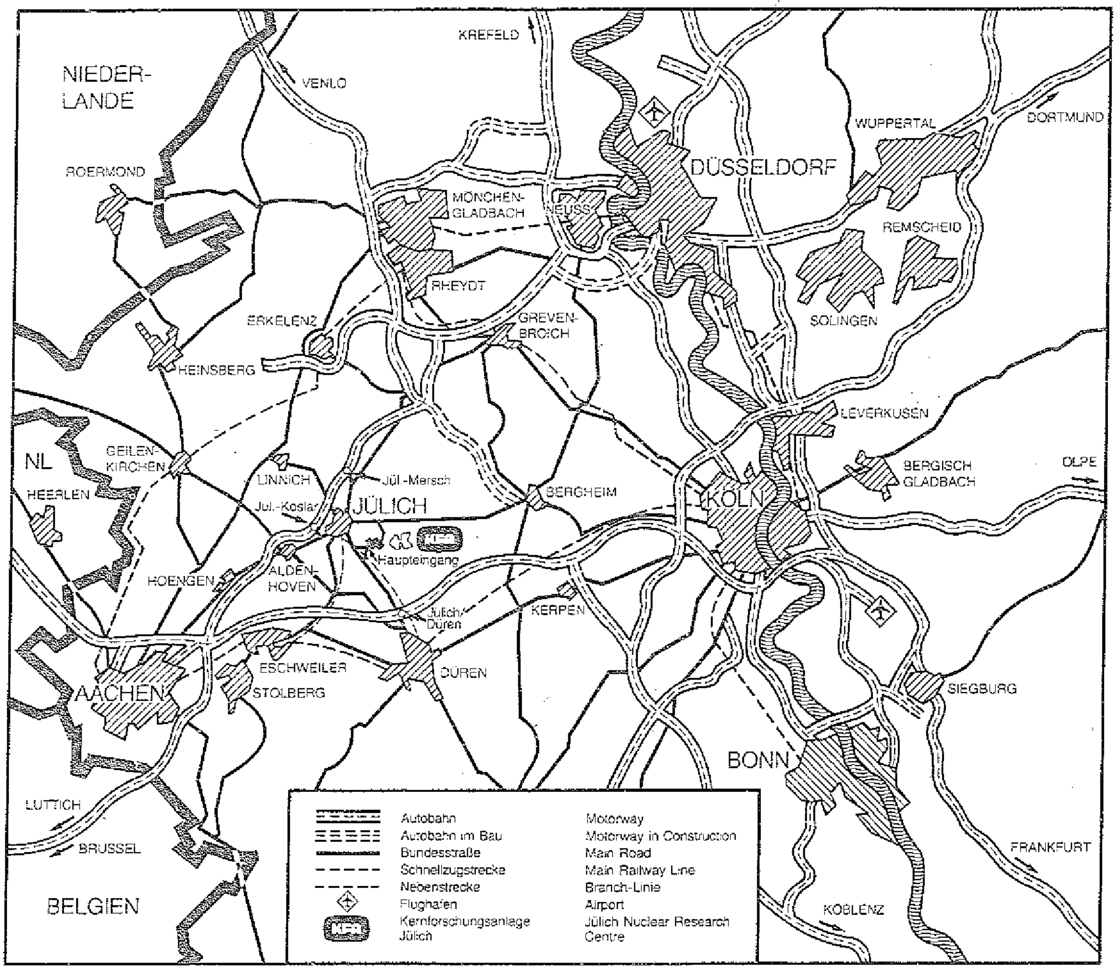

Als Manuskript gedruckt

Berichte der Kernforschungsanlage Jülich – Nr. 2125

Institut für Plasmaphysik Association EURATOM-KFA Jül – 2125

Zu beziehen durch: ZENTRALBIBLIOTHEK der Kernforschungsanlage Jülich GmbH

Postfach 1913 · D-5170 Jülich (Bundesrepublik Deutschland)

Telefon: 02461/610 · Telex: 833556-0 kf d

Calculation of Poloidal Rotation in the Edge Plasma of Limiter Tokamaks

by

Hartmut Gerhauser
Hans Arno Claaßen

Calculation of Poloidal Rotation in the Edge Plasma of Limiter Tokamaks

by H. Gerhauser and H.A. Claaßen

Institut für Plasmaphysik der Kernforschungsanlage Jülich GmbH
Association EURATOM/KFA

Abstract

The existing 2-d two-fluid code for computing the plasma profiles in the scrape-off layer of limiter tokamaks has been further developed to include the effect of poloidal rotation in the basic equations. This rotation is produced by radial electric fields which arise in the limiter shadow due to radial gradients in the Langmuir sheath potential in front of the limiter. As a consequence slight deviations from ambipolar motion must occur. A strong increase of rotation near the separatrix is connected with an electric current circuit closed via the limiter edge. The 2-d profiles of all relevant quantities are calculated and discussed for TEXTOR-typical parameters including also the effect of limiter recycled neutrals. The results agree well with the known experimental evidence on poloidal rotation and should be transferable to all limiter tokamaks.

Contents

A) Introduction

In recent years the plasma behaviour in the scrape-off layer of limiter or divertor tokamaks has been investigated by several authors /1,2,3,4/ resorting to the numerical solution of fluid equations. These computer codes use simplified versions of the two-fluid equations described in the original work of Braginskij /5/ and discretize them on a rectangular grid with one coordinate in the radial direction and the other in the toroidal direction parallel to the magnetic field. One basic assumption in the equations is the ambipolar motion of electrons and ions, which means that there are no electric currents flowing in the scrape-off plasma. Furthermore it is assumed that the plasma velocity has no component in the poloidal direction, which means that a poloidal rotation does not occur. However, these assumptions may lead to inconsistencies. First it is clear that the plasma must be in radial equilibrium, so we must have $j_{pol}\ B_{tor} = \frac{\partial p}{\partial r}$, which requires the presence of poloidal currents j_{pol}. Secondly the calculation of the spatial dependence of the electrostatic potential ϕ shows the existence of radial electric fields with an associated $\vec{E} \times \vec{B}$ - drift in the poloidal direction which cannot be compensated by the ∇p_i - drift. Hence a poloidal rotation will always be produced. The basic physical mechanism behind this effect is the formation of the electrostatic Langmuir sheath in front of the limiter or divertor target plate. If the impinging plasma flow consists of equal or almost equal numbers of electrons and ions, the potential drop across the plasma sheath must be $\phi \sim 3\ kT_e$ for a hydrogen plasma, and integration along the magnetic field lines until the symmetry plane gives $\phi \sim 3.5\ kT_e$. Since the electron temperature T_e at the plasma edge is usually a strongly decreasing function of radius, considerable radial gradients of the plasma potential can be built up. We will find that the poloidal rotation velocity is typically of the order of twice the geometric mean of the radial diffusion velocity and the maximum toroidal convection velocity (which is taken to be of the order of the sound velocity). When crossing the separatrix from the limiter shadow towards the plasma core, the plasma potential is no longer subject to the constraint of following the Langmuir potential at the space charge sheath formed due to the contact with the limiter. There is, however, another constraint inside the separatrix. The inertia of the relatively massy plasma core will prevent it from being dragged along with the rotation of the narrow scrape-off layer. This means that the plasma rotation velocity must fall steeply to zero inside the separatrix. Consequently the potential ϕ must pass a maximum near the separatrix and the gradient $\partial\phi/\partial r$ must change its sign such that the $\vec{E} \times \vec{B}$ - drift can compensate the ∇p_i-drift within the plasma core. Eventually ϕ itself must change its sign and take large negative values when approaching the center of the plasma column. Remarkably enough all these theoretically predicted characteristic features of the radial profiles of the plasma potential and the poloidal rotation have been confirmed by measurements in different tokamak experiments /6,7,8/. It is thus worthwhile to study these effects in some more detail with the help of the existing 2-d code /1/ by taking into account those terms in the basic two-fluid equations that have been omitted in the previous treatments /1,2,3,4/. One interesting phenomenon to be discussed is the generation of electric currents by the presence of differential rotation, i.e. a shear in the rotational velocity. The highest currents arise near the separatrix because, as explained above, there are the steepest radial gradients of the rotation. We will show that the current circuit is an elongated vortex flow closed via the limiter edge. The connection between rotation and electric current flow had already been pointed out in ref. /9/. Clearly the occurrence of currents with components in the radial and toroidal directions entails that the assumption of ambipolar motion of electrons and ions is no longer fulfilled. However, in contrast to /9/ we find that the deviations from ambipolarity are small, of the order of 1 % or smaller. The reason is that, with parameters typical for the scrape-off layer of tokamaks like TEXTOR, the ion gyro radius is much smaller than characteristic radial lengths like density decay length or radial extent of the limiter, namely of the order of 10 % or smaller. But small currents at the limiter will cause only small changes of the potential and the rotation, which in turn will cause even smaller changes of the currents, and so on. Hence it is easy to determine numerically self-consistent plasma profiles by rapidly convergent iteration. The analytical treatment of /9/, on the contrary, relies on large deviations from ambipolarity introduced by large ion gyro radii. Furthermore, to make the solution analytically tractable, additional simplifications have been used in /9/ such as zero ion temperature (i.e. the ion gyro radius must be calculated with the electron temperature) and classical instead of anomalous values for diffusion and thermal conduction.

In this paper a numerical investigation of the plasma behaviour in the scrape-off layer is performed which is based on the full set of 2-d two-fluid equations and which takes into account the effect of electrical currents and poloidal rotation selfconsistently. Included are also the source terms by limiter recycled neutrals. The basic physical concepts involved in the model are presented and some numerical details outlined. The results are calculated with TEXTOR relevant parameters and the qualitative agreement with existing experimental evidence is shown. We conclude then that similar results should be obtained in all limiter tokamaks of this kind.

B) Basic Two-Fluid Equations

We consider a plasma consisting of electrons and hydrogen ions in the scrape-off layer of a limiter tokamak. The toroidal geometry is approximated by a right-handed Cartesian coordinate system. We denote the toroidal direction (parallel to the magnetic field) by x, the radial direction by y and the poloidal direction by z. All quantities are assumed to be independent of the poloidal coordinate so that $\frac{\partial}{\partial z} \equiv 0$ everywhere. If $\vec{u}$ is the velocity of the electrons and $\vec{v}$ the velocity of the ions, the electrical current density is defined by

$$\vec{j} = en\,(\vec{v} - \vec{u}) \tag{1}$$

We remind that we have <u>not</u> made the usual assumption of ambipolar motion /1,2,3,4/, so $\vec{j} \neq 0$ in general, whereas the assumption of quasineutrality $n = n_e = n_i$ is maintained. After these preliminaries we can state the basic equations following essentially the original work of Braginskij /5/ but introducing also some significant modifications.

1) Equations of continuity

Electrons $\qquad \frac{\partial n}{\partial t} + \nabla\cdot(n\vec{u}) = S_n \qquad (2)$

Ions $\qquad \frac{\partial n}{\partial t} + \nabla\cdot(n\vec{v}) = S_n \qquad (3)$

The source term S_n represents the creation of electrons and ions by the ionization of limiter recycled neutral particles. Subtracting (2) from (3) and using (1), we find that in agreement with the quasineutrality condition the current density must be divergence free:

$$\nabla \cdot \vec{j} = \frac{\partial j_x}{\partial x} + \frac{\partial j_y}{\partial y} + \frac{\partial j_z}{\partial z} = 0$$

which on account of $\partial/\partial z \equiv 0$ simplifies to

$$\frac{\partial j_x}{\partial x} + \frac{\partial j_y}{\partial y} = 0 \qquad (4)$$

This shows the existence of a stream function ψ that can be defined by

$$j_y = \frac{\partial \psi}{\partial x} \quad , \quad j_x = - \frac{\partial \psi}{\partial y} \qquad (5)$$

2) Equation of motion for the electrons (Ohm's law)

Neglecting electron inertia and viscous effects the momentum equation for the electrons leads to the generalized Ohm's law:

$$-\nabla p_e - en\,(\vec{E} + \vec{u} \times \vec{B}) + \vec{R} = 0 \qquad (6)$$

The term $\vec{R}$ represents the transfer of momentum from ions to electrons by collisions and consists of the friction force and the thermal force:

$$\vec{R} = en\,\left(\frac{\vec{j}_{\parallel}}{\sigma_{\parallel}} + \frac{\vec{j}_{\perp}}{\sigma_{\perp}}\right) - 0.71\, n\, \nabla_{\parallel} T_e - \frac{3}{2}\,\frac{n}{\omega_e \tau_e}\;\vec{e}_{\parallel} \times \nabla T_e \qquad (7)$$

The electrical conductivities in the friction force have the form

$$\frac{en}{\sigma_{\parallel}} = 0.51\,\frac{en}{\sigma_{\perp}} = 0.51\,\frac{B}{\omega_e \tau_e} \qquad (8)$$

In TEXTOR typical plasma edge parameters are T_e = 25 eV, n = 2 x 10^{12} cm^{-3} and B = 2 Tesla. With these values the product of the electron cyclotron frequency and the electron collision time is found to be

$\omega_e\tau_e \approx 6 \times 10^5$. This means that those terms in $\vec{R}$ that contain the factor $1/\omega_e\tau_e$ are extremely small compared to all other terms, they should be neglected. As a consequence it is not possible to use Ohm's law in the usual way for determining $\vec{j}_{\parallel}$ and $\vec{j}_{\perp}$. To see what it determines instead, we consider the three components separately. In the parallel direction we get

$$-\frac{\partial p_e}{\partial x} + en\frac{\partial \phi}{\partial x} + en\frac{j_x}{\sigma_{\parallel}} - 0.71\, n\frac{\partial T_e}{\partial x} = 0 \tag{9}$$

where ϕ is the electrostatic potential defined by $\vec{E} = -\nabla\phi$. For $\sigma_{\parallel} \to \infty$ equation (9) obviously links the parallel gradients of ϕ, p_e and T_e so that $\phi(x,y)$ is determined everywhere if the radial dependence $\phi(y)$ is known at a specified toroidal position x. In the radial direction we get

$$-\frac{\partial p_e}{\partial y} + en\frac{\partial \phi}{\partial y} + (j_z - en\, v_z)\, B + en\frac{j_y}{\sigma_{\perp}} = 0 \tag{10}$$

As will soon be shown, radial equilibrium requires

$$j_z B = \frac{\partial p}{\partial y} = \frac{\partial p_e}{\partial y} + \frac{\partial p_i}{\partial y} \tag{11}$$

Hence for $\sigma_{\perp} \to \infty$ equation (10) reads

$$\frac{\partial p_i}{\partial y} + en\frac{\partial \phi}{\partial y} - en\, B\, v_z = 0 \tag{12}$$

This obviously determines the poloidal velocity $v_z(x,y)$ everywhere in terms of the z-components of the $\vec{E} \times \vec{B}$ - drift and the diamagnetic ∇p_i-drift. If $\partial\phi/\partial y$ is defined by (9), i.e. independently of $\partial p_i/\partial y$, a poloidal mass rotation of the plasma must be produced. In the poloidal direction we get

$$-\frac{\partial p_e}{\partial z} + en\frac{\partial \phi}{\partial z} + en\, u_y B + en\frac{j_z}{\sigma_{\perp}} - \frac{3}{2}\frac{n}{\omega_e\tau_e}\frac{\partial T_e}{\partial y} = 0$$

For $\frac{\partial}{\partial z} \equiv 0$ and $\omega_e\tau_e$, $\sigma_{\perp} \to \infty$ this yields $u_y \to 0$. This means that the classical radial particle transport is very small. However, because of the steep gradients in the plasma edge, drift-type instabilities maintain a large turbulent fluctuation level, which induces an anomalous radial diffusion flux. Dependent on the phase correlation between the density fluctuations $\tilde{n}$ and the electrostatic potential fluctuations $\tilde{\phi}$ there is a non-vanishing time average of the form

$$nu_y \approx nv_y = - \left\langle \tilde{n} \frac{1}{B} \frac{\partial \tilde{\phi}}{\partial z} \right\rangle = \left\langle \tilde{n}\ \tilde{v}_y \right\rangle$$
$$\Gamma^{\perp} = nv_y = - D^{\perp} \frac{\partial n}{\partial y} \tag{13}$$

In this way the fluctuating radial $\tilde{\vec{E}}_z \times \vec{B}$ - drift velocity is described by the phenomenological anomalous diffusion coefficient $D^{\perp}$. We take it to be constant and of the order of the Bohm coefficient.

We conclude that with the assumptions made for our scrape-off plasma Ohm's law reduces to fixing the potential ϕ, the rotation v_z and the radial particle flux $\Gamma^{\perp}$ in terms of the density n and the temperatures T_e and T_i.

3) Equation of motion for the plasma

We start with the momentum balance equation for the ions ($m = m_i$):

$$\frac{\partial}{\partial t} (mn\vec{v}) + \nabla\cdot(mn\vec{v}\vec{v}) + \nabla p_i + \nabla\cdot\overleftrightarrow{\pi} - en\ (\vec{E} + \vec{v} \times \vec{B}) + \vec{R} = \vec{S}_p \tag{14}$$

The source term $\vec{S}_p$ represents the momentum transfer by the recycled neutrals. We combine equation (14) for the ions with equation (6) for the electrons to get the equation of motion for the electron-ion-ensemble:

$$\frac{\partial}{\partial t} (mn\vec{v}) + \nabla\cdot(mn\vec{v}\vec{v}) + \nabla p + \nabla\cdot\overleftrightarrow{\pi} - \vec{j} \times \vec{B} = \vec{S}_p \tag{15}$$

By using the equation of continuity (3) for the ions this takes the form

$$mn\ (\frac{\partial}{\partial t} + \vec{v}\cdot\nabla)\ \vec{v} = -\nabla p - \nabla\cdot\overleftrightarrow{\pi} + \vec{j} \times \vec{B} + \vec{S}_p - m\vec{v}\ S_n \tag{16}$$

Again it is useful to consider the three components separately. We retain only the dominant component π_{xx} of the viscosity tensor $\overleftrightarrow{\pi}$ and suppress all terms with $\partial/\partial z$:

$$mn(\frac{\partial}{\partial t} + v_x \frac{\partial}{\partial x} + v_y \frac{\partial}{\partial y})\ v_x = -\frac{\partial p}{\partial x} - \frac{\partial \pi_{xx}}{\partial x} + S_{px} - mv_x S_n \tag{17}$$

$$mn\ (\frac{\partial}{\partial t} + v_x \frac{\partial}{\partial x} + v_y \frac{\partial}{\partial y})\ v_y = -\frac{\partial p}{\partial y} + j_z\ B + S_{py} - mv_y\ S_n \tag{18}$$

$$mn\ (\frac{\partial}{\partial t} + v_x \frac{\partial}{\partial x} + v_y \frac{\partial}{\partial y})\ v_z = -\ j_y\ B + S_{pz} - mv_z\ S_n \tag{19}$$

Whereas the toroidal equation (17) can be fully exploited for determining the time evolution $\partial v_x/\partial t$, the radial equation (18) degenerates to the equilibrium condition (11), because the diffusion velocity v_y is extremely small compared to the sound velocity and already determined by (13). For TEXTOR parameters $v_y \sim 10^{-3}\sqrt{\frac{p}{mn}}$, so that terms containing v_y in (18) must be neglected. Turning finally to the poloidal equation (19), we see that it can be used to define the unknown radial current density j_y in terms of gradients of the already known rotation velocity v_z, if the time evolution $\partial v_z/\partial t$ plays a minor role. By virtue of (5) this also defines j_x. This introduces deviations from the ambipolar motion of electrons and ions. We estimate the order of magnitude from (19) and (12) in regions far from the limiter edge, where the sources S_n and S_{pz} are very small:

$$\frac{j_y}{env_y} \sim \frac{m}{eB}\frac{\partial v_z}{\partial y} \sim \frac{m_i}{e^2B^2}\frac{\partial^2 T_i}{\partial y^2} \sim \frac{r_i^2}{\lambda_y^2} \tag{20}$$

For $T_i = T_e = 25$ eV and for deuterons the ion gyroradius in the magnetic field of TEXTOR results to be $r_i \approx 0.36$mm. This is certainly less than 10 % of characteristic radial scale lengths λ_y , so that the nonambipolar corrections are less than 1 %. The calculations will show, that indeed also $j_x/env_x \lesssim 1$ % even in front of the limiter. We note that the smallness of the nonambipolarity constitutes a major difference to Boozer's /9/ work. Nevertheless j_y is essential for setting up a considerable poloidal rotation. Since we are only interested in approaching the stationary state, the time derivative in (19) can be regarded as small compared to the convective derivative. If we content ourselves with calculating the time evolution of v_z and j_x, j_y only approximately, this has a negligible influence on the behaviour of n, v_x, T_e and T_i due to the smallness of the nonambipolar corrections. Hence we neglect this second order effect and define j_y by

$$j_y B = - mn(v_x \frac{\partial}{\partial x} + v_y \frac{\partial}{\partial y}) v_z + S_{pz} - mv_z S_n \tag{21}$$

This equation shows the close connection between a current density and a differential (i.e. a spatially non constant) plasma rotation.

4) Equation of electron energy balance

We start from the equation

$$\frac{\partial}{\partial t} (\frac{3}{2} n T_e) + \nabla \cdot (\frac{5}{2} n T_e \vec{u} + \vec{q}_e) = - en \vec{E} \cdot \vec{u} + \vec{R} \cdot \vec{v} + Q_{ei} + W_e \tag{22}$$

with the heat flux defined by

$$\vec{q}_e = - \chi_e^{\parallel} \nabla_{\parallel} T_e - \chi_e^{\perp} \nabla_{\perp} T_e - \frac{5}{2} \frac{nT_e}{eB} \vec{e} \times \nabla T_e - 0.71 \frac{T_e}{e} \vec{j}_{\parallel} - \frac{3}{2} \frac{T_e}{e\omega_e \tau_e} \vec{e} \times \vec{j} \tag{23}$$

Because of $\frac{\partial}{\partial z} \equiv 0$ the third component q_{ez} is not needed. The other components are

$$q_{ex} = - \chi_e^{\parallel} \frac{\partial T_e}{\partial x} - 0.71 \frac{T_e}{e} j_x \tag{24}$$

$$q_{ey} = - \chi_e^{\perp} \frac{\partial T_e}{\partial y} + \frac{3}{2} \frac{T_e}{e\omega_e \tau_e} j_z \tag{25}$$

We assume a classical parallel heat conductivity $\chi_e^{\parallel}$, but an anomalous perpendicular one:

$$\chi_e^{\perp} = n\ D^{\perp} \tag{26}$$

Introducing the equilibrium condition (11) in (25) gives

$$q_{ey} = -\ n\ D^{\perp}\ \frac{\partial T_e}{\partial y} + \frac{3}{2\omega_e\tau_e}\ \frac{T_e}{eB}\ \frac{\partial p}{\partial y} \tag{27}$$

and since $\frac{1}{\omega_e\tau_e} \to 0$ the second term in (25) and (27) must be neglected. The right-hand side of (22) contains the energy exchange Q_{ei} between electrons and ions tending to temperature equilibration and the energy loss W_e by ionization and excitation of the recycled neutrals. The remaining terms must be further transformed with the help of Ohm's law (6):

$$\begin{aligned} -\ en\ \vec{E}\cdot\vec{u} + \vec{R}\cdot\vec{v} &= (\vec{j} - en\vec{v})\cdot\vec{E} + \vec{R}\cdot\vec{v} \\ &= \vec{j}\cdot\vec{E} + \vec{v}\cdot(\vec{R} - en\ \vec{E}) \\ &= \vec{j}\cdot\vec{E} + \vec{v}\cdot(\nabla p_e + en\ \vec{u}\ \mathrm{x}\ \vec{B}) \\ &= -\ \vec{j}\cdot\nabla\phi + \vec{v}\cdot(\nabla p_e - \vec{j}\ \mathrm{x}\ \vec{B}) \end{aligned} \tag{28}$$

The hitherto performed numerical 2-d calculations /1,2,3,4/ retained only the $\vec{v}\cdot\nabla p_e$-term in (28). But even for ambipolar motion $j_x=j_y=0$ with a vanishing Ohmic power production $\vec{j}\cdot\vec{E}$ a Lorentz-force $\vec{j}\mathrm{x}\vec{B}$ in the radial direction must be taken into account to ensure radial equilibrium. By using (9,11,12) we finally get:

$$\begin{aligned} -\ en\ \vec{E}\cdot\vec{u} + \vec{R}\cdot\vec{v} &= v_x\ \frac{\partial p_e}{\partial x} + v_y\left(\frac{\partial p_e}{\partial y} - j_z B\right) - j_x\ \frac{\partial\phi}{\partial x} + \left(v_z B - \frac{\partial\phi}{\partial y}\right)\ j_y \\ &= v_x\ \frac{\partial p_e}{\partial x} - v_y\ \frac{\partial p_i}{\partial y} - \frac{j_x}{en}\ \left(\frac{\partial p_e}{\partial x} + 0.71\ n\ \frac{\partial T_e}{\partial x}\right) + \frac{j_y}{en}\ \frac{\partial p_i}{\partial y} \\ &= u_x\ \frac{\partial p_e}{\partial x} - u_y\ \frac{\partial p_i}{\partial y} - 0.71\ \frac{j_x}{e}\ \frac{\partial T_e}{\partial x} \end{aligned} \tag{29}$$

In order to obtain an equation for $\frac{\partial T_e}{\partial t}$ alone we combine (22) with the continuity equations (2,3):

$$\frac{3}{2}\ n\ \frac{\partial T_e}{\partial t} + \frac{3}{2}\ T_e S_n + T_e\ \nabla\cdot(n\vec{u}) + \frac{5}{2}\ n\vec{u}\cdot\nabla T_e + \nabla\cdot\vec{q}_e =$$

$$= u_x \frac{\partial p_e}{\partial x} - u_y \frac{\partial p_i}{\partial y} - 0.71 \frac{j_x}{e} \frac{\partial T_e}{\partial x} + Q_{ei} + W_e$$

$$\frac{3}{2} n \frac{\partial T_e}{\partial t} + T_e \nabla\cdot(n\vec{v}) - \frac{\partial}{\partial x} (\chi_e^{\parallel} \frac{\partial T_e}{\partial x}) - \frac{\partial}{\partial y} (\chi_e^{\perp} \frac{\partial T_e}{\partial y}) =$$

$$= u_x (\frac{\partial p_e}{\partial x} - \frac{5}{2} n \frac{\partial T_e}{\partial x}) - u_y (\frac{\partial p_i}{\partial y} + \frac{5}{2} n \frac{\partial T_e}{\partial y}) + 0.71 \frac{T_e}{e} \frac{\partial j_x}{\partial x}$$

$$+ Q_{ei} + W_e - \frac{3}{2} T_e S_n \tag{30}$$

The correction terms introduced by a nonvanishing j_x and j_y are easily identified on the right-hand side of equation (30).

5) Equation of ion energy balance

We start from the equation

$$\frac{\partial}{\partial t} (\frac{3}{2} n T_i + \frac{mn}{2} \vec{v}^2) + \nabla\cdot [(\frac{5}{2} n T_i + \frac{mn}{2} \vec{v}^2) \vec{v} + \overleftrightarrow{\pi}\cdot\vec{v} + \vec{q}_i] =$$

$$= (en \vec{E} - \vec{R})\cdot\vec{v} - Q_{ei} + W_i \tag{31}$$

with the heat flux defined by

$$\vec{q}_i = - \chi_i^{\parallel} \nabla_{\parallel} T_i - \chi_i^{\perp} \nabla_{\perp} T_i \tag{32}$$

The source term W_i describes the energy change by charge exchange with and ionization of the recycled neutrals, Q_{ei} is again the temperature equilibration term. The other terms on the right-hand side of (31) represent the work done by the electric field and the friction with the electron. They also occur in the electron equation (22), but with the opposite sign, and constitute the energy transfer between electrons and ions. We can simplify (31) and get an equation for $\partial T_i/\partial t$ alone.

$$(\frac{3}{2} T_i + \frac{m}{2} \vec{v}^2) \frac{\partial n}{\partial t} + (\frac{5}{2} T_i + \frac{m}{2} \vec{v}^2) \nabla\cdot(n\vec{v}) + \frac{3}{2} n \frac{\partial T_i}{\partial t} +$$

$$+ n(\frac{\partial}{\partial t} + \vec{v}\cdot\nabla) \frac{m}{2} \vec{v}^2 + \frac{5}{2} n \vec{v}\cdot\nabla T_i + \vec{v}\cdot(\nabla\cdot\overleftrightarrow{\pi}) + (\overleftrightarrow{\pi}\cdot\nabla)\cdot\vec{v} + \nabla\cdot\vec{q}_i =$$

$$= - \vec{v}\cdot(\nabla p_e - \vec{j} \times \vec{B}) - Q_{ei} + W_i \tag{33}$$

Now multiplying the continuity equation (3) by $\frac{3}{2} T_i + \frac{m}{2} \vec{v}^2$, taking the scalar product of the equation of motion (16) with $\vec{v}$, and inserting into (33) yields

$$(\frac{3}{2} T_i + \frac{m}{2} \vec{v}^2) S_n + T_i \nabla\cdot(n\vec{v}) + \frac{3}{2} n \frac{\partial T_i}{\partial t} + \vec{v}\cdot(-\nabla p_i + \vec{S}_p - m\vec{v} S_n) +$$

$$+ \frac{5}{2} n \vec{v} \cdot \nabla T_i + (\overleftrightarrow{\pi}\cdot\nabla)\cdot\vec{v} + \nabla\cdot\vec{q}_i = - Q_{ei} + W_i \tag{34}$$

We retain only π_{xx} and neglect terms with v_y^2 compared to v_x^2 and v_z^2. This puts the T_i-equation in the final form

$$\frac{3}{2} n \frac{\partial T_i}{\partial t} + T_i \nabla\cdot(n\vec{v}) + \pi_{xx} \frac{\partial v_x}{\partial x} - \frac{\partial}{\partial x} (\chi_i^{\parallel} \frac{\partial T_i}{\partial x}) - \frac{\partial}{\partial y} (\chi_i^{\perp} \frac{\partial T_i}{\partial y}) =$$

$$= v_x (\frac{\partial p_i}{\partial x} - \frac{5}{2} n \frac{\partial T_i}{\partial x}) + v_y (\frac{\partial p_i}{\partial y} - \frac{5}{2} n \frac{\partial T_i}{\partial y}) - v_x S_{px} - v_z S_{pz}$$

$$- (\frac{3}{2} T_i - \frac{m}{2} v_x^2 - \frac{m}{2} v_z^2) S_n - Q_{ei} + W_i \tag{35}$$

The correction terms introduced by the finite poloidal rotation velocity v_z are easily identified on the right-hand side of equation (35).

C) Geometry and Boundary Conditions

We model the edge region of the tokamak plasma in the rectangular domain ACDF

Fig.1: Geometry of Scrape-off and Transition Layer

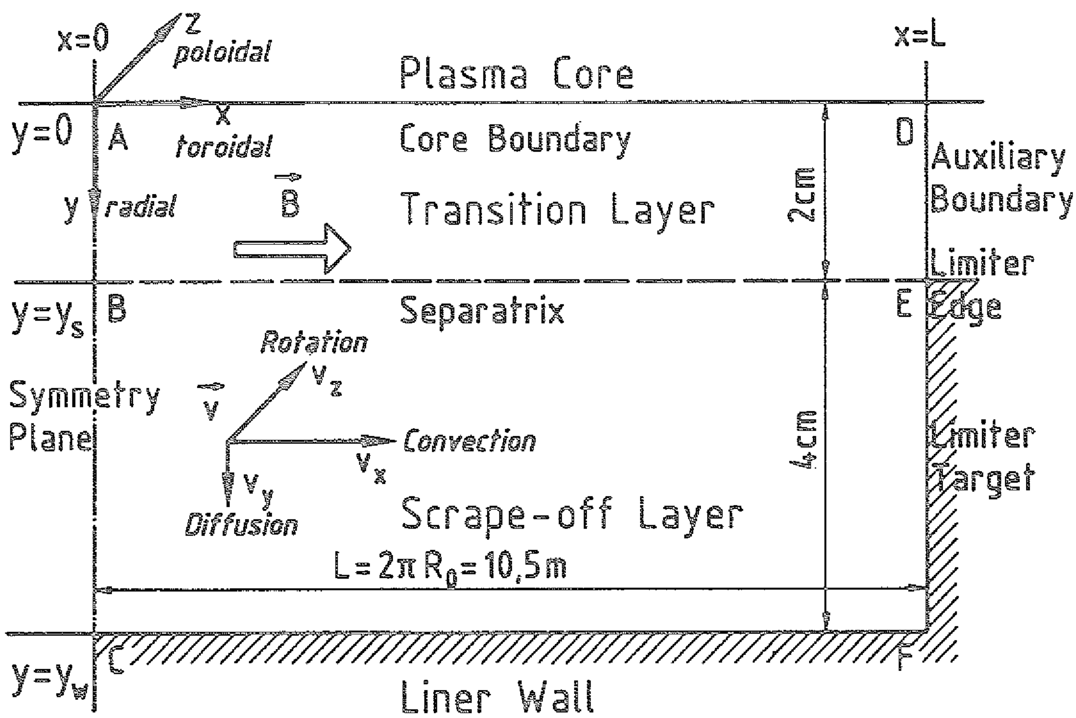

of fig. 1. It consists of the scrape-off layer (abbreviation: s.o.l.) in the limiter shadow and a transition layer between the separatrix (defined by the limiter edge) and the plasma core.

The length L of the s.o.l. between the symmetry plane and the limiter plane is taken to be one torus circumference of TEXTOR. This takes account of the fact that the poloidal limiter of this tokamak is not closed but consists of four separated segments so that a magnetic field line starting from one side of the limiter travels on the average at least twice around the torus before hitting the limiter again. The complicated poloidal structure of the s.o.l. cannnot be described by our 2d-model. We also neglect the finite toroidal width of the limiter compared to the connexion length of 2L. For this reason the physical quantities near the auxiliary boundary DE, defined as the continuation of the limiter surface EF into the transition region, must have similar symmetry properties as those near the symmetry plane AC.

In principle we have ten scalar quantities involved in the problem, namely the density n, the velocity $\vec{v} = (v_x, v_y, v_z)$, the temperatures T_e and T_i, the electric current density $\vec{j} = (j_x, j_y, j_z)$ and the electrostatic potential ϕ. However only four of them, namely n, v_x, T_e, T_i, must be determined from the simultaneous solution of four coupled partial differential equations subject to appropriate boundary conditions. We may call them the primary variables. The six remaining quantities can all be expressed directly in terms of the primary variables and their spatial derivatives. Two of these secondary variables are eliminated from the beginning, namely the radial diffusion velocity v_y and the poloidal current density j_z by equations (13) and (11). The other four secondary variables must be determined by an iterative procedure, as will be outlined below.

1) Boundary conditions for the primary variables

The required number of physical boundary conditions depends on the order of the differential equations. We first rewrite (3) and (17) in the form

$$\frac{\partial n}{\partial t} = - \frac{\partial}{\partial x} (nv_x) + \frac{\partial}{\partial y} (D^{\perp} \frac{\partial n}{\partial y}) + S_n \tag{36}$$

$$mn \frac{\partial v_x}{\partial t} = - mn\ v_x \frac{\partial v_x}{\partial x} + mD^{\perp} \frac{\partial n}{\partial y} \frac{\partial v_x}{\partial y} - \frac{\partial}{\partial x} (n\ T_e + n\ T_i) + \frac{4}{3} \frac{\partial}{\partial x} (\eta \frac{\partial v_x}{\partial x}) + Sp_x - m\ v_x\ S_n \tag{37}$$

Here η is the parallel viscosity contained in the stress tensor element

$$\pi_{xx} = - \frac{4}{3} \eta \frac{\partial v_x}{\partial x} \tag{38}$$

We see that the equation (36) for the density is of second order in y, but only of first order in x. Therefore if we prescribe a boundary condition for n in the symmetry plane, no physical boundary condition is available for the limiter plane. Similarly equation (37) for the velocity is of second order in x, but only of first order in y. Therefore if we prescribe a boundary condition for v_x at the core boundary, no physical boundary condition is available for the liner wall. In these cases we must introduce numerical boundary conditions by using quadratic space extrapolation. This means that the boundary value $n_o = n(L)$ at the limiter is obtained from the densities at equidistant points in front of the limiter

$$n_{-k} = n(L - k \cdot \Delta x), \quad k = 1,2,3$$

by requiring that n_o fits to the parabola defined by n_{-k}:

$$n_o = n_{-3} + 3(n_{-1} - n_{-2})$$

A similar procedure is applied to the velocity v_x at the liner wall. It can be shown that linear space extrapolation or other pescriptions may lead to unphysical oscillations of the solution.
The equations (30) for $\partial T_e/\partial t$ and (35) for $\partial T_i/\partial t$ are of second order in both directions via the χ-terms.
We now discuss the conditions at the different boundaries in detail.

a) Plasma core boundary AD

If the transition layer is deep enough, the limiter induced toroidal convection velocity v_x should be vanishingly small. This is not necessarily true for the poloidal rotation velocity v_z. The density should be constant along the boundary, but the value of the constant is not known. On the other hand a reasonable total particle flux $\Gamma^{\perp}_{tot}$ crossing the boundary can be prescribed, but the distribution of the flux density along the boundary is not known. This leads to a sort of mixed boundary condition, and the same holds for the temperatures and the total energy fluxes $Q_e^{\perp}{}_{tot}$ and $Q_i^{\perp}{}_{tot}$. We write the conditions in the form

$$v_x = 0$$

$$\int_0^L \Gamma^{\perp}(x)\, dx = \Gamma^{\perp}_{tot} \quad \text{and} \quad n = \text{constant} \tag{39}$$

$$\int_0^L Q_e^{\perp}(x)\, dx = Q_e^{\perp}{}_{tot} \quad \text{and} \quad T_e = \text{constant} \tag{40}$$

$$\int_0^L Q_i^{\perp}(x)\, dx = Q_i^{\perp}{}_{tot} \quad \text{and} \quad T_i = \text{constant} \tag{41}$$

Here the radial particle flux density is as in (13)

$$\Gamma^{\perp} = nv_y = nu_y = - D^{\perp} \frac{\partial n}{\partial y}$$

and the energy flux densities comprise heat convection and heat conduction:

$$Q_e^{\perp} = \frac{5}{2} T_e \Gamma^{\perp} + q_e^{\perp} \qquad = \frac{5}{2} T_e \Gamma^{\perp} - \chi_e^{\perp} \frac{\partial T_e}{\partial r} \tag{42}$$

$$Q_i^{\perp} = (\frac{5}{2} T_i + \frac{m}{2} v_z^2) \Gamma^{\perp} + q_i^{\perp} = (\frac{5}{2} T_i + \frac{m}{2} v_z^2) \Gamma^{\perp} - \chi_i^{\perp} \frac{\partial T_i}{\partial r} \tag{43}$$

b) Symmetry plane AC and auxiliary boundary DE

The obvious symmetry conditions are vanishing velocity and vanishing derivatives of the other quantities:

$$v_x = 0$$

$$\frac{\partial T_e}{\partial x} = \frac{\partial T_i}{\partial x} = 0 \quad \text{and} \quad \frac{\partial n}{\partial x} = 0 \tag{44}$$

It is remembered that vanishing $\partial n/\partial x$ can be prescribed only in the symmetry plane, not in the limiter plane.

c) Liner wall CF

There is little information about the densities and temperatures at the wall besides the fact that they are "small" in some sense. Instead of prescribing fixed values of n_w, T_{ew} and T_{iw} we found it better to use adaptively floating boundary conditions, i.e. the boundary values are adapted to the radial profiles of the solution such as to disturb it as little as possible in front of the wall. This presupposes that the solution at a certain distance away from the wall is relatively insensitive to the precise boundary values, but this is indeed the case, because the particle and energy fluxes to the wall are always much smaller than those to the limiter. A possible prescription is

$$n_w = \frac{1}{16} n_s, \quad T_{ew} \lesssim T_{e\ w-1}, \quad T_{iw} \lesssim T_{i\ w-1} \tag{45}$$

where the index s denotes the separatrix and the index w-1 the wall minus Δy.

d) Limiter EF

As is well known a collisionfree space charge sheath with the thickness of a few Debye lengths is built up in front of the limiter. In the potential drop of this Langmuir sheath the ions are accelerated and the electrons are decelerated. One edge of the sheath faces the s.o.l. plasma, which is assumed as collision dominated. The particle and energy fluxes leaving the s.o.l. plasma and arriving at the edge must fulfil certain transition conditions when entering the sheath, in order to ensure the continuity of the fluxes. Since on our length scale the sheath edge and the limiter surface coincide, these transition conditions take the role of boundary conditions for our calculations.
The flow velocity of the plasma entering the Langmuir sheath must reach a minimum value of the order of the sound velocity, in order to satisfy Bohm's criterion. We write

$$v_x = \delta_s c_s = \delta_s \sqrt{\frac{T_e + T_i}{m_i}} \tag{46}$$

The energy fluxes are subject to the following relations:

$$Q_e^{\parallel} = \frac{5}{2} T_e n u_x + q_e^{\parallel} = \delta_e T_e n u_x \tag{47}$$

$$Q_i^{\parallel} = [\frac{5}{2} T_i + \frac{m}{2} (v_x^2 + v_z^2) - \frac{4}{3} \frac{\eta}{n} \frac{\partial v_x}{\partial x}] nv_x + q_i^{\parallel} = \delta_i T_i \; nv_x \tag{48}$$

Appropriate numbers for the factors δ_s, δ_e and δ_i must be derived from a kinetic theory. In the appendix we have calculated approximate formulae on the basis of certain commonly adopted simplifying assumptions. However, a detailed and reliable theory on the sheath and presheath, where the plasma in accelerated to sound velocity and the distribution functions get more and more non-Maxwellian by the distortions due to the absorbing wall, is still missing. For this reason we simply use the following pure numbers having the right order of magnitude:

$$\delta_s = 1, \; \delta_e = 5.5, \; \delta_i = 3.5 \tag{49}$$

This also justifies neglecting v_z^2 in (48) and replacing u_x by v_x in (47).

e) <u>Limiter edge E</u>

At the limiter edge the velocity v_x will experience an abrupt change from zero to sound velocity c_s. But in real physics a step function cannot occur, and also from numerical reasons it is not tolerable. Therefore v_x is smoothed out on a length scale ε with

<u>Fig. 2:</u>
<u>Velocity</u>

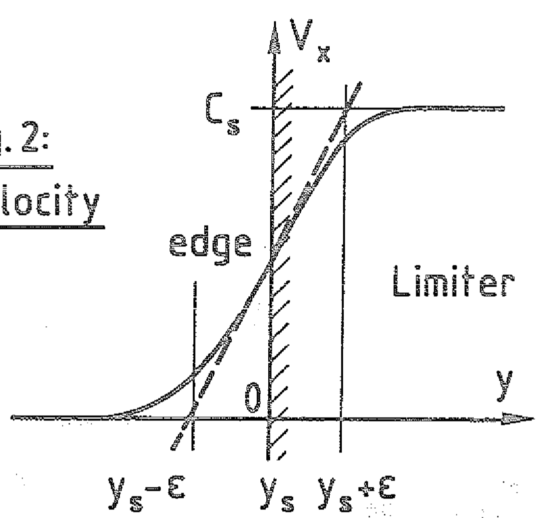

$$0.3 \text{ mm} \sim r_i \ll \varepsilon \ll \lambda_y \sim 20 \text{ mm} \tag{50}$$

where r_i is the ion gyro radius and λ_y the density scale length. We choose $\varepsilon = 2.5$ mm.

2) Boundary conditions for the secondary variables

a) Potential ϕ at limiter EF

We put the limiter target surface itself to zero potential. Then the potential at the Langmuir sheath edge facing the s.o.l. plasma is given by the potential drop in the sheath. From the appendix eq. (A18) we have for $v_x = c_s$:

$$e\phi = e\Delta\phi = -T_e \ln\left[\sqrt{\frac{2\pi m_e}{m_i}\frac{T_e+T_i}{T_e}}\left(1 - \frac{j_x}{enc_s}\right)\right] \tag{51}$$

For small non-ambipolarity $j_x \ll enc_s$ this simplifies to

$$e\phi = e\Delta\phi \approx \frac{1}{2} T_e \ln\left(\frac{m_i}{2\pi m_e}\frac{T_e}{T_e+T_i}\right) + T_e\frac{j_x}{enc_s} \tag{52}$$

In the special case of deuterons, zero ion temperature and vanishing j_x this yields $e\Delta\phi = 3.2\ T_e$. In general one may estimate $e\phi \sim 3T_e$ near the limiter. From the limiter potential we obtain $\phi(x,y)$ everywhere in the limiter shadow region by integrating eq. (9) along x:

$$e\frac{\partial\phi}{\partial x} = \frac{T_e}{n}\frac{\partial n}{\partial x} + 1.71\frac{\partial T_e}{\partial x} \tag{53}$$

By applying (12) we get also the poloidal rotation velocity $v_z(x,y)$ everywhere in the limiter shadow:

$$eBv_z = \frac{T_i}{n}\frac{\partial n}{\partial y} + \frac{\partial T_i}{\partial y} + e\frac{\partial\phi}{\partial y} \tag{54}$$

This determines especially the values $\phi(0,y_s)$ and $v_z(0,y_s)$ at the intersection point B of the symmetry plane and the separatrix.

b) Rotation v_z along AB

We assume that the rotation beyond the separatrix quickly decays to the value $v_z = 0$ inside the plasma core. Since the rotation is mainly caused by the contact of the plasma with the limiter, it is reasonable to assume an exponential radial decay at large toroidal distances from the limiter. Hence we take v_z along AB, the intersection line of the symmetry plane with the transition zone, to have the following form:

$$v_z(0,y) = v_z(0,y_s)\, e^{(y-y_s)/\varepsilon} \quad \text{for} \quad y \leqslant y_s \tag{55}$$

It is consistent to choose again $\varepsilon = 2.5$ mm similar to the behaviour of v_x near the limiter edge. From (55) and from $\phi(0,y_s)$ we now find $\phi(0,y)$ by integrating (54) along y from B to A. Having defined $\phi(0,y)$ on the line AB, the potential $\phi(x,y)$ in the whole transition layer follows by integration of (53) along x, and the rotation $v_z(x,y)$ by application of (54). This completes the determination of ϕ and v_z everywhere.

c) Streamfunction ψ in the symmetry plane AC

From symmetry reasons the toroidal current density j_x must vanish:

$$j_x = -\frac{\partial \psi}{\partial y} = 0 \quad \text{so that } \psi(0,y) = \text{constant} = 0 \tag{56}$$

The stream function must be constant along the symmetry plane, and we choose the constant to be zero. The radial current density j_y was given by (21):

$$Bj_y = B\frac{\partial \psi}{\partial x} = -mn\left(v_x \frac{\partial v_z}{\partial x} + v_y \frac{\partial v_z}{\partial y}\right) + S_{pz} - mv_z S_n \tag{57}$$

Integration of (57) along x determines $\psi(x,y)$ and hence j_x and j_y everywhere. Especially we get $j_x(L,y)$ at the limiter.

d) Iteration of the secondary variables

When starting the time relaxation of the primary variables the current density j_x at the limiter is not yet known. Therefore we must iterate and go several times through the equations (51), (53), (54), (55) and (57). Schematically this reads as follows:

$$\begin{tikzcd} j_x\Big|_{Lim} = 0 \arrow[r] & \phi, v_z \arrow[r] & \psi \arrow[r] & j_x\Big|_{Lim} \arrow[r] & \boxed{\text{Conv. ?}} \arrow[r, "\text{yes}"] \arrow[llll, bend left, "\text{Iteration}", "\text{no}"'] & {} \end{tikzcd} \qquad (58)$$

After four iterations of the zero approximation, j_x at the limiter is exact up to an error of at most 1%. During the time relaxation $j_x\Big|_{Lim}(t-\Delta t)$ is a very good approximation for $j_x\Big|_{Lim}(t)$, so that two iteration cycles are fully sufficient.

D) Recycling of Neutrals and Interaction with S.o.l. Plasma

1) Modelling the Recycling of Neutrals

The D^+-ions impinging on the limiter target are nearly monoenergetic with near-normal incidence due to the acceleration in the Langmuir sheath. According to (48) and (49) the kinetic energy of the ions just before this acceleration is $\delta_i T_i = 3.5\ T_i$. The energy transferred to the ions during their acceleration in the Langmuir sheath is given by the Langmuir potential (52) and of the order of $e\Delta\phi \sim 3\ T_e$. In the model we take the total kinetic energy of the ions when hitting the limiter target to be

$$E_i = 3\ (T_e + T_i) = 6\ \frac{m_i c_s^2}{2} \tag{59}$$

instead of 3 T_e + 3.5 T_i. In reality E_i will be even smaller, because we have not taken into account the reduction of the potential drop by the emission of secondary electrons, and above all, we have not included the reduction of the electron temperature by the ionization and dissocation of hydrogen molecules.

After the neutralization of the D^+-ions at the limiter surface part of them are reflected as D^o-atoms with slightly reduced energy. We call them "fast neutrals" with flux density Γ_o^f and energy E_o^f:

$$\Gamma_o^f = n_o^f\ v_o^f, \quad E_o^f = \frac{m_i\ (v_o^f)^2}{2} \lesssim E_i \tag{60}$$

The rest of the former D^+-ions is released as D_2-molecules with thermal energy. However, these are very short-lived and undergo predominantly the following electron impact reactions (see e.g. /10/ or /11/ and assume same coefficents for deuterium as for hydrogen):

1) $D_2 + e^- \xrightarrow{S_d^o} D^o + D^o + e^-$

2) $D_2 + e^- \xrightarrow{S_i^o} D_2^+ + 2e^- \xrightarrow{S_d^+} D^+ + D^o + 2e^-$

For electron temperatures in the range of 10 to 20 eV the rate coefficents $\langle \sigma v \rangle$ for dissociation and ionization are approximately

$$S_d^o \approx 10^{-8}\ \frac{cm^3}{sec}, \quad S_i^o \approx 0.5 \text{ to } 2 \times 10^{-8}\ \frac{cm^3}{sec}, \quad S_d^+ \approx 10^{-7}\ \frac{cm^3}{sec}$$

so that a combined rate coefficient for the decay of molecules is

$$S^o_{tot} \approx S^o_d + S^o_i \approx 1.5 \text{ to } 3 \times 10^{-8} \frac{cm^3}{sec}$$

For $n_e = 2 \times 10^{12}$ cm^{-3} the mean free path or decay length for thermal D_2 thus results to be

$$\lambda_{mfp} = \frac{v_{th}}{n_e S^o_{tot}} \approx \frac{1.2 \times 10^5}{2 \times 10^{12} \times (1.5 \text{ to } 3) \times 10^{-8}} \approx 2 \text{ to } 4 \text{ cm}$$

With our present integration grid the toroidal mesh size is $\Delta x = 17.5$ cm. Therefore we cannot resolve the history of the molecules and treat them simply as Frank-Condon neutrals emitted from the limiter surface. We also neglect the D^+-ions formed by reaction 2). This relatively small fraction of 20 to 30 % is swept back to the limiter by the fluid flow, where it has a good chance to be finally reemitted as D^o-neutrals. In addition, as pointed out by /11/, there might also occur volume recombination with negative ions D^- formed due to electron attachment to vibrationally excited D_2. Since typical energies of Frank-Condon neutrals created from the dissociation of D_2-molecules are of the order of 3 to 5 eV, we call them "slow neutrals" with flux density Γ^s_o, and for simplicity we assign to them a fixed energy $E_o{}^s$:

$$\Gamma^s_o = n^s_o \, v^s_o \; , \quad E^s_o = \frac{m_i (v^s_o)^2}{2} = 5 \text{ eV} \tag{61}$$

The definitions (60) and (61) are completed by using the empirical particle and energy reflexion coefficients R_N, R_E from Cupini et al. /12/. This yields the energy of the recycled fast neutrals in the form

$$E_o^f = \frac{R_E}{R_N} E_i = \frac{0.75 - 0.25 \log_{10}\varepsilon_i}{0.868 - 0.2265 \log_{10}\varepsilon_i} E_i \tag{62}$$

where ε_i [eV] is a reduced energy in the range $2\ \mathrm{eV} \lesssim \varepsilon_i \lesssim 100\ \mathrm{eV}$. For hydrogen or deuterium projectiles on an iron target $\varepsilon_i \approx 0.4\ E_i$. The flux densities are

$$\begin{aligned} \Gamma_o^f &= n_o^f\, v_o^f = -R_N\, n(L)\, v_x(L) = -R_N\, n(L)\, c_s(L) = -R_n\, \Gamma^{\parallel}(L) \\ \Gamma_o^s &= n_o^s\, v_o^s = -\,(1-R_N)\, \Gamma^{\parallel}(L) \end{aligned} \tag{63}$$

For TEXTOR parameters about half of the neutrals are slow or fast:

$$\Gamma_o^f \sim \Gamma_o^s \sim -\frac{1}{2}\,\Gamma^{\parallel}$$

In addition to neglecting the rapidly transient molecular states the model must introduce a second quite restrictive assumption. The reason is again the constraint of the toroidal mesh size of the present integration grid. We assume that the neutral particles are emitted perpendicular or almost perpendicular to the limiter surface and move parallel or at small angles to the toroidal magnetic field. The emission from the limiter is either purely normal or it has a narrow angular distribution around the normal direction with discrete angles corresponding to discrete grid vectors. Every grid point of the limiter surface emits neutral particles in 11 different directions (and with 2 different energies corresponding to the "fast" and to the "slow" fraction). As is shown in Fig. 3, the angular distribution is similar to a cos-distribution, but squeezed to an angle range of $\pm\ 3^o$ close to the limiter normal.

Note that in the picture the radial scale length Δy has been multiplied by a factor of about 100 so that it seems to have the same value as the toroidal scale length Δx. Hence the directions of propagation are in reality much less oblique. Neutral particles hitting the liner wall are assumed to

Fig.3 : Angular Distribution of Recycled Neutrals

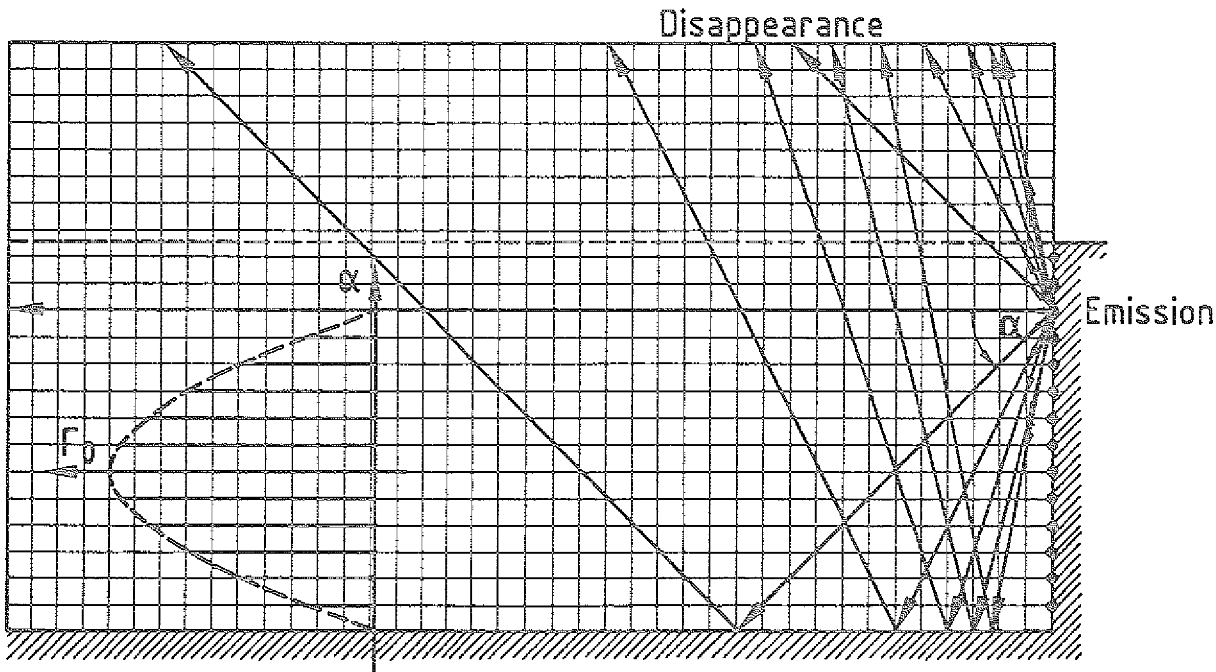

be reflected elastically and specularly, which is indeed the case for the grazing incidence of our neutrals. For simplicity we further assume that there are no velocity components in the poloidal z-direction.
In reality, of course, the neutral particles will be emitted with an angular distribution that is rather similar to an ordinary cosine destribution. As a consequence most particles travel very quickly through the s.o.l. plasma and have a good chance to be lost directly without undergoing any interaction, be it ionization or charge exchange. To some extent this can be simulated also by the present code by introducing a recycling factor $R \leq 1$ at the limiter so that 1-R represents the fraction of lost particles.

2) Modelling the Interaction with S.o.l. Plasma

We denote the two kinds of particles by k, so that k = f (fast) or k = s (slow). The eleven discrete directions of emission may be called beam directions and are characterized by their angles α with the limiter normal.

$\mathrm{tg}\,\alpha$ has the values

$$\mathrm{tg}\,\alpha = 0, \pm \frac{\Delta y}{\Delta x}, \pm \frac{2\Delta y}{\Delta x}, \ldots, \pm \frac{5\Delta y}{\Delta x} \tag{64}$$

The length element along the straight particle trajectories is given by

$$ds^2 = dx^2 + dy^2 , \quad ds = \frac{dx}{\cos\alpha} \tag{65}$$

At each grid point of the limiter we know E_o^k and hence $v_o^k = -\sqrt{2E_o^k/m_i}$. We also know Γ_o^k and define $\Gamma_o^{k\alpha}$ so that $\Gamma_o^k = \sum_\alpha \Gamma_o^{k\alpha}$, e.g. according to the squeezed cosine-distribution of Fig. 3. Because of

$$\Gamma_o^{k\alpha} = n_o^{k\alpha} v_o^k \cos\alpha \tag{66}$$

the density at the limiter must be written in the form

$$n_o^k = \sum_\alpha n_o^{k\alpha} = \sum_\alpha \frac{\Gamma_o^{k\alpha}}{v_o^k \cos\alpha} \tag{67}$$

The neutral densities for each beam decay exponentially along the trajectories ξ, η with $\eta = y - (\xi - x)\,\mathrm{tg}\,\alpha$:

$$n_o^{k\alpha}(x,y) = n_o^{k\alpha}(L, y - (L-x)\,\mathrm{tg}\,\alpha) \exp\left(- \int_L^x \frac{\nu_I(\xi,\eta) + \nu_{cx}(\xi,\eta)}{v_o^{k\alpha}} \frac{d\xi}{\cos\alpha}\right) \tag{68}$$

and the same is true for $\Gamma_o^{k\alpha}$ replacing $n_o^{k\alpha}$. Here ν_I and ν_{cx} are the frequencies of electron impact ionization and of charge exchange collisions. The velocity refers to the emission point: $v_o^{k\alpha} = v_o^k\,(L, y - (L-x)\,\mathrm{tg}\,\alpha)$. The reflexion of neutrals at the liner wall is described by introducing fictitious particle sources on the mirror image of the limiter. By superposing all kinds and beams of neutrals we find the total neutral density everywhere:

$$n_o(x,y) = \sum_{k\alpha} n_o^{k\alpha}(x,y) \tag{69}$$

The interaction of all these neutrals with the s.o.l. plasma yields the following source terms in the basic fluid equations.

Ion production rate $\quad S_n = \nu_I \; n_o \quad$ (70)

Momentum transfer rates

$$S_{px} = \nu_I \sum_{\alpha k} m_i \; \Gamma_o^{k\alpha} + \nu_{cx} \sum_{\alpha k} m_i \; (\Gamma_o^{k\alpha} - n_o^{k\alpha} v_x) \tag{71}$$

$$S_{pz} = - \nu_{cx} \sum_{\alpha k} m_i n_o^{k\alpha} \; v_z = - \nu_{cx} \; m_i \; n_o \; v_z \tag{72}$$

Particle energy transfer rate

$$W_i = \nu_I \sum_{\alpha k} n_o^{k\alpha} \frac{m_i}{2} (v_o^{k\alpha})^2 + \nu_{cx} \sum_{\alpha k} n_o^{k\alpha} \left\{\frac{m_i}{2} \left[(v_o^{k\alpha})^2 - v_x^2 - v_z^2\right] - \frac{3}{2} T_i\right\} \tag{73}$$

Electron energy loss rate

$$W_e = - \nu_I \; n_o \; E_I - \nu_* \; n_o \; E_* \tag{74}$$

We have included in W_e radiation losses by electron impact excitation with the frequency ν_*. The different interaction frequencies $\nu_{int} = \nu_I, \nu_{cx}, \nu_*$ are calculated according to $\nu_{int} = nS_{int} = n \left\langle \sigma_{int} v \right\rangle$. Polynomial approximations for the rate coefficients $S_I(Te)$ and $S_{cx}(Ti)$ are taken from Freeman and Jones /13/. The charge exchange losses in equations (71, 72, 73) are somewhat underestimated because in reality hotter plasma ions (in the tail of the Maxwell distribution) will undergo charge exchanges more frequently than colder ones so that more momentum and more energy is carried away than suggested by our simplified averaging. Instead of $S_{cx}(T_i)$ we use a corrected rate coefficent for charge exchange $S_{cx}(T_{eff})$ with

$$T_{eff} = T_i + \frac{\pi}{8} m_i \, (v_x - v_o^s)^2 \tag{75}$$

This takes account of the fact that there is a relative velocity between the ions flowing with $v_x \geqslant 0$ towards the limiter and the neutrals flying at least with $v_o^s \leqslant 0$ away from the limiter. Because of the weak temperature dependence $S_{cx} \sim T_i^{1/3}$ for temperatures below 100 eV this approximation (75) is sufficient, and the same is true also with respect to the forementioned underestimation of charge exchange loss rates. For the excitation rate coefficient $S_*(T_e)$ we use a corona model for the first excited hydrogen level, assuming that the energy E_* transferred by excitation is fully radiated away by spontaneous emission. For hydrogen $E_* = \frac{3}{4} E_I = \frac{3}{4}$ 13.6 eV = = 10.2 eV. However, the number of excitations is larger than the number of ionizations, so that $\nu_* E_*$ exceeds $\nu_I E_I$ by about 10 to 20 % in the range of relevant temperatures.

We remind that the exponential decay (68) is true in view of the very elongated s.o.l. geometry which implies that charge exchange neutrals are almost completely lost to the plasma core. For slow neutrals we have

$$v_o^s = - \sqrt{\frac{2E_o^s}{m_i}} \approx - 2.2 \times 10^6 \ \frac{\text{cm}}{\text{sec}}$$

For $T_e = T_i = 20$ eV the rate coefficients taken from /10/ are approximately

$$S_i \approx 1.4 \times 10^{-8} \ \frac{\text{cm}^3}{\text{sec}} \, , \; S_{cx} \approx 3 \times 10^{-8} \ \frac{\text{cm}^3}{\text{sec}}$$

Taking $n = n_e = n_{D^+} = 2 \times 10^{12} \text{cm}^{-3}$ the mean free path or decay length for D-atoms results to be

$$\lambda_{mfp} = \frac{|v_o^s|}{n\,(S_i + S_{cx})} = \frac{2.2 \times 10^6}{2 \times 10^{12} \times 4.4 \times 10^{-8}} = 25 \text{ cm}$$

For fast neutrals λ_{mfp} is about three times larger. This allows us to use a numerical integration grid with a toroidal mesh size of 17.5 cm for calculating neutral density profiles.

E) Numerical Procedure

1) Discretization and Time Relaxation

We start from our four basic equations, the equations of continuity (36), of motion (37), or electron energy (30) and of ion energy (35). Let us introduce the vector of primary variables

$$\vec{w} = (n,\ v_x,\ T_e,\ T_i) \tag{76}$$

Then the basic equations can be visualized as giving the time derivative of $\vec{w}$ explicitly in terms of $\vec{w}$ and its spatial derivatives plus additional terms describing non-local integrated effects:

$$\frac{\partial \vec{w}}{\partial t} = \vec{f}\,\left(\vec{w}, \frac{\partial \vec{w}}{\partial x}, \frac{\partial^2 \vec{w}}{\partial x^2}, \frac{\partial \vec{w}}{\partial y}, \frac{\partial^2 \vec{w}}{\partial y^2}\right) + \text{source terms from neutrals}$$
$$+ \text{ nonambipolar corrections with } j_x,\ j_y,\ v_z \tag{77}$$

The function $\vec{f}$ is highly nonlinear, but it does not contain mixed derivatives $\partial^2\vec{w}/\partial x \partial y$. Of course the transport coefficients may also depend on $\vec{w}$ (except v_x). The source terms introduce nonlocal dependencies by integrating along particle paths. The same is true for the nonambipolar corrections, because the iteration procedure (58) determines ϕ and ψ by integrations along x. Hence in principle we have a system of coupled nonlinear partial integro-differential equations of the parabolic type. It is clear that for solving such a complex problem one must resort to numerical methods.

We discretize the equations in the rectangular integration domain of fig. 1. Two spatial grids have been used until now, the one with the wider mesh size is a 40 x 22 grid and is shown in fig. 3, the other with the finer mesh size is a 60 x 33 grid and has been used for the computer plots displaying our numerical results. The notation is given in table 1.

Table 1	wider mesh size	finer mesh size	
toroidal direction $x_1=0$, $x_l=(l-1)\Delta x$	$\Delta x = L/40$ $x_{41} = L$	$\Delta x = L/60$ $x_{61} = L$	 $= 10.5$ m
radial direction $y_1=0$, $y_m=(m-1)\Delta y$ separatrix	$\Delta y = y_w/22$ $y_{23} = y_w$ $y_s = (y_8+y_9)/2$	$\Delta y = y_w/33$ $y_{34} = y_w$ $y_s = (y_{11}+y_{12})/2$	 $=$ 6 cm $\approx$ 2cm

x_1 is the symmetry plane and $x = L$ the limiter plane. Note that the separatrix is located half-way between two gridlines. Also the radial fluxes entering or leaving the edge region are calculated half-step from y_1 and y_w, so that $y = (y_1+y_2)/2$ is the true plasma core boundary and $y = (y_w+y_{w-1})/2$ is the true liner wall, where incident neutral particles should be reflected. The variables $\vec{w}$ are relaxed in time with a time step Δt until the profiles become stationary, starting from an initial guess at $t_0=0$ which should not be too far away from the final stationary state at $t_n=n\Delta t\to\infty$ to ensure convergence. This can always be managed if the parameters and boundary conditions are changed only by a small amount from run to run, once that one solution for a special set of parameters and boundary conditions has been found.

We apply the Mc Cormack integration procedure /14/ which is second order accurate by using forward and backward spatial differencing alternately.

Every time step Δt is composed of two substeps, the predictor and the corrector step. As an example, we show the method for the equation of continuity with the mass density $\rho = m \cdot n$:

$$\frac{\partial \rho}{\partial t} = -\rho \frac{\partial v}{\partial x} - v \frac{\partial \rho}{\partial x} + \frac{\partial}{\partial y}\left(D \frac{\partial \rho}{\partial y}\right) \quad , \quad v = v_x, \ D = D^{\perp}$$

The source term has been omitted for simplicity.

Predictor step:

$$\frac{\overline{\rho_{lm}^{n+1}} - \rho_{lm}^{n}}{\Delta t} = -\left[\rho_l^n \frac{v_l^n - v_{l-1}^n}{\Delta x} + v_l^n \frac{\rho_l^n - \rho_{l-1}^n}{\Delta x}\right]_m$$
$$+ \frac{1}{\Delta y}\left[\frac{D_{m+1}^n + D_m^n}{2}\,\frac{\rho_{m+1}^n - \rho_m^n}{\Delta y} - \frac{D_m^n + D_{m-1}^n}{2}\,\frac{\rho_m^n - \rho_{m-1}^n}{\Delta y}\right]_l \tag{78}$$

Corrector step:

$$\frac{\overline{\overline{\rho_{lm}^{n+1}}} - \overline{\rho_{lm}^{n+1}}}{\Delta t} = -\left[\overline{\rho_l^{n+1}} \frac{\overline{v_{l+1}^{n+1}} - \overline{v_l^{n+1}}}{\Delta x} + \overline{v_l^{n+1}} \frac{\overline{\rho_{l+1}^{n+1}} - \overline{\rho_l^{n+1}}}{\Delta x}\right]_m$$
$$+ \frac{1}{\Delta y}\left[\frac{D_{m+1}^n + D_m^n}{2}\,\frac{\overline{\rho_{m+1}^{n+1}} - \overline{\rho_m^{n+1}}}{\Delta y} - \frac{D_m^n + D_{m-1}^n}{2}\,\frac{\overline{\rho_m^{n+1}} - \overline{\rho_{m-1}^{n+1}}}{\Delta y}\right]_l \tag{79}$$

Total time step: $$\rho_{lm}^{n+1} = \frac{\rho_{lm}^n + \overline{\overline{\rho_{lm}^{n+1}}}}{2} \tag{80}$$

The transport coefficients are advanced in time only after the total time step. First derivatives in the radial direction are treated in an analogous manner, so that a term like $\partial\rho/\partial y$ reads $(\rho_{lm}^n - \rho_{l,\,m-1}^n)/\Delta y$ for the predictor step and $(\overline{\rho_{l,\,m+1}^{n+1}} - \overline{\rho_{lm}^{n+1}})/\Delta y$ for the corrector step. However, in order to avoid asymmetries, we interchange the role of forward and backward radial differences from time step to time step, so that for odd time steps $\partial\rho/\partial y$ reads $(\rho_{l,\,m+1}^n - \rho_{lm}^n)/\Delta y$ for the predictor step and

$(\overline{\rho^{n+1}_{lm}} - \overline{\rho^{n+1}_{l,\,m-1}})/\Delta y$ for the corrector step. For this reason the whole computation cycle restarts identically only after every double time step. The source terms and nonambipolar corrections may be kept constant during several time cycles. It is fully sufficient to recalculate them only after every twenty double time steps.

For the decay of neutral particles according to equation (68) we need the evaluation of a path integral. As an example let us take tg $\alpha = -3\Delta y/\Delta x$ and let $\nu = \nu_I + \nu_{cx}$. Then the integral along the path from grid point (l,m) to grid point (l-1, m-3) is written as a weighted sum in the following form:

$$\int_{l,m}^{l-1,\,m-3} \nu \frac{dx}{\cos\alpha} = -\Big[\frac{1}{6}\nu_{lm} + \Big(\frac{2}{9}\nu_{l,\,m-1} + \frac{1}{9}\nu_{l-1,\,m-1}\Big) + \Big(\frac{1}{9}\nu_{l,\,m-2} + \frac{2}{9}\nu_{l-1,\,m-2}\Big) + \frac{1}{6}\nu_{l-1,\,m-3}\Big]\sqrt{\Delta x^2 + (3\Delta y)^2} \tag{81}$$

This may be easily generalized to arbitrary descrete emission angles α. This reflexion of neutral particles at the liner wall being supposed as elastic and specular is most easily treated by using mirror images of the limiter sources and the scrape-off plasma.

2) Implicit Modification for Numerical Stability

The time step Δt for the explicit time integration method is limited by the usual Courant-Friedrichs-Levy criterion for numerical stability

$$\Delta t \leqslant \mathrm{Min}\left(\frac{\Delta x}{v_x + \sqrt{2}\, c_s}, \frac{(\Delta x)^2}{\frac{8}{3}\frac{\eta}{nm}}, \frac{(\Delta y)^2}{2D^{\perp}}, \frac{(\Delta x)^2}{\frac{4}{3}\frac{\chi_e^{\parallel}}{n}}, \text{etc.}\right) \tag{82}$$

If this condition is not fulfilled, short-wave numerical oscillations develop rapidly. Now the parallel heat conductivities $\chi_e^{\parallel}$ and $\chi_i^{\parallel}$ are extremely large, so that the CFL-criterion imposes time steps about 10^{-3} smaller along x than necessary along y. In view of this strong anisotropy we derive an implicit modification of the Mc Cormack procedure /14/ restricted to the x-direction only. This means that we deal only with those terms in the basic equations (77) that contain $\frac{\partial}{\partial x}$ and $\frac{\partial^2}{\partial x^2}$, and leave all other terms with y-derivatives, source terms and nonambipolar corrections unchanged. We illustrate the method for the electron temperature equation (30) and the predictor step. Let

$$T = T_e(t), \; \tilde{T} = T_e(t+\Delta t), \quad v = v_x, \quad \chi = \chi_e^{\parallel} \tag{83}$$

Then we have to consider the following equation:

$$\frac{3}{2} n \frac{\partial T}{\partial t} + T(n \frac{\partial v}{\partial x} + v \frac{\partial n}{\partial x}) - \frac{\partial}{\partial x} (\chi \frac{\partial T}{\partial x}) =$$
$$= v \; (n \frac{\partial T}{\partial x} + T \frac{\partial n}{\partial x} - \frac{5}{2} n \frac{\partial T}{\partial x}) + \text{further terms}$$

$$\frac{\partial T}{\partial t} = - \frac{2}{3} T \frac{\partial v}{\partial x} - v \frac{\partial T}{\partial x} + \frac{2}{3n} \frac{\partial}{\partial x} (\chi \frac{\partial T}{\partial x}) + \ldots . \tag{84}$$

Hence the explicit temperature change ΔT_l for the predictor step is

$$\Delta T_l = \tilde{T}_l - T_l = \frac{\Delta t}{\Delta x} \{- \frac{2}{3} T_l(v_l - v_{l-1}) - v_l \; (T_l - T_{l-1})$$
$$+ \frac{\chi_{l+1} + \chi_l}{3n_l \; \Delta x} (T_{l+1} - T_l) - \frac{\chi_l + \chi_{l-1}}{3n_l \; \Delta x} (T_l - T_{l-1})\} + \ldots . \tag{85}$$

Introducing the abbreviations

$$\mu = \frac{\Delta t}{2\Delta x} , \quad X_{l\pm 1/2} = \frac{2}{3} \frac{\chi_l + \chi_{l\pm 1}}{n_l \; \Delta x} \tag{86}$$

equation (85) simplifies to

$$\frac{1}{\mu}\,\Delta T_l = -\frac{4}{3}\,T_l\,(v_l - v_{l-1}) - 2v_l\,(T_l - T_{l-1}) + X_{l+1/2}\,(T_{l+1} - T_l) - X_{l-1/2}\,(T_l - T_{l-1}) + \ldots. \tag{87}$$

We call the implicit temperature change δT_l and take it to be

$$\begin{aligned}\frac{1}{\mu}\,\delta T_l = &-\frac{2}{3}\,\tilde{T}_l(v_l - v_{l-1}) - \tilde{v}_l(T_l - T_{l-1})\\ &-\frac{2}{3}\,T_l(\tilde{v}_l - \tilde{v}_{l-1}) - v_l(\tilde{T}_l - \tilde{T}_{l-1})\\ &+ X_{l+1/2}(T_{l+1} - T_l) - X_{l-1/2}(\tilde{T}_l - \tilde{T}_{l-1}) + \ldots.\end{aligned} \tag{88}$$

The method is time-centered similar to Crank-Nicholson (after combining predictor and corrector), and it is therefore unconditionally stable. Further transformation of (88) yields

$$\begin{aligned}\frac{1}{\mu}\,\delta T_l = &-\frac{2}{3}\,\delta T_l\,(v_l - V_{l-1}) - \delta v_l\,(T_l - T_{l-1})\\ &-\frac{2}{3}\,T_l\,(\delta v_l - \delta v_{l-1}) - v_l\,(\delta T_l - \delta T_{l-1})\\ &- X_{l-1/2}\,(\delta T_l - \delta T_{l-1}) + \frac{1}{\mu}\,\Delta T_l\end{aligned}$$

Neglecting differences $v_l - v_{l-1}$ against v_l and $T_l - T_{l-1}$ against T_l we finally get

$$\delta T_l = \frac{-\frac{2}{3}\,\mu\,T_l(\delta v_l - \delta v_{l-1}) + \mu(v_l + X_{l-1/2})\,\delta T_{l-1} + \Delta T_l}{\mu\,(v_l + X_{l-1/2}) + 1} \tag{89}$$

Thus the implicit δT_l is a weighted average of the previously calculated explicit ΔT_l and the implicit δT_{l-1} with an admixture of δv_l and δv_{l-1}, such that with increasing Δt and μ the neighbouring δT_l and δT_{l-1} become strongly correlated, which smoothes out unstable oscillations. The unknown changes $\delta\vec{w}$ at point l are calculated simultaneously from the known changes at point l-1 by the straightforward inversion of a sparsely occupied 4 x 4 matrix, so that we end up with a very simple linear relation of the form

$$\delta\vec{w}_l = \overleftrightarrow{A}_l \cdot \delta\vec{w}_{l-1} + \overleftrightarrow{B}_l \cdot \Delta\vec{w}_l \tag{90}$$

In summary we require only the solution of upper or lower bidiagonal instead of the usual block-tridiagonal equations, and the additional CPU-time per time step for the implicit modification is only about 50 % of the time needed for the explicit method. We routinely use a 100-fold CFL time step with a corresponding reduction in computing time. Furthermore the vectorization capabilities of the KFA Cray X-MP computer can be fully exploited, which gives a speed-up factor of about 25 over IBM 3081. In this way the time relaxation procedure for the 33 x 60 grid converges within a total CPU-time of about 2 minutes.

F) Discussion of the Results and Comparison with Experimental Evidence

1) Neutral Particles

We have compiled 2 x 17 computer plots of the profiles of all relevant plasma variables for TEXTOR-typical parameters. The upper plots with the letter (a) refer to a recycling of the neutral particles with an emission perpendicular to the limiter surface and parallel to the magnetic field. The lower plots with the letter (b) refer to a recycling with the angular distribution described by fig. 3. The neutral density itself is shown by plots 1a,b and 2a,b. The limiter edge is indicated by a vertical arrow in plots 1a,b and by a vertical broken line in plots 2a,b. Obviously an angular distribution leads to a steeper decay of the neutral density in the toroidal direction and to an accumulation of neutral particles in front of the liner wall where they are reflected. The discrete beams are well recognized by the steps in the profiles of plots 1b and 2b. Some neutral particles are lost directly across the boundary to the plasma core.

Fig.4: Particle Flow Diagram [10^{19} / sec / m]

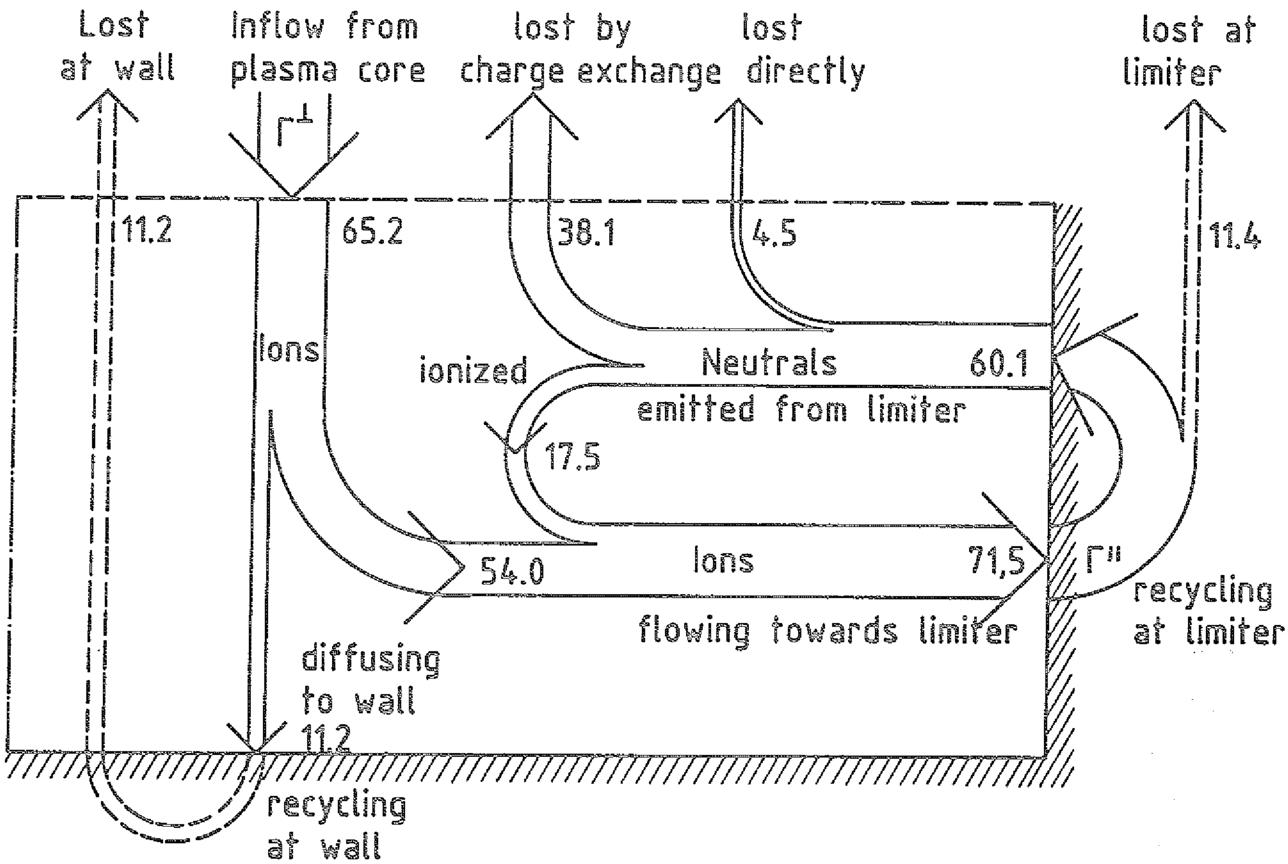

Fig.5: Energy Flow Diagram [kW/m]

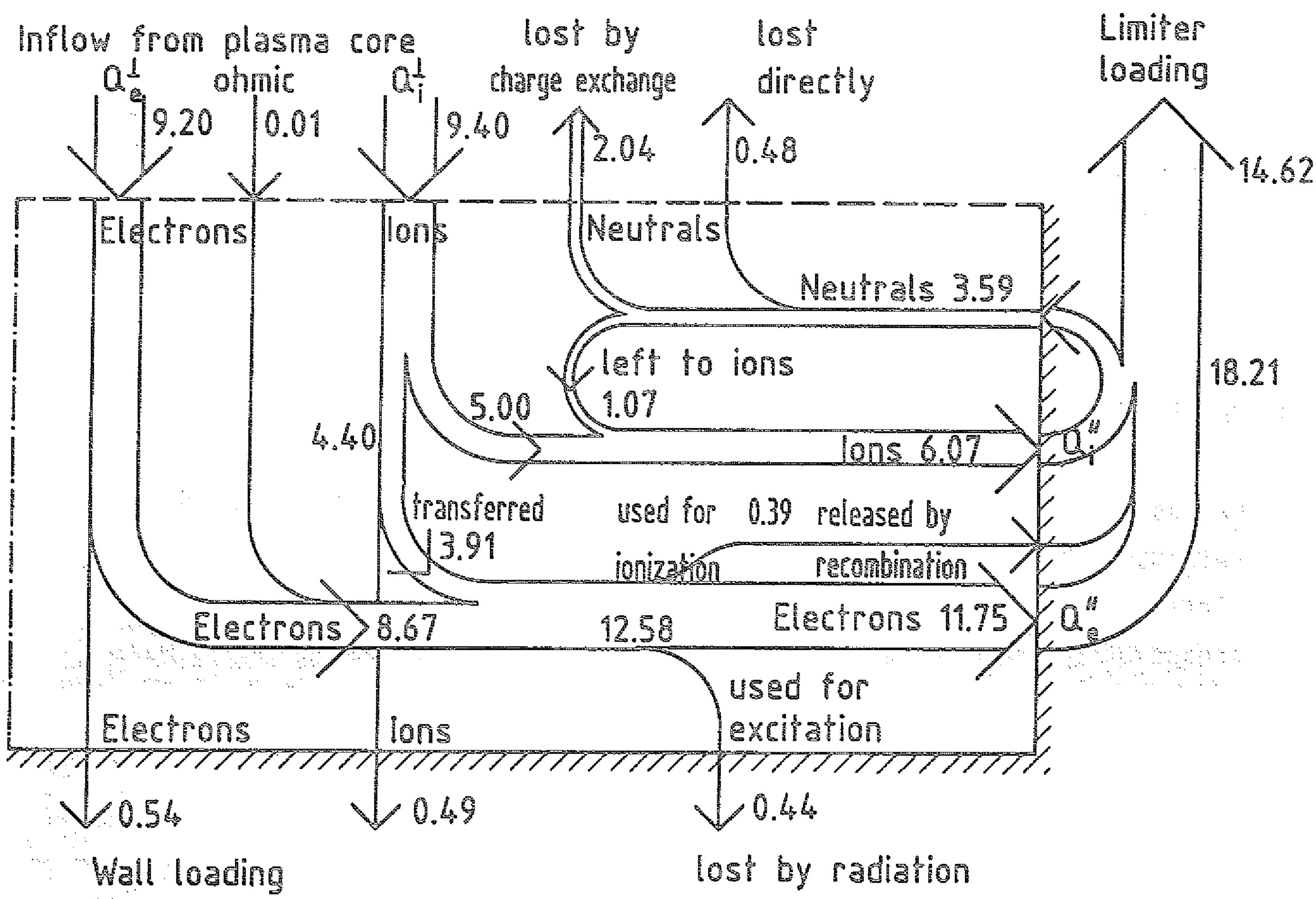

2) Particle and Energy Balances

The computer code also analyzes the particle and energy flows in the scrape-off and transition layer and checks the balances. For case (b) the particle flow diagram is displayed by fig. 4 and the energy flow diagram by fig. 5. All numbers are total fluxes and refer to a poloidal length of 1 m along one side of the (segmented) poloidal limiter. For simplicity the schematic drawings represent only the scrape-off layer, but the interactions and interchanges taking place in the transition layer are contained in the calculated numbers. The input parameters that mainly determine the plasma behaviour in the edge region are the particle and energy inflows from the plasma core entering across the core boundary. A particle recycling factor of 84 % at the limiter target has been assumed, the rest is treated as lost. In reality all particles are recycled, but since a large number of them travel at oblique angles, these will be lost as well without undergoing any interaction with the edge plasma. The particle flow diagram shows that charge exchange plays a major role compared to ionization. In the energy flow diagram an energy input about equally distributed among the electrons and the ions has been assumed. Consequently the electron and ion temperatures tend to reach about the same levels. However, a considerable amount of energy is transferred from the ions to the electrons along their way to the limiter. This energy is gained back by the ions in the Langmuir sheath (not shown in the diagram). The amounts of electron energy needed for ionization and for excitation are relatively small. According to /11/, when taking all excitation levels into account, excitation should consume approximately 20 % more energy than ionization, which shows that our simple model using only the first excited level is not too bad.

3) Density Constriction and Velocity Steepening

Let us now discuss the plasma density displayed by plots 3a,b and the flow velocity displayed by plots 4a,b and 5a,b. Radial profiles are shown by plots 6a,b, toroidal profiles by plots 7a,b. We observe a monotonic decrease of the density when approaching the limiter connected with a marked constriction of the radial profiles. In case (a) the radial decay lengths at the symmetry plane, at half meter in front of the limiter and at the limiter itself are 23 mm, 12 mm and 8 mm respectively. In case (b) the effect is somewhat less pronounced, and the corresponding numbers are 22/12/9 mm. The increase of the toroidal velocity, on the other hand, shows a marked steepening when approaching the limiter. In case (a) with a linear extrapolation the velocity would tend to 0.26 of the sound velocity c_s at the limiter, in case (b) the effect is again somewhat less pronounced, and the extrapolated value is 0.33 c_s. The density constriction and the velocity steepening are clearly correlated and both largely due to the braking action of counter-streaming neutral particles being ionized and charge exchanged. The radial density decay length far from the limiter may be estimated in the following way:

$$\lambda_r \sim \sqrt{D^{\perp} \tau_{\parallel}} \sim \sqrt{D^{\perp} / \frac{\partial v_x}{\partial x}}$$

$$\lambda_r \sim \sqrt{D^{\perp} / \frac{0.3 \; c_s}{L}} \tag{91}$$

Taking $D^{\perp}$ = 6000 cm²/sec , c_s = 42000 m/sec , L = 10.5 m yields

$$\lambda_r \sim \sqrt{\frac{6000 \times 10.5}{0.3 \times 42000}} = \sqrt{5} = 2.24 \text{ cm}$$

in agreement with the above mentioned values. The reduction of the radial decay length near the limiter to about half its value as compared to the symmetry plane is confirmed by experimental evidence in TEXTOR. The measured density profiles in fig. 6 are taken from ref. /15/ and nicely reproduce the shape of the calculated profiles in plots 6a,b. However, the absolute values of the experimental decay lengths are only 16/8 mm. These lengths are smaller because the experiment was made with hydrogen instead of deuterium. Since $c_s \sim m_i^{-1/2}$ the decay length is $\lambda_r \sim m_i^{1/4}$. Furthermore $D^{\perp}$ might be smaller for H^+ than for D^+. It is pointed out that the computer calculations have been performed with only one tenth of the classical value for the viscosity η. Larger values remove the velocity steepening as well as the density constriction, in contradiction to the experimental findings. Since both η and the parallel heat conductivity $\chi_i^{\parallel}$ have the same temperature dependence $\sim T_i^{5/2}$, we have also reduced $\chi_i^{\parallel}$ to one tenth of its classical value. As an additional information we have plotted the electric field $E_{\parallel} = - \partial\phi/\partial x$ normalized to its limiter value in plots 7a,b.

Fig. 6: Measured Density Profiles
at symmetry plane (A) and near limiter (B)

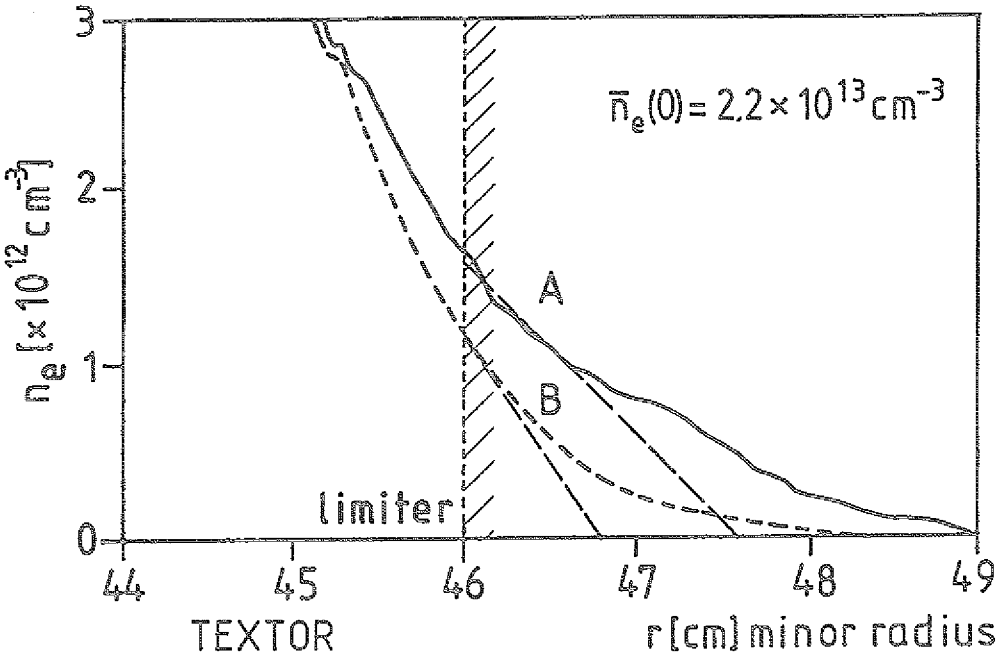

The electric field increases towards the limiter in close correlation with the neutral density. In plot 7b several discontinuous rises of n_0 are accompanied by corresponding rises in $E_{\parallel}$. The reason is that more neutral particles imply more momentum transfer, so that a higher electric field is needed to overcome the increased friction force in order to ensure a monotonic growth of the total fluid velocity of the edge plasma towards the limiter.

4) Electrostatic Potential and Poloidal Rotation

a) Calculated Profiles

We now turn to the potential and the other derived secondary variables. They depend heavily on the temperature profiles. The electron temperature in plots 8a,b is only slightly decreasing in the toroidal direction as a consequence of the very large parallel electron heat conductivity $\chi_e^{\parallel}$. The radial profiles are too flat near the liner wall and especially near the plasma core boundary. In reality there is also impurity radiation which will cause the profiles to be much steeper. The ion temperature in plots 9a,b exhibits a strong cooling effect due to cold neutrals in the vicinity of the limiter edge. Far enough from the limiter the radial T_i-profiles are almost linearly increasing towards the plasma core. The electrostatic plasma potential energy $e\phi$ is displayed by plots 10a,b, radial profiles are shown by plots 11a,b. Remember that the values at the limiter surface are prescribed by the potential drop across the space charge sheath in front of the limiter. This Langmuir potential is of the order of $3T_e$. The values at the symmetry plane are higher by an additional floating potential of the order of 10 eV. The radial profiles of the potential exhibit a characteristic maximum near the separatrix. It is shifted somewhat towards the plasma core. If the potential continues decreasing within the plasma core with the same gradient of about 10 eV/cm, it must change its sign at a minor radius of about r=36 cm. Because of the close connection of the potential with the rotational velocity both must be discussed together. The rotational velocity in the ion diamagnetic direction is displayed by plots 12a,b and 13a,b, radial profiles are shown by plots 14a,b. Apart from distortions near the limiter due to the influence of neutral particles the rotational velocity is essentially constant in the toroidal direction. Remember that we had introduced the constraint of exponentially vanishing plasma core rotation in the symmetry plane. This leads to a steep radial increase of the rotational velocity everywhere along the separatrix, a maximum shifted somewhat into the limiter shadow and a subsequent decrease towards the liner wall. Whereas in the scrape-off layer the electric drift and the ∇p_i-drift act in the same direction and produce a considerable rotation, these drifts must compensate each other in the core such as to leave the plasma at rest, which is related to the change of sign of $\nabla\phi$ in the transition layer. We estimate the order of magnitude of the rotational velocity v_z near the separatrix from eq. (54):

$$v_z \approx \frac{1}{eB} \left(\frac{T_i}{n}\frac{\partial n}{\partial y} + \frac{\partial T_i}{\partial y} + 3\,\frac{\partial T_e}{\partial y}\right) \tag{92}$$

We neglect $\partial T_i/\partial y$ compared to $\partial T_e/\partial y$, take the same radial decay length for T_e as for n and put $T_e = T_i = T$:

Fig.7: Measured Radial Profiles
in the Edge Plasma of the TEXT Tokamak

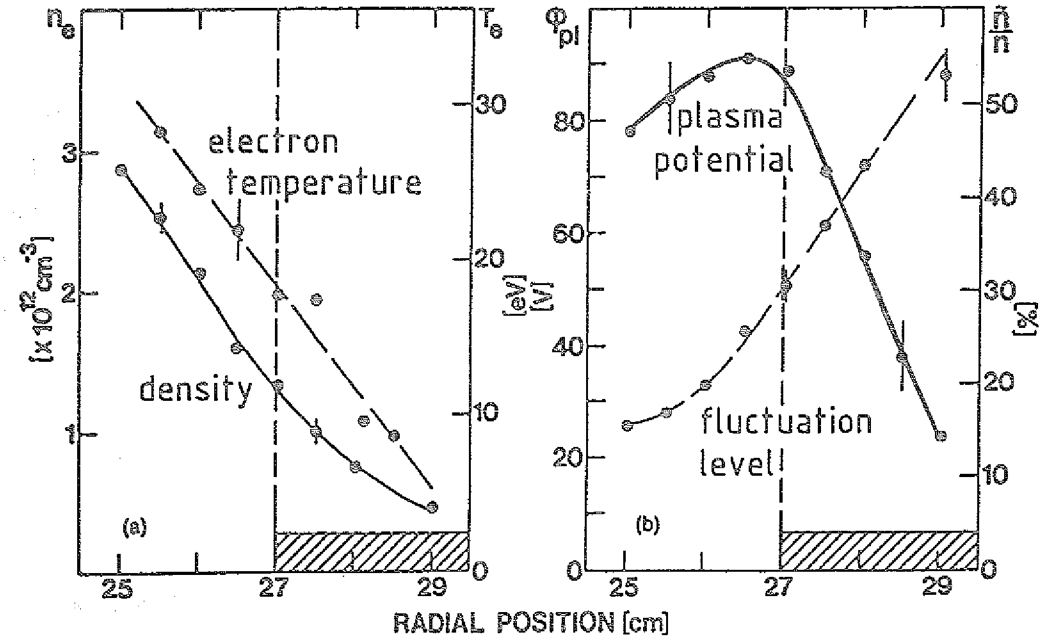

Fig. 8: Measured Poloidal Drift Velocities
in the Edge Plasma of the TEXT Tokamak

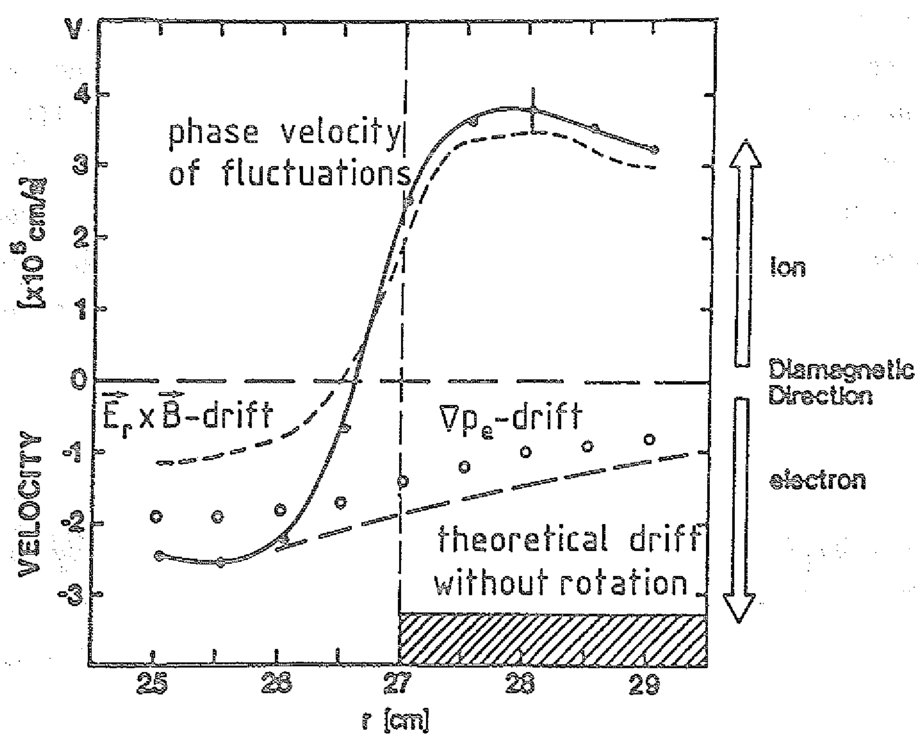

$$v_z \approx - \frac{1}{eB} \left(\frac{T_i}{\lambda_r} + 0 + 3 \frac{T_e}{\lambda_r}\right) = - \frac{4T}{eB\lambda_r} \tag{93}$$

Inserting T = 25 eV, B = 2 Vs/m² and λ_r = 2.2 cm yields

$$v_z \approx - \frac{4 \times 25}{2 \times 0.022} \approx - 2270 \frac{m}{sec}$$

in agreement with plots 14a,b. Note that $-v_z$ is the velocity in the ion diamagnetic direction. Another way of looking at the order of magnitude of v_z is the following. We write (93) in a more complicated manner and use (91) and the definition of v_y:

$$v_z \approx - \frac{4T}{D^{\perp}eB} \sqrt{\frac{D^{\perp}}{\lambda_r}} \sqrt{\frac{D^{\perp}}{\lambda_r}} \approx - \frac{4T}{D^{\perp}eB} \sqrt{\frac{D^{\perp}}{n} \frac{\partial n}{\partial y}} \sqrt{\frac{0.3\ c_s \lambda_r}{L}}$$

$$v_z \approx - \frac{4T}{D^{\perp}eB} \sqrt{\frac{0.3\lambda_r}{L}} \sqrt{v_y\ c_s} \approx - 2 \sqrt{v_y\ c_s} \tag{94}$$

Thus $-v_z$ is about twice the geometric mean of the diffusion velocity $v_y \approx 30$ m/sec and the sound velocity $c_s \approx 42000$ m/sec.

b) Comparison with Experimental Results of three Tokamaks

Our results concerning the behaviour of the potential and the rotation are confirmed by experimental evidence in TEXT /6/. The TEXT tokamak at Austin is smaller (R = 100 cm, a = 27 cm, B = 1T) than the TEXTOR tokamak at Jülich (R = 175 cm, a = 46 cm, B = 2T), but the edge conditions are quite similar. A square array of four single Langmuir probes was used to sample the density, electron temperature and floating potential at the top of the tokamak and located about 80 cm away from the limiter in the (toroidal) electron drift direction. The probe array was moved radially from shot to shot. The measured radial profiles are shown by fig. 7, and we may state that the characteristic features of the general shape of the plasma potential are nicely reproduced by our plots 11a,b. The measurements also allowed to compute the S(k,ω) spectrum for density and potential fluctuations where S(k,ω) represents the power of the fluctuations as a function of frequency ω and of the component of the wave vector k in the poloidal direction. The power-weighted phase velocity

$$v_{ph}(\omega) = \frac{\Sigma_k \frac{\omega}{k} S(k,\omega)}{\Sigma_k S(k,\omega)} \qquad (95)$$

is nearly independent of frequency, and a cubic spline fit to the measured phase velocity for both density and potential fluctuations is plotted in fig. 8. Obviously the phase velocity changes from propagation in the electron diamagnetic direction in the bulk plasma to propagation in the ion diamagnetic direction in the scrape-off plasma. However, the drift velocity of the turbulent fluctuations for drift wave theories is predicted to be in the electron diamagnetic direction and should follow the ∇p_e-drift as indicated by the fat broken line in fig. 8. The difference between the actual measured phase velocity and the theoretical drift is easily explained by a rotation of the plasma as a whole and nicely reproduced by our plots 14a,b. Note that in TEXT the values of the rotational velocities must be doubled because of the smaller magnetic field (1T instead of 2T). The $\vec{E}_r \times \vec{B}$ - drift velocity is also shown in fig. 8 and is the dominant contribution to the change in the measured phase velocity. If we assume $\nabla p_i \approx \nabla p_e$ so that the ion diamagnetic drift is about minus the electron diamagnetic drift, the curves of fig. 8 are consistent with the picture that the electric drift should be about three times the ion diamagnetic drift in the scrape-off plasma and about minus the ion diamagnetic drift in the core plasma. The measured data were also used to calculate a fluctuation induced transport $\Gamma^{\perp}(\omega)$ from the correlation and phase angle $\Theta(\omega)$ between $\tilde{\phi}(\omega)$ and $\tilde{n}(\omega)$ by Fourier analyzing eq. (13). The radial particle flux is for all r and ω in the outward direction and decreases with r in the limiter shadow, in qualitative agreement with our anomalous diffusion flux.

Further experimental evidence on plasma rotation follows from detailed investigations of the structure of edge plasma turbulence in the Caltech tokamak /7/. This tokamak is even smaller (R = 45 cm, a = 14 cm, B = 0.35 T), but the edge parameters $n_e(a) \approx 10^{12}$ cm^{-3}, $T_e(a) \approx 25$ eV and $e\phi(a) \approx$ ≈ 60 eV are again quite similar to those of the other tokamaks. A two-dimensional probe array was used consisting of an 8 x 8 square matrix of Langmuir probes with a total extent of 1.8 cm in both the poloidal and the radial direction. It was fixed at the outer equatorial plane and covered a radial range from r = 13.7 to r = 15.5 cm. The wall was at 16 cm. The measurements concentrated on the evaluation of cross-correlation functions defined by

$$C_{1n}(\tau) = \frac{\Sigma\ S_1(t)\ S_n(t+\tau)}{\sqrt{\Sigma\ S_1^2\ \Sigma\ S_n^2}} \quad , \quad \Sigma = \int_{t=0}^{T} \ldots\ dt \tag{96}$$

with S_n denoting the signal of probe number n, and T = 0.8 msec. The poloidal propagation velocity of $\tilde{n}$ and $\tilde{\phi}$ versus radius was measured as the group velocity derived from the delay time to the peak of the cross-correlation function between probes separated by 0.75 cm poloidally. Since the experiment was restricted to the scrape-off layer $r \gtrsim a$, only the radial decay of $e\phi(r) \sim 3T_e(r)$ could be measured, the transition layer with the maximum of the potential was beyond the range of the probes. However, the reversal of the poloidal propagation velocity from the ion diamagnetic direction to the electron diamagnetic direction just beyond the separatrix at $r \approx 13.8$ cm could be detected. The measured group speed in the limiter shadow region is typically 7000 m/sec, the electric drift velocity is about 6000 m/sec, and the ∇p_e-drift velocity is about -2000 m/sec. According to non-linear collisional drift-wave models turbulent fluctuations should propagate at velocities near the ∇p_e-drift. Hence we must again superimpose a plasma rotation composed of a ∇p_i-drift ($\nabla p_i \approx \nabla p_e$) and the electric drift to obtain the measured propagation. The radial particle flux was calculated from the correlation of $\tilde{n}$ and $\tilde{v}_r = \tilde{E}_{pol}/B$ in the form

$$\Gamma^{\perp} = \left\langle \tilde{n}\ \tilde{v}_r \right\rangle = C_{nE}(0)\ \left\langle \tilde{n} \right\rangle \left\langle \tilde{v}_r \right\rangle = -\ D^{\perp}\ \frac{\partial n}{\partial r} = \frac{D^{\perp} n}{\lambda_r} \tag{97}$$

where $C_{nE}(0) \approx 0.2$ is the zero-time correlation coefficient between $\tilde{n}$ and $\tilde{E}_{pol}$, and $\langle \tilde{n} \rangle$ and $\langle \tilde{v}_r \rangle$ are the root-mean-square fluctuation levels. The calculated fluxes were large and outward, $D^{\perp}$ was found to be about twice the Bohm diffusion coefficient, and it was concluded in /7/ that this diffusion process may be comprehensible in terms of non-linear edge instability theory.

Some additional information is reported from the TM-4 tokamak /8/. In this small tokamak (R = 53 cm, a = 8.5 cm, B = 1.4 T) the measurements were restricted to the plasma core inside the separatrix. Radial profiles of the plasma potential were determined by using a beam of fast Cs^+-ions as a probe. The potential was positive at the periphery, but it decreased to large negative values $e\phi \leq -T_i$ in the center of the column, which is qualitatively what we would expect, too. The poloidal (and toroidal) rotation velocities were determined from the Doppler shift of spectral lines of carbon and oxygen impurities. In the central part of the plasma column the poloidal velocity was directed along the electron diamagnetic drift and coincided with neoclassical predictions of impurity velocity. At the periphery, however, the poloidal rotation changed sign, indicating a plasma rotation in the ion diamagnetic direction as seen in the other tokamaks.

5) Electric Currents

We finish the discussion by directing the attention to our last twice three computer plots. Plots 15a,b display the stream function Ψ in A per poloidal m as a measure of the nonambipolarity by the occurrence of radial and toroidal electric currents. The contour lines of equal Ψ represent the current density lines and are projected in plots 16a,b. We observe a marked and very elongated current vortex flow along the separatrix to be closed via the limiter edge. This current eddy is clearly connected with the steep radial increase of plasma rotation along the separatrix. A second much weaker and counteroriented current eddy is connected with the decrease of rotation in the limiter shadow. The third and weakest eddy in front of the liner wall depends on the boundary conditions for the plasma variables which are not very well known. The understanding of the physics in the transition region just in front of the limiter head is outside the scope of the present model which treats the limiter as infinitely thin. It is clear, however, that the limiter has a finite width and that there must be electric currents leaving the limiter head in the radial direction to ensure a divergence free closure of the dominant current vortex. Plots 17a,b show the toroidal currents j_x in the limiter plane. The negative currents beyond the separatrix are those which must emerge from the limiter head.

LITERATURE

/1/ H. Gerhauser, H.A. Claaßen, Proc. 12th Eur. Conf. on Contr. Fus. and Plasma Physics, Budapest, Part II, p. 464 (1985)

/2/ B.J. Braams, ibidum, p. 480

/3/ R. Simonini, W. Feneberg, A. Taroni, ibidum, p. 484

/4/ Yu.L. Igitkhanov et al., ibidum, p. 488

/5/ S.I. Braginskij, Rev. Plasma Physics Vol. 1, p. 205 (1965)

/6/ Ch.P. Ritz et al., Phys. Fluids 27, p. 2956 (1984)

/7/ S.J. Zweben, R.W. Gould, Nucl. Fus. 25, p. 171 (1985)

/8/ V.I. Bugarya et al., JETP Letters 38, p. 404 (1983)

/9/ A.H. Boozer, Phys. Fluids 19, p. 1210 (1976)

/10/ M.F.A. Harrison, Atomic and Molecular Collisions in the Plasma Boundary, Report CLM-P746 (1985)

/11/ R.K. Janev et al., J. Nucl. Materials 121, p. 10 (1984)

/12/ E. Cupini et al., NIMBUS Report Part I, 127/83-1/Fu-I/NET (1983)

/13/ R.L. Freeman, E.M. Jones, Report CLM-R137 (1974)

/14/ R.W. Mac Cormack, AIAA Journal 20, p. 1275 (1982)

/15/ U. Samm et al., 7th Int. Conf. on Plasma Surface Interactions in Contr. Fus. Devices, Princeton 1986, J. of Nuclear Materials 145-147, 206 (1987)

/16/ K.U. Riemann, Phys. Fluids 24, p. 2163 (1981)

ACKNOWLEDGEMENT

Stimulating discussions with Prof. G. Ecker and his co-workers in Bochum and the valuable programming assistance of G. Giesen are gratefully acknowledged.

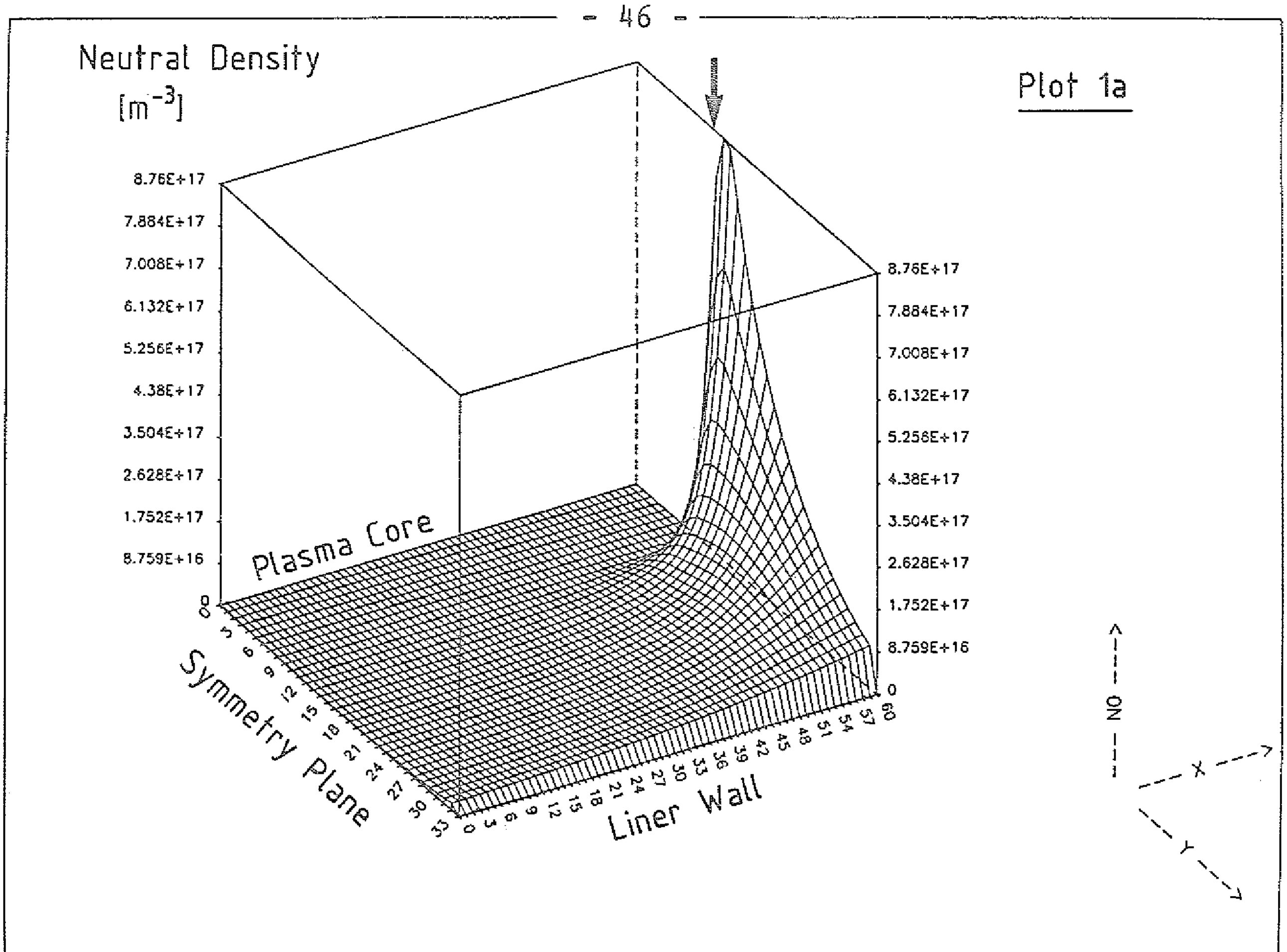
Neutral Density
[m^{-3}]
Plot 1a
8.76E+17
7.884E+17
7.008E+17
6.132E+17
5.256E+17
4.38E+17
3.504E+17
2.628E+17
1.752E+17
8.759E+16
0
Plasma Core
Symmetry Plane
Liner Wall
NO
X
Y

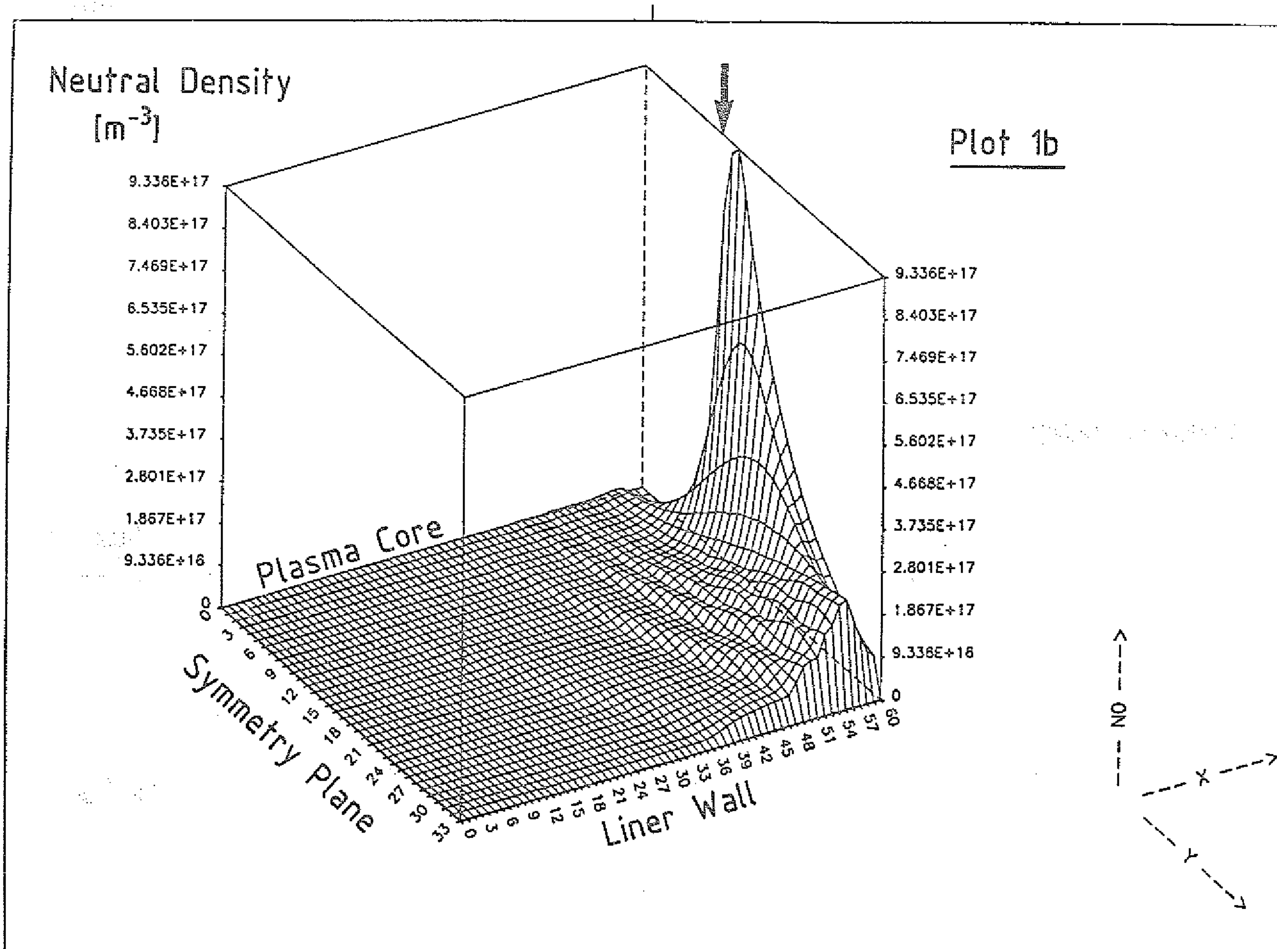
Neutral Density
[m^{-3}]
Plot 1b
9.336E+17
8.403E+17
7.469E+17
6.535E+17
5.602E+17
4.668E+17
3.735E+17
2.801E+17
1.867E+17
9.336E+16
0
Plasma Core
Symmetry Plane
Liner Wall
NO
X
Y

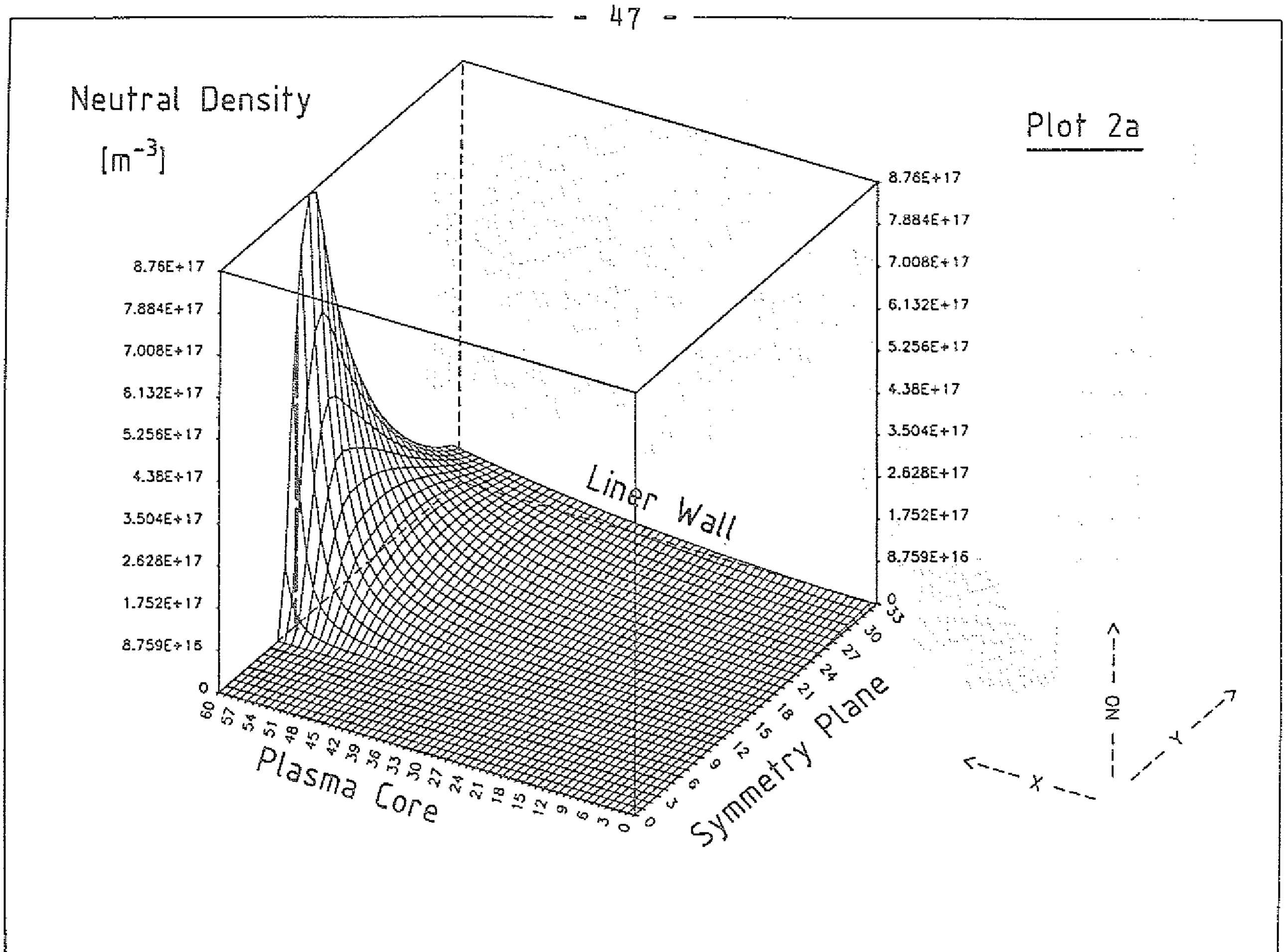
Neutral Density
[m^-3]
Plot 2a
8.76E+17
7.884E+17
7.008E+17
6.132E+17
5.256E+17
4.38E+17
3.504E+17
2.628E+17
1.752E+17
8.759E+16
0
Liner Wall
Plasma Core
Symmetry Plane
X
Y
NO

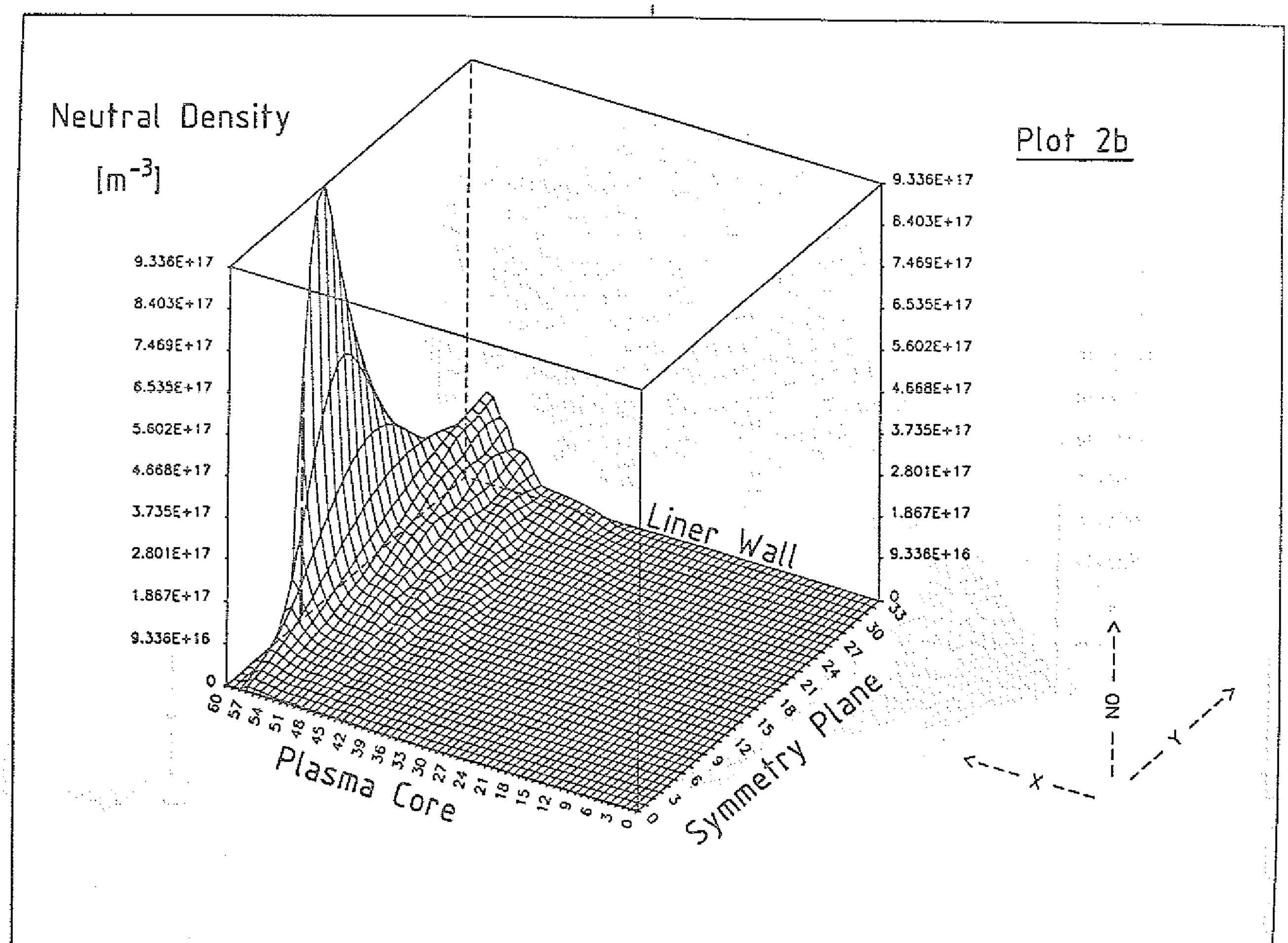
Neutral Density
[m^-3]
Plot 2b
9.336E+17
8.403E+17
7.469E+17
6.535E+17
5.602E+17
4.668E+17
3.735E+17
2.801E+17
1.867E+17
9.336E+16
0
Liner Wall
Plasma Core
Symmetry Plane
X
Y
NO

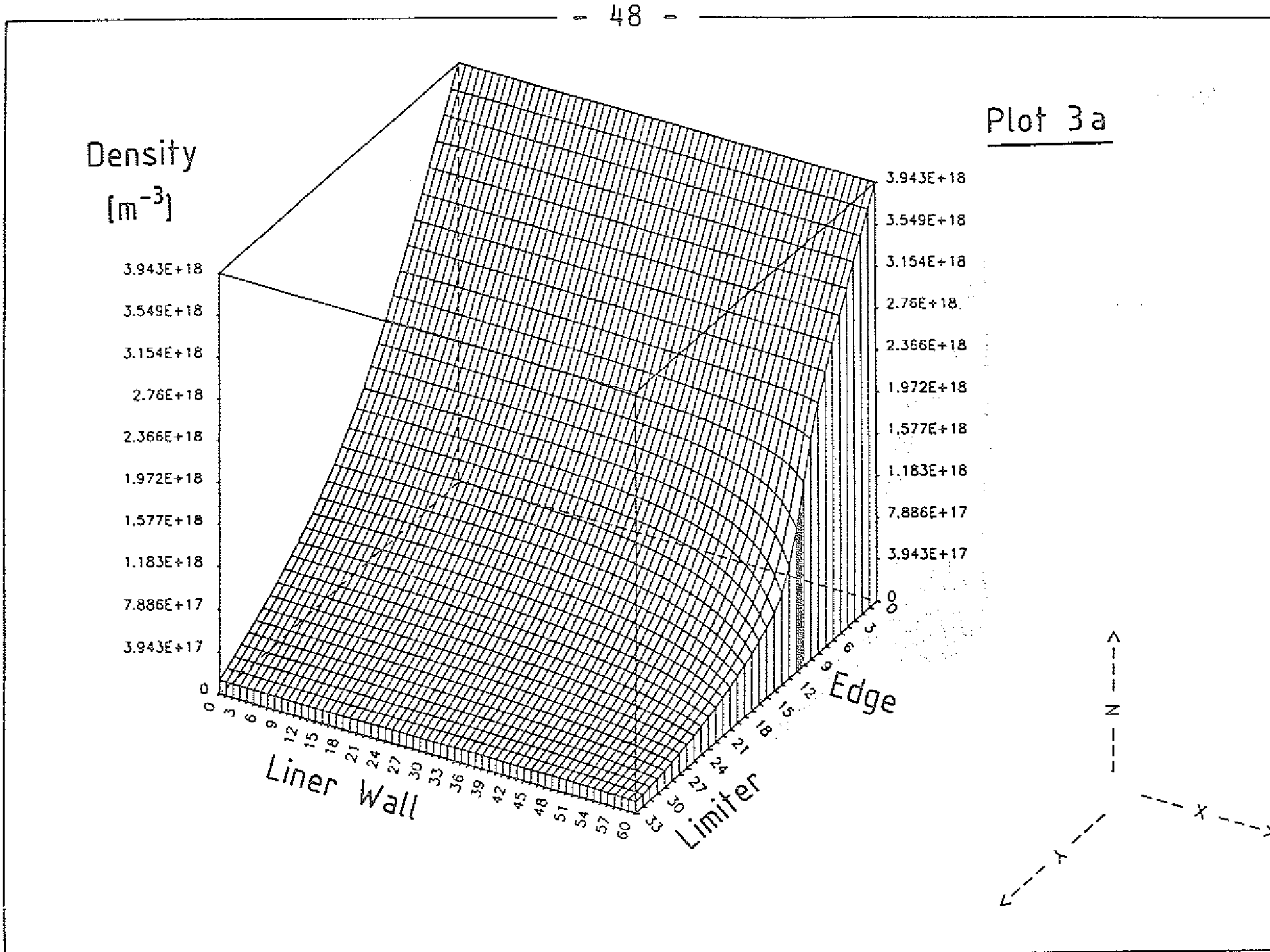
Plot 3a
Density
[m^-3]
3.943E+18
3.549E+18
3.154E+18
2.76E+18
2.366E+18
1.972E+18
1.577E+18
1.183E+18
7.886E+17
3.943E+17
0
Liner Wall
Limiter
Edge
N
X
Y

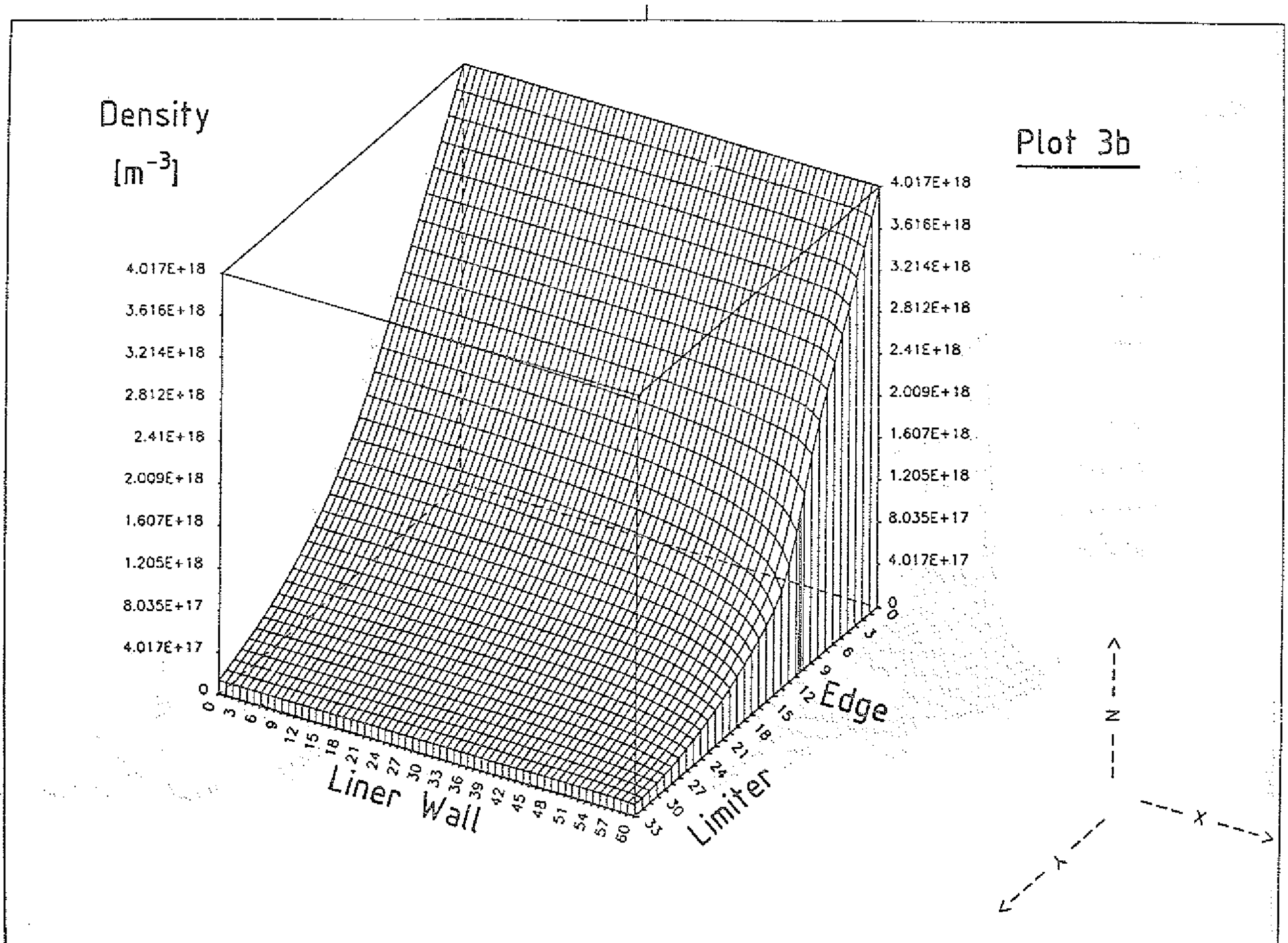
Plot 3b
Density
[m^-3]
4.017E+18
3.616E+18
3.214E+18
2.812E+18
2.41E+18
2.009E+18
1.607E+18
1.205E+18
8.035E+17
4.017E+17
0
Liner Wall
Limiter
Edge
N
X
Y

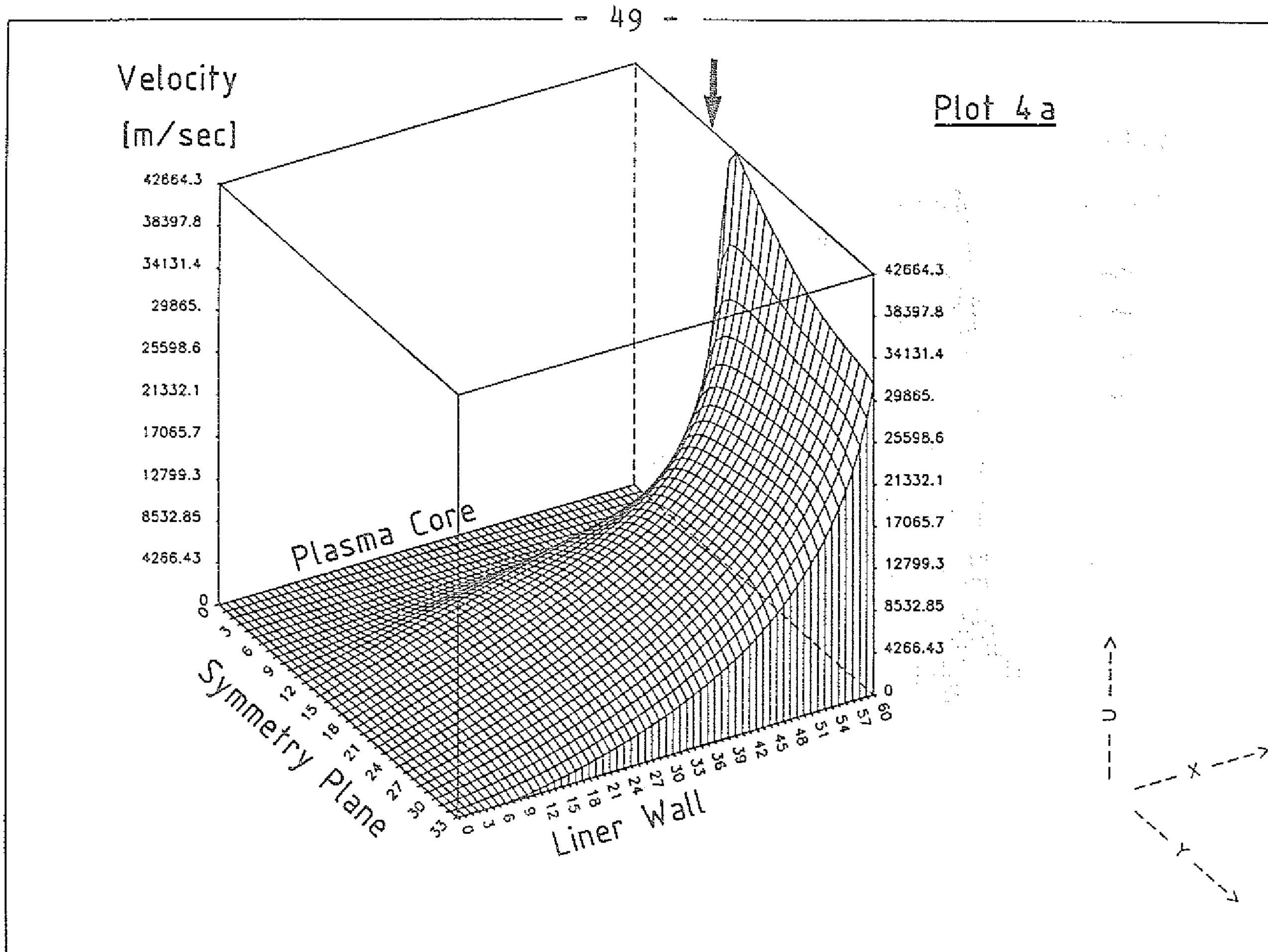
Velocity
[m/sec]
Plot 4a
Plasma Core
Symmetry Plane
Liner Wall
42664.3
38397.8
34131.4
29865.
25598.6
21332.1
17065.7
12799.3
8532.85
4266.43
0
U
X
Y

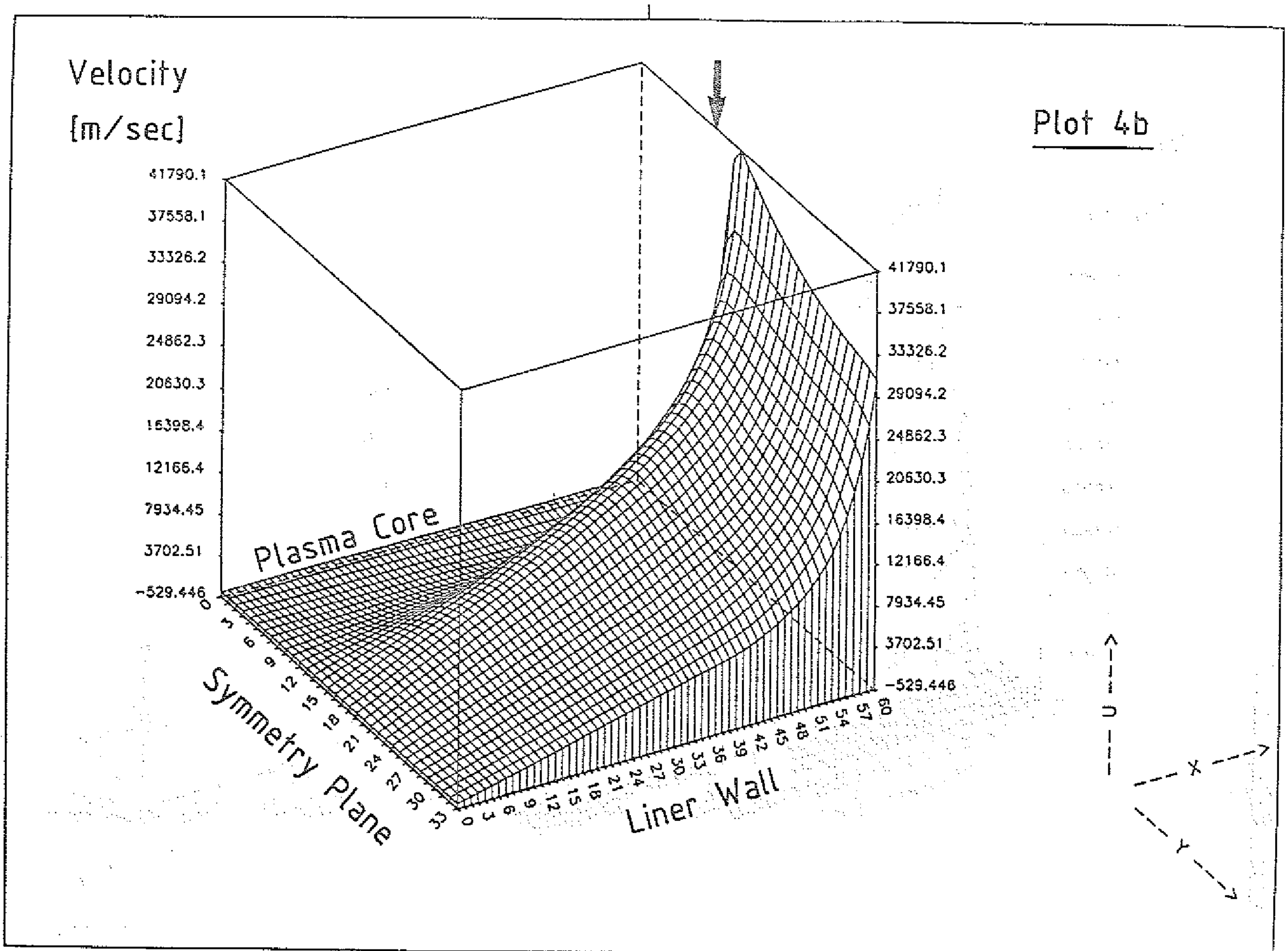
Velocity
[m/sec]
Plot 4b
Plasma Core
Symmetry Plane
Liner Wall
41790.1
37558.1
33326.2
29094.2
24862.3
20630.3
16398.4
12166.4
7934.45
3702.51
-529.446
U
X
Y

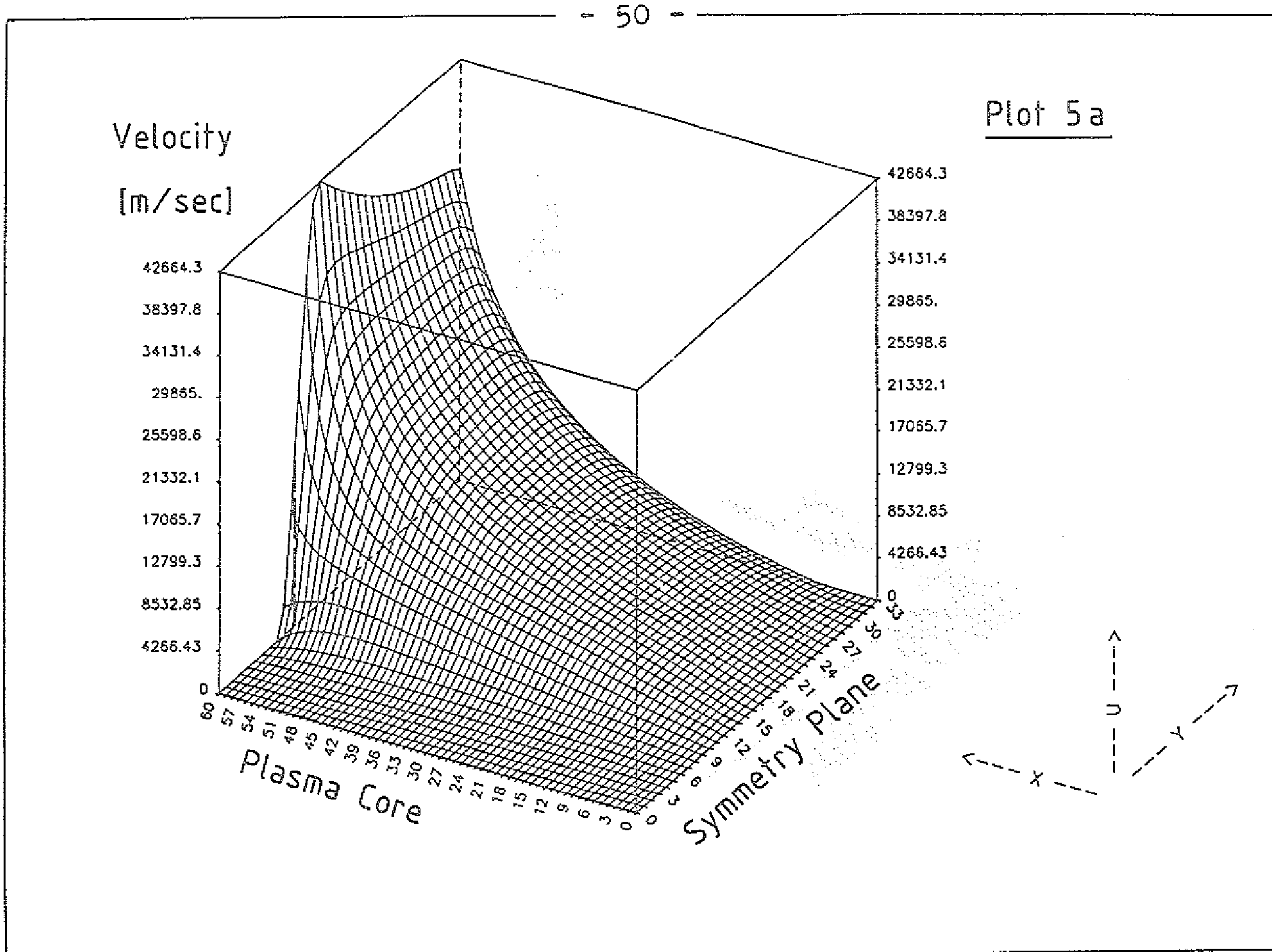
Plot 5a
Velocity
[m/sec]
42664.3
38397.8
34131.4
29865.
25598.6
21332.1
17065.7
12799.3
8532.85
4266.43
0
60 57 54 51 48 45 42 39 36 33 30 27 24 21 18 15 12 9 6 3 0
Plasma Core
0 3 6 9 12 15 18 21 24 27 30 33
Symmetry Plane
U
Y
X

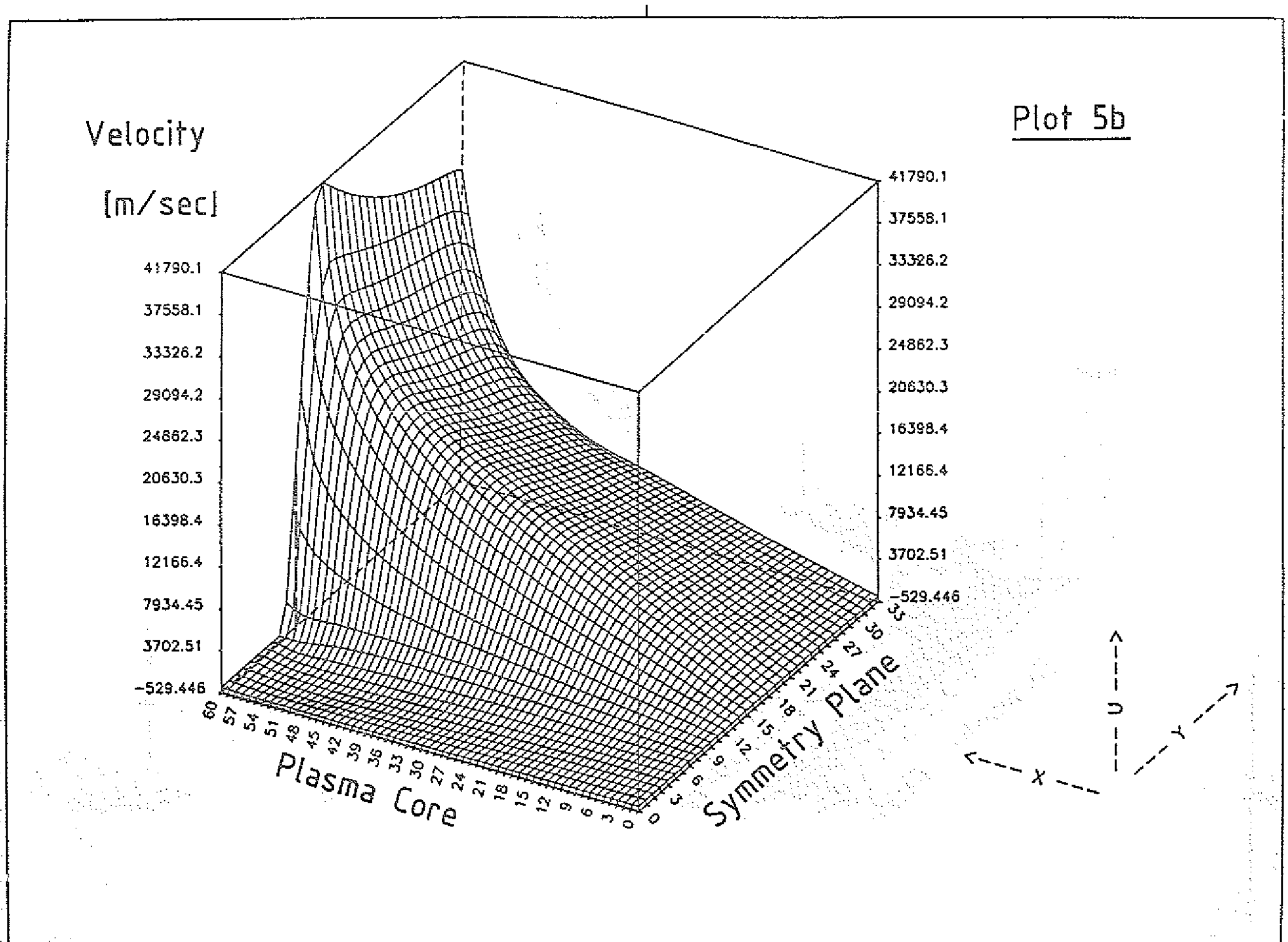
Plot 5b
Velocity
[m/sec]
41790.1
37558.1
33326.2
29094.2
24862.3
20630.3
16398.4
12166.4
7934.45
3702.51
-529.446
60 57 54 51 48 45 42 39 36 33 30 27 24 21 18 15 12 9 6 3 0
Plasma Core
0 3 6 9 12 15 18 21 24 27 30 33
Symmetry Plane
U
Y
X

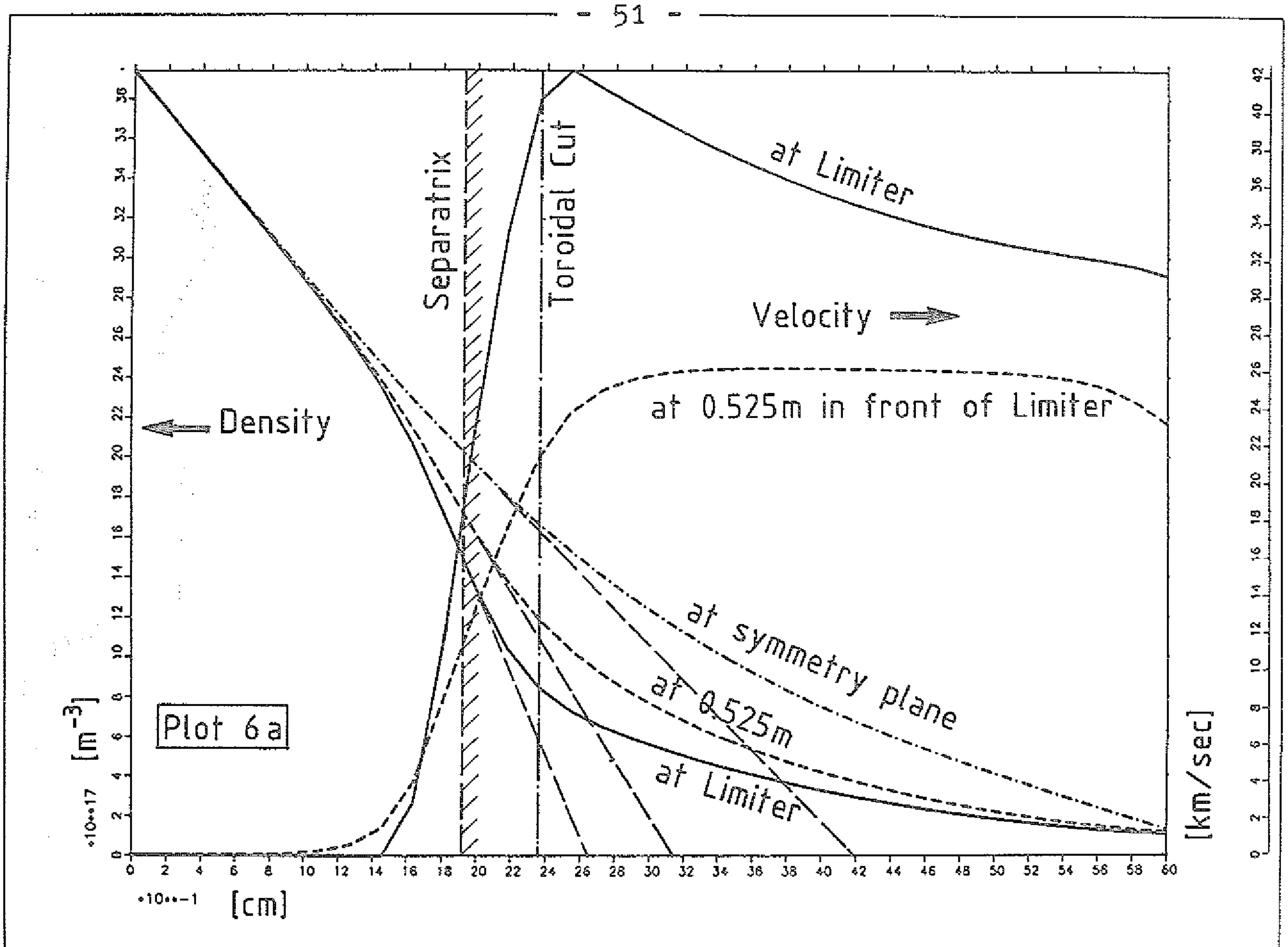
Separatrix
Toroidal Cut
at Limiter
Velocity
at 0.525m in front of Limiter
Density
at symmetry plane
at 0.525m
at Limiter
Plot 6a
[m^-3]
*10**17
[km/sec]
*10**-1
[cm]

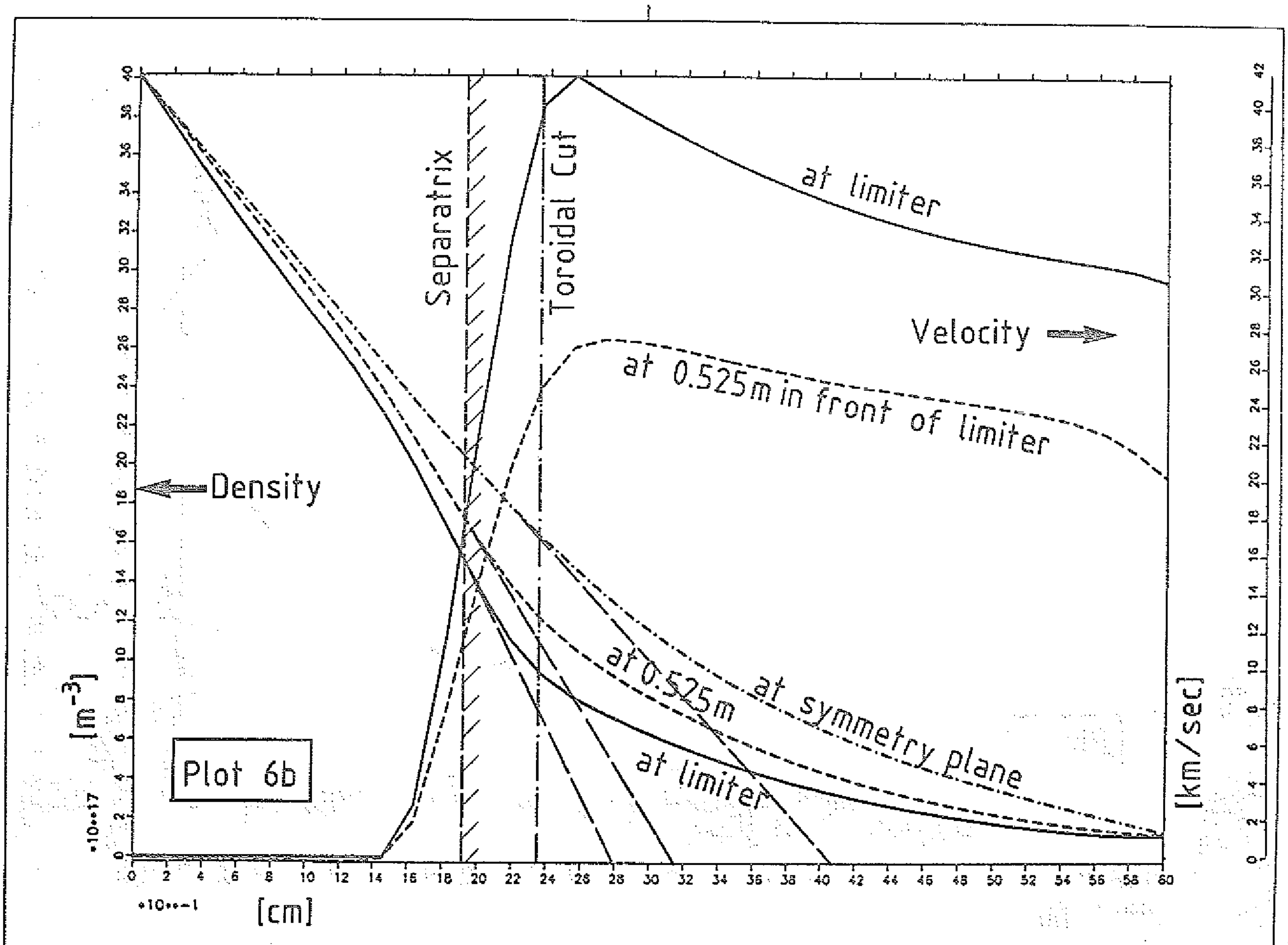
Separatrix
Toroidal Cut
at limiter
Velocity
at 0.525m in front of limiter
Density
at 0.525m
at symmetry plane
at limiter
Plot 6b
[m^-3]
*10**17
[km/sec]
*10**-1
[cm]

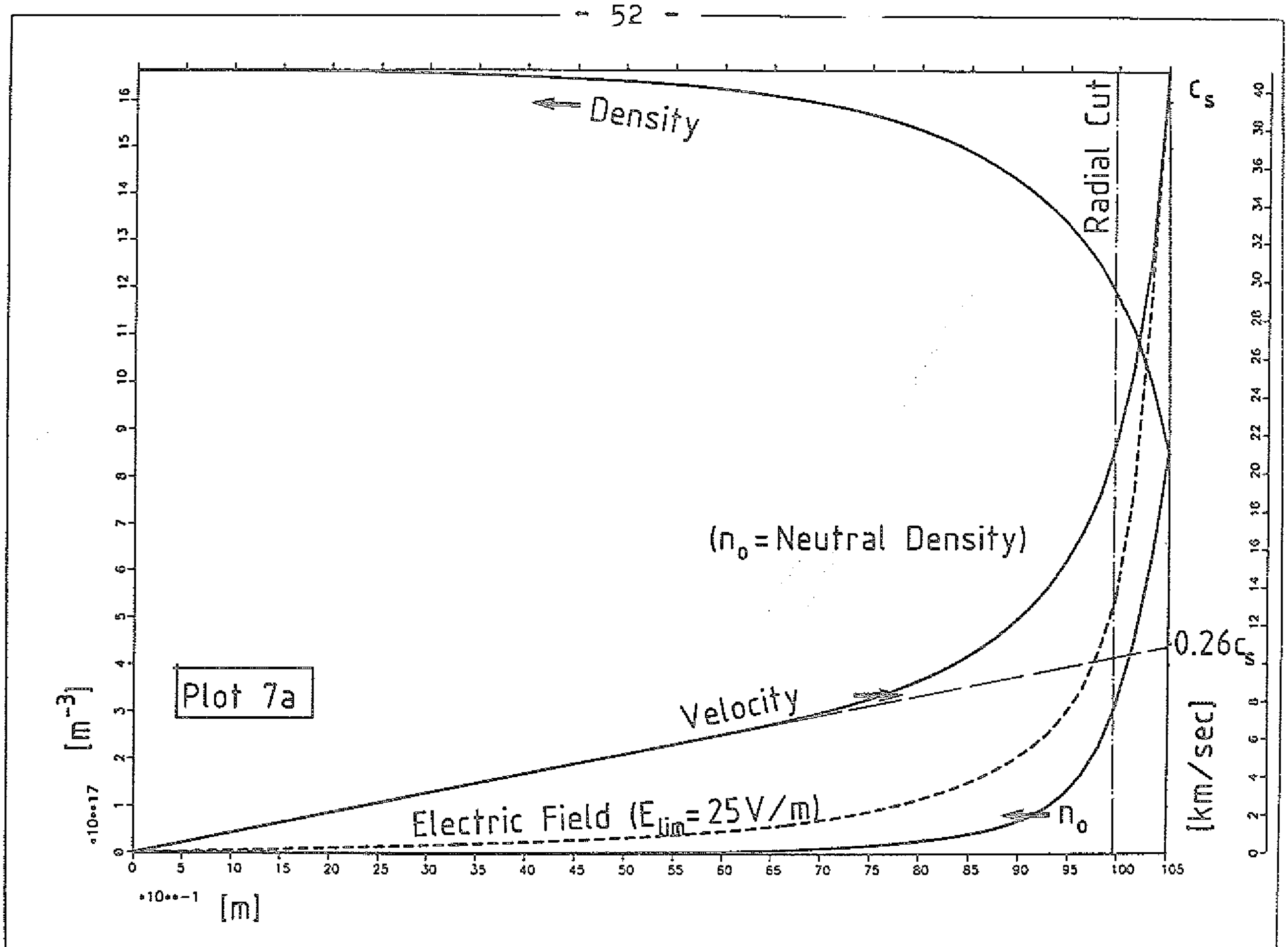

Density
Radial Cut
c_s
(n_o = Neutral Density)
0.26c_s
Plot 7a
Velocity
Electric Field (E_{lim} = 25 V/m)
n_o
[m^{-3}]
*10**17
*10**-1
[m]
[km/sec]

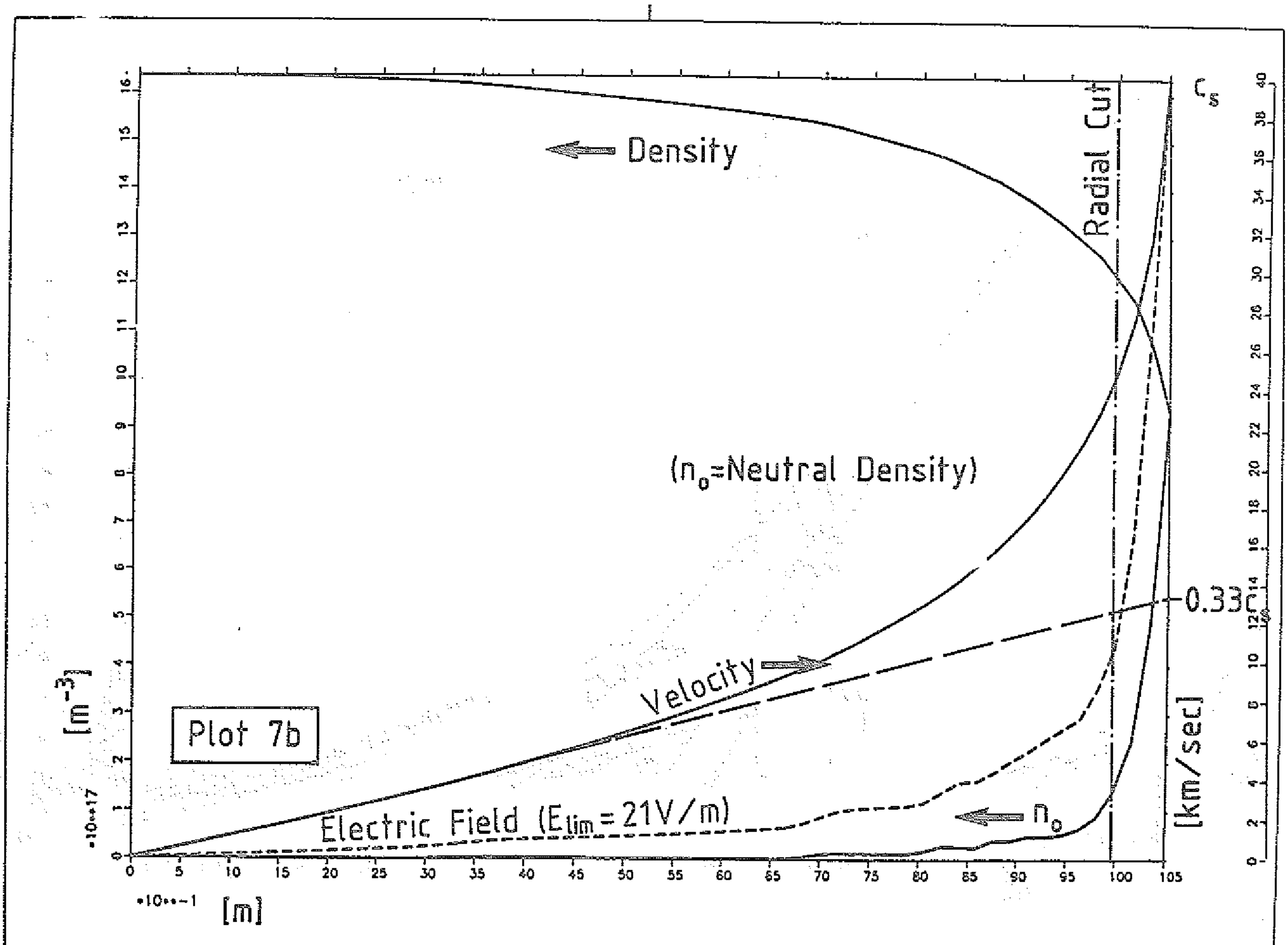

Density
Radial Cut
c_s
(n_o=Neutral Density)
0.33c_s
Velocity
Plot 7b
Electric Field (E_{lim} = 21 V/m)
n_o
[m^{-3}]
*10**17
*10**-1
[m]
[km/sec]

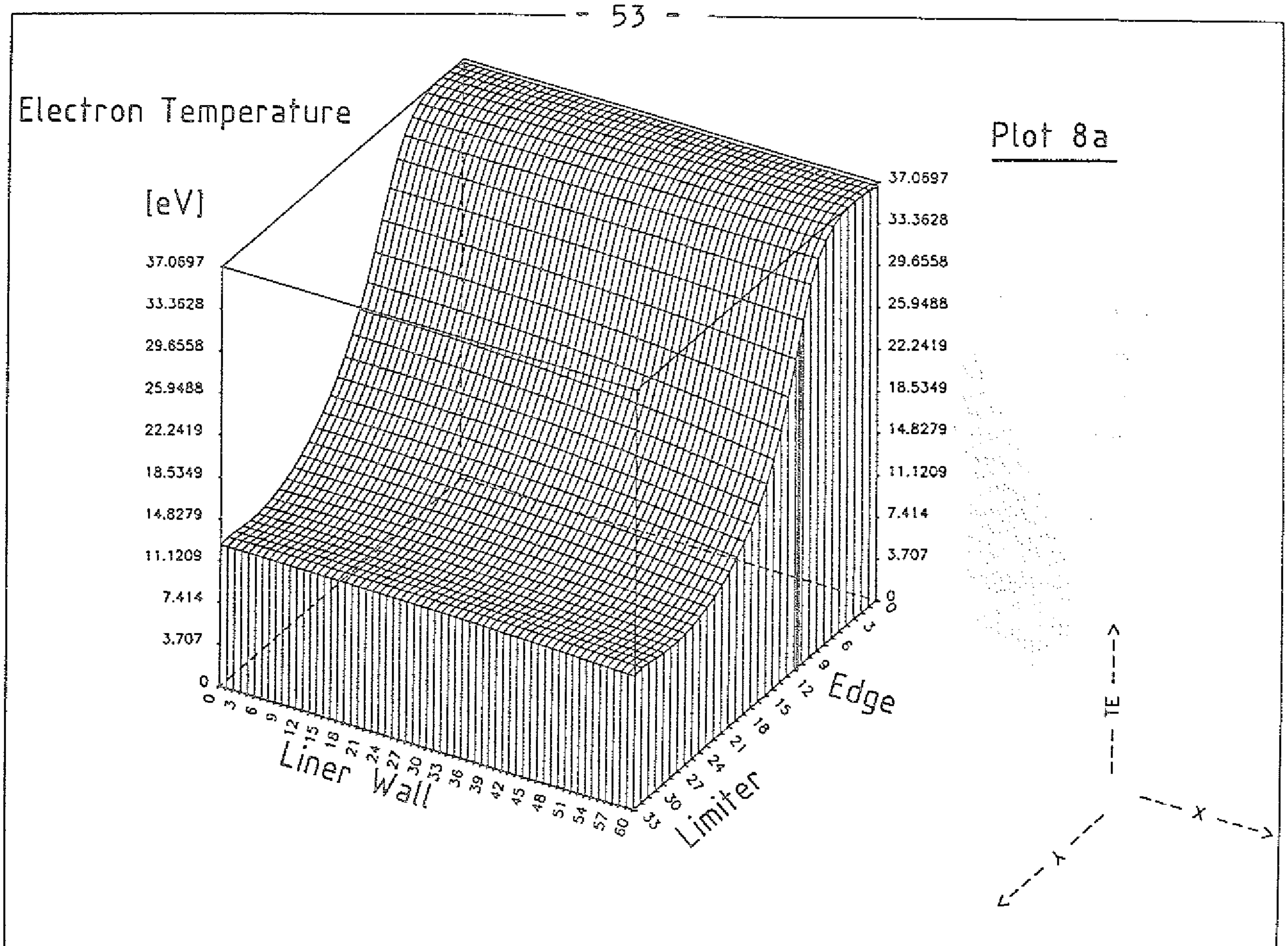

Electron Temperature
[eV]
Plot 8a
37.0697
33.3628
29.6558
25.9488
22.2419
18.5349
14.8279
11.1209
7.414
3.707
0
Liner Wall
Edge
Limiter
TE
X
Y

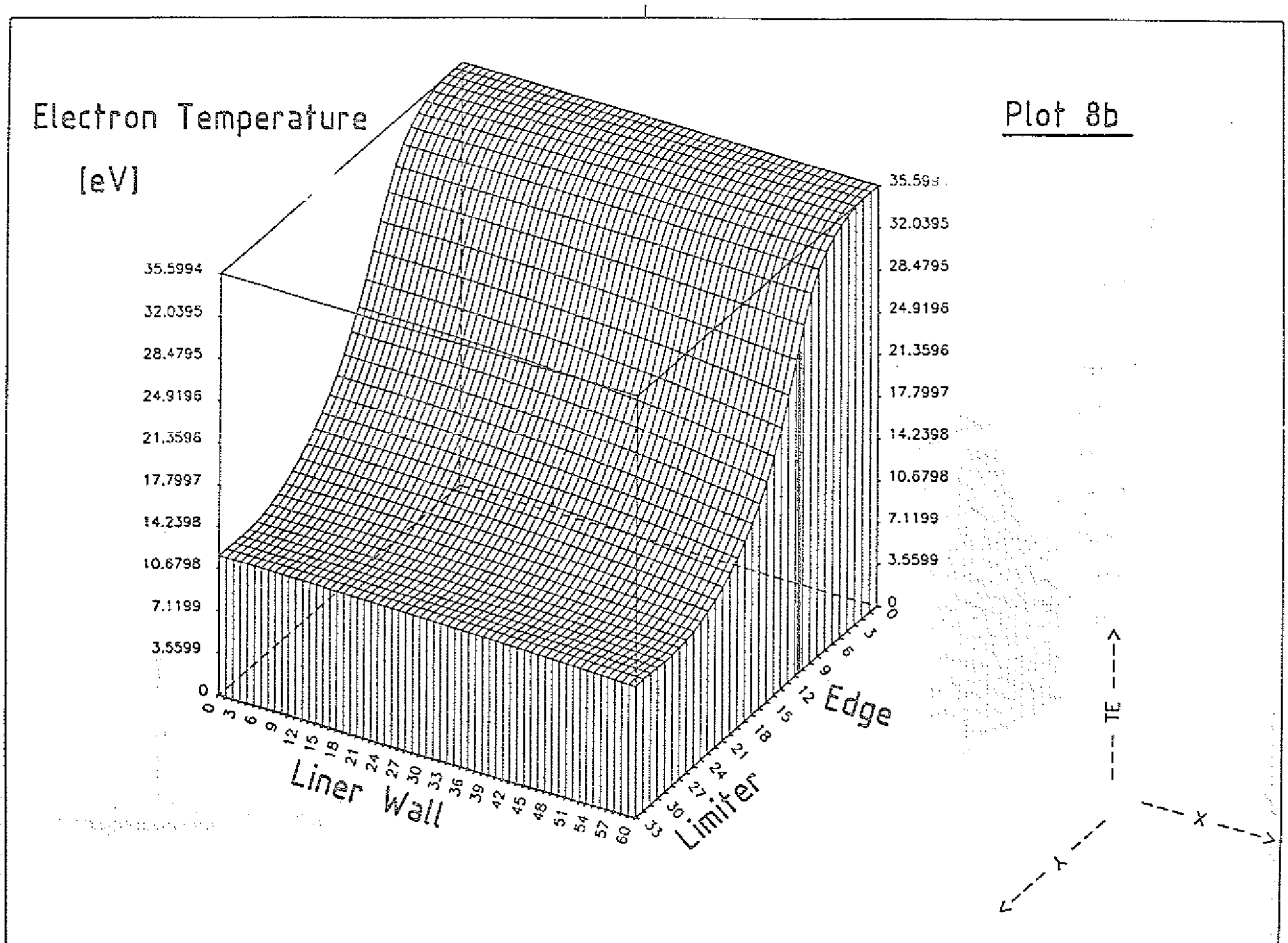

Electron Temperature
[eV]
Plot 8b
35.5994
32.0395
28.4795
24.9196
21.3596
17.7997
14.2398
10.6798
7.1199
3.5599
0
Liner Wall
Edge
Limiter
TE
X
Y

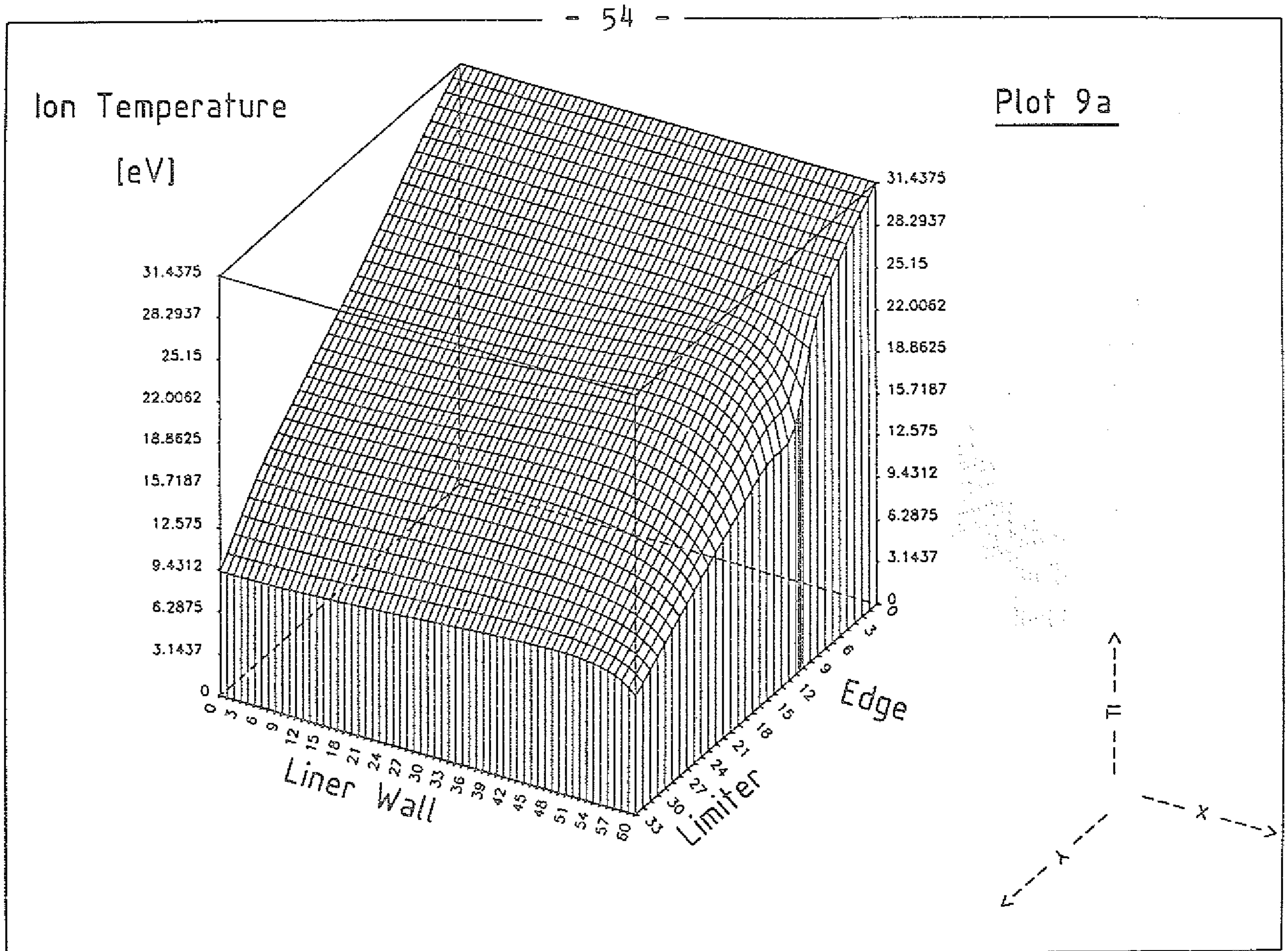
Ion Temperature
[eV]
Plot 9a
31.4375
28.2937
25.15
22.0062
18.8625
15.7187
12.575
9.4312
6.2875
3.1437
0
Liner Wall
Limiter
Edge
T
x
y

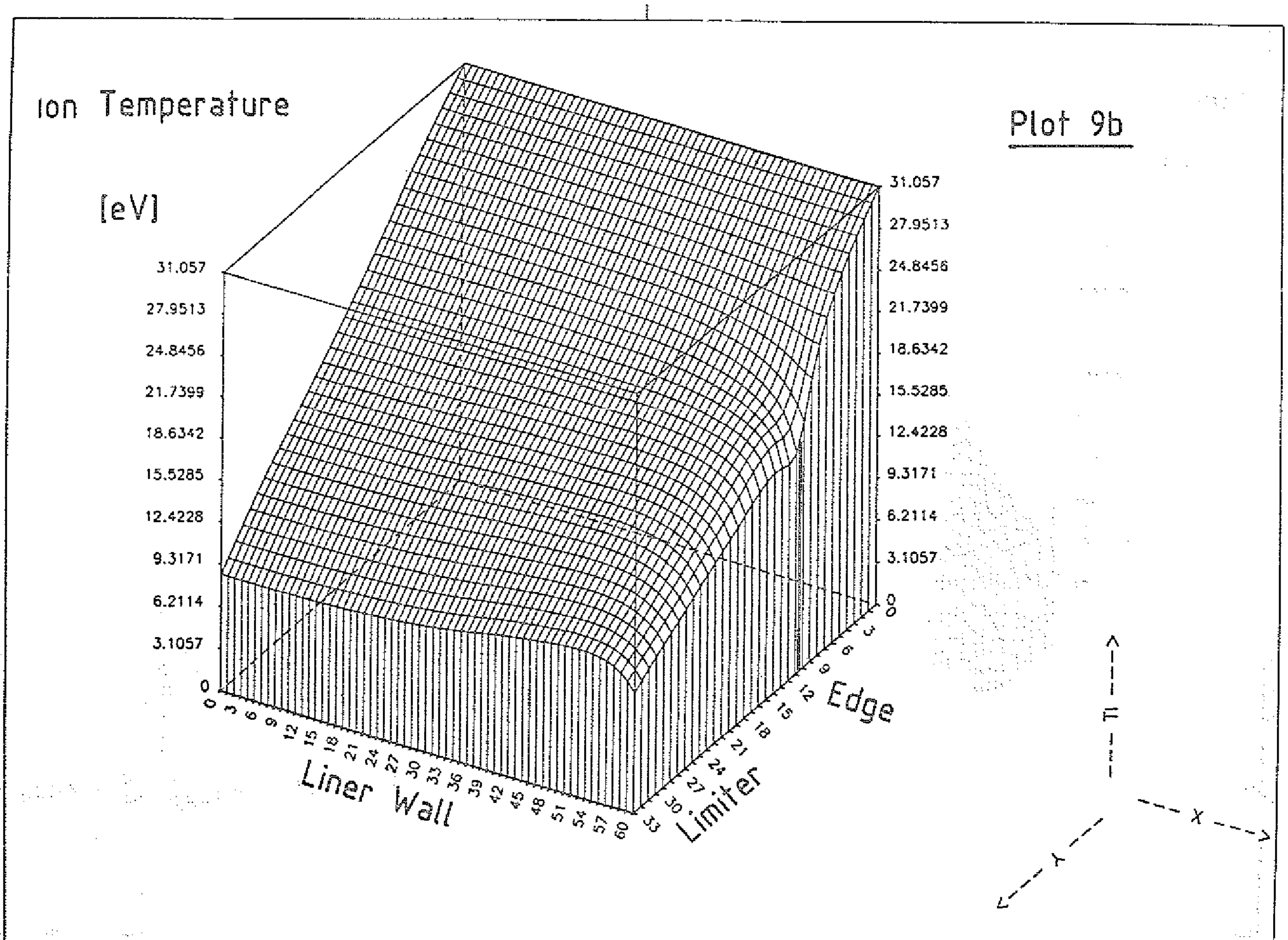
Ion Temperature
[eV]
Plot 9b
31.057
27.9513
24.8456
21.7399
18.6342
15.5285
12.4228
9.3171
6.2114
3.1057
0
Liner Wall
Limiter
Edge
T
x
y

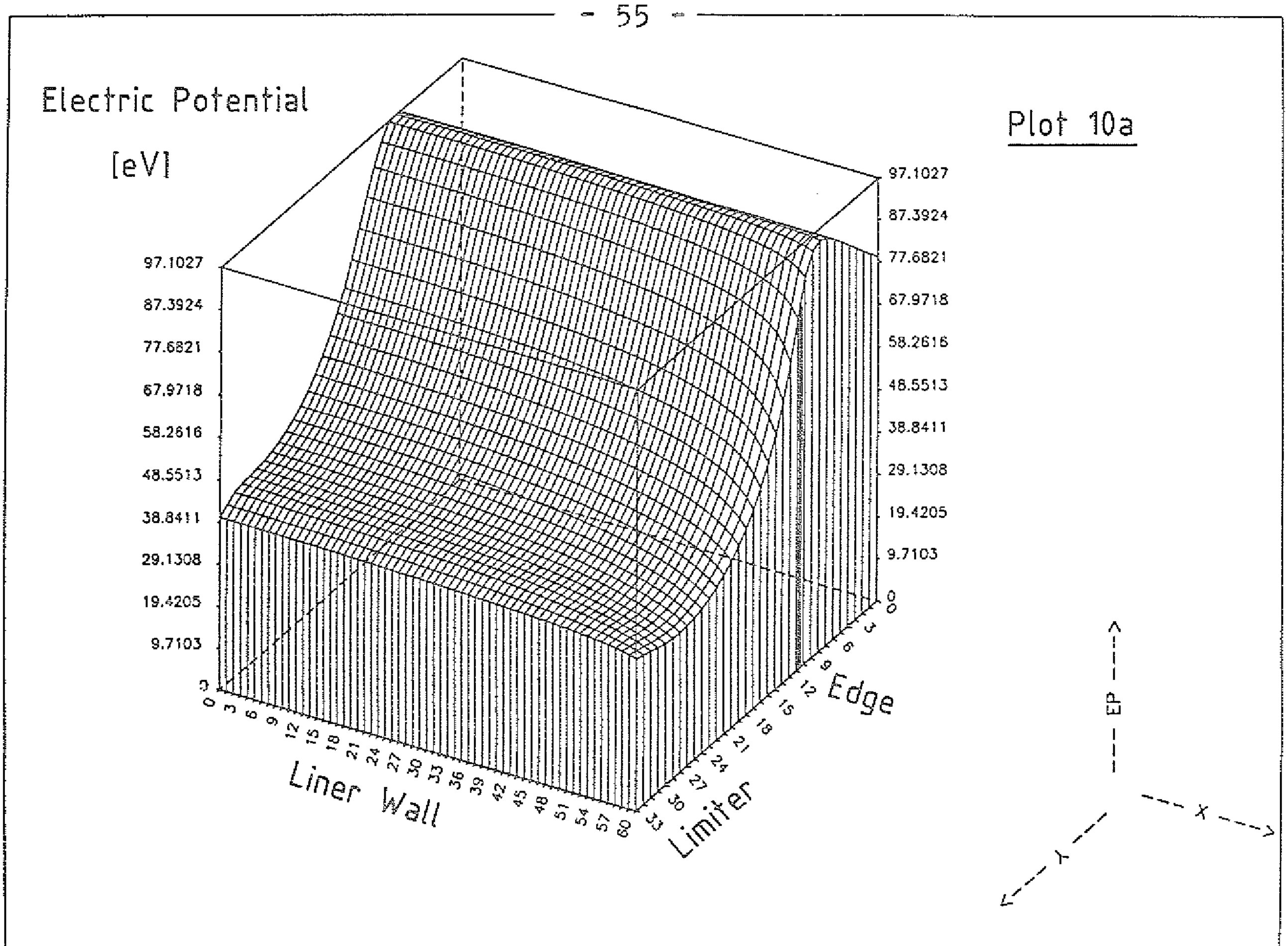
Electric Potential
[eV]
Plot 10a
97.1027
87.3924
77.6821
67.9718
58.2616
48.5513
38.8411
29.1308
19.4205
9.7103
0
Liner Wall
Limiter
Edge
EP
X
Y

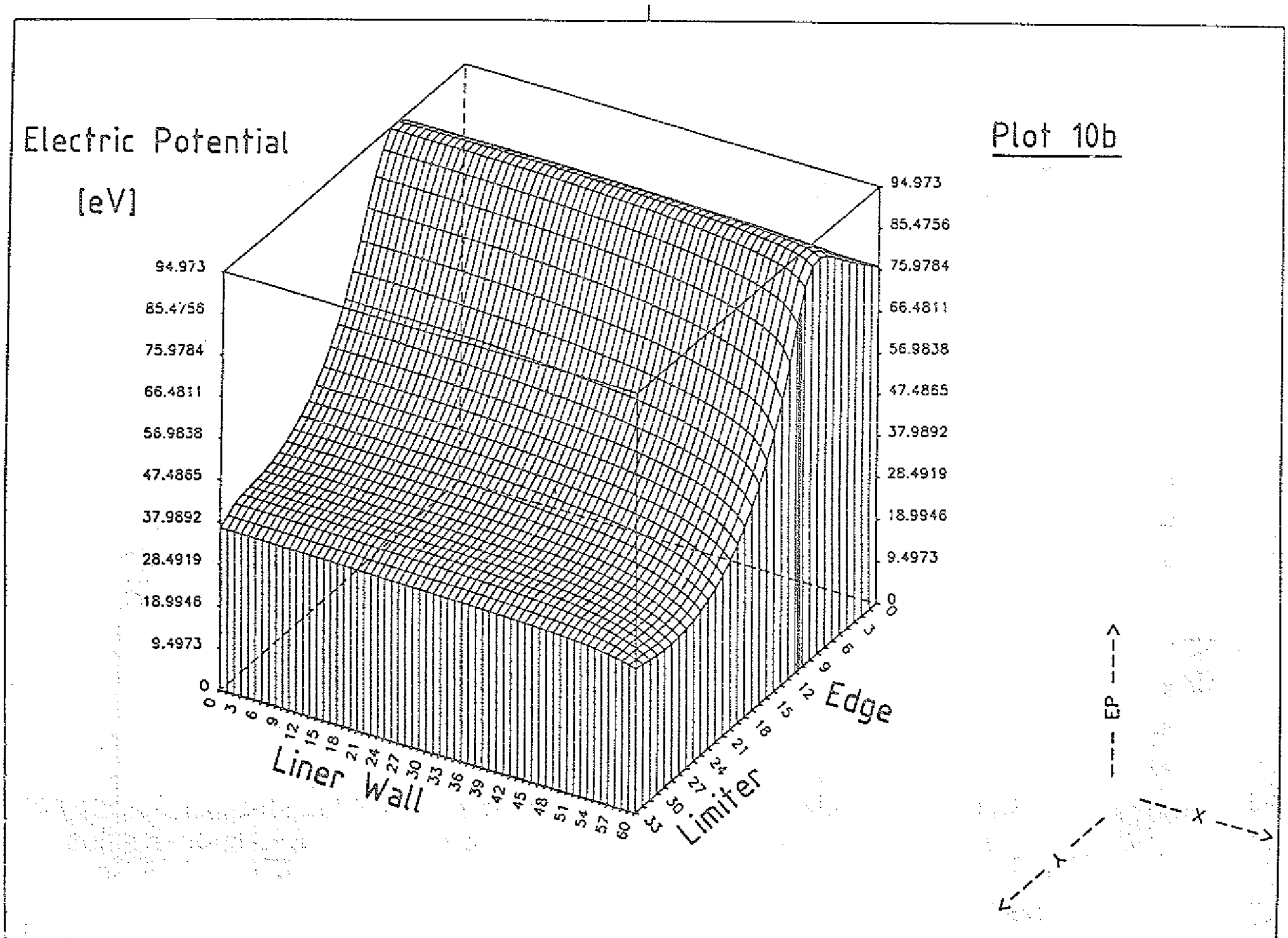
Electric Potential
[eV]
Plot 10b
94.973
85.4756
75.9784
66.4811
56.9838
47.4865
37.9892
28.4919
18.9946
9.4973
0
Liner Wall
Limiter
Edge
EP
X
Y

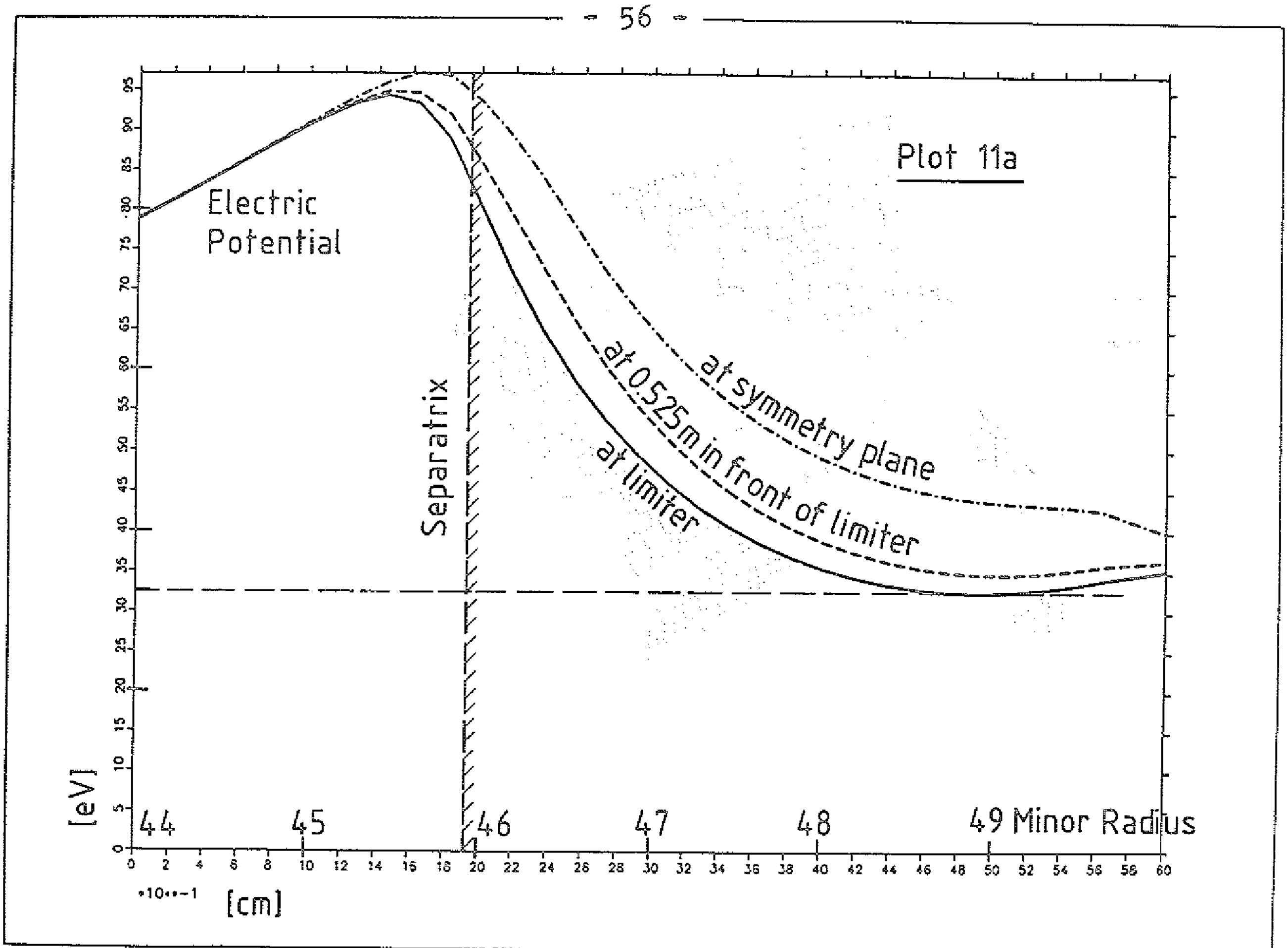
Plot 11a
Electric
Potential
Separatrix
at symmetry plane
at 0.525m in front of limiter
at limiter
[eV]
44
45
46
47
48
49 Minor Radius
*10**-1
[cm]

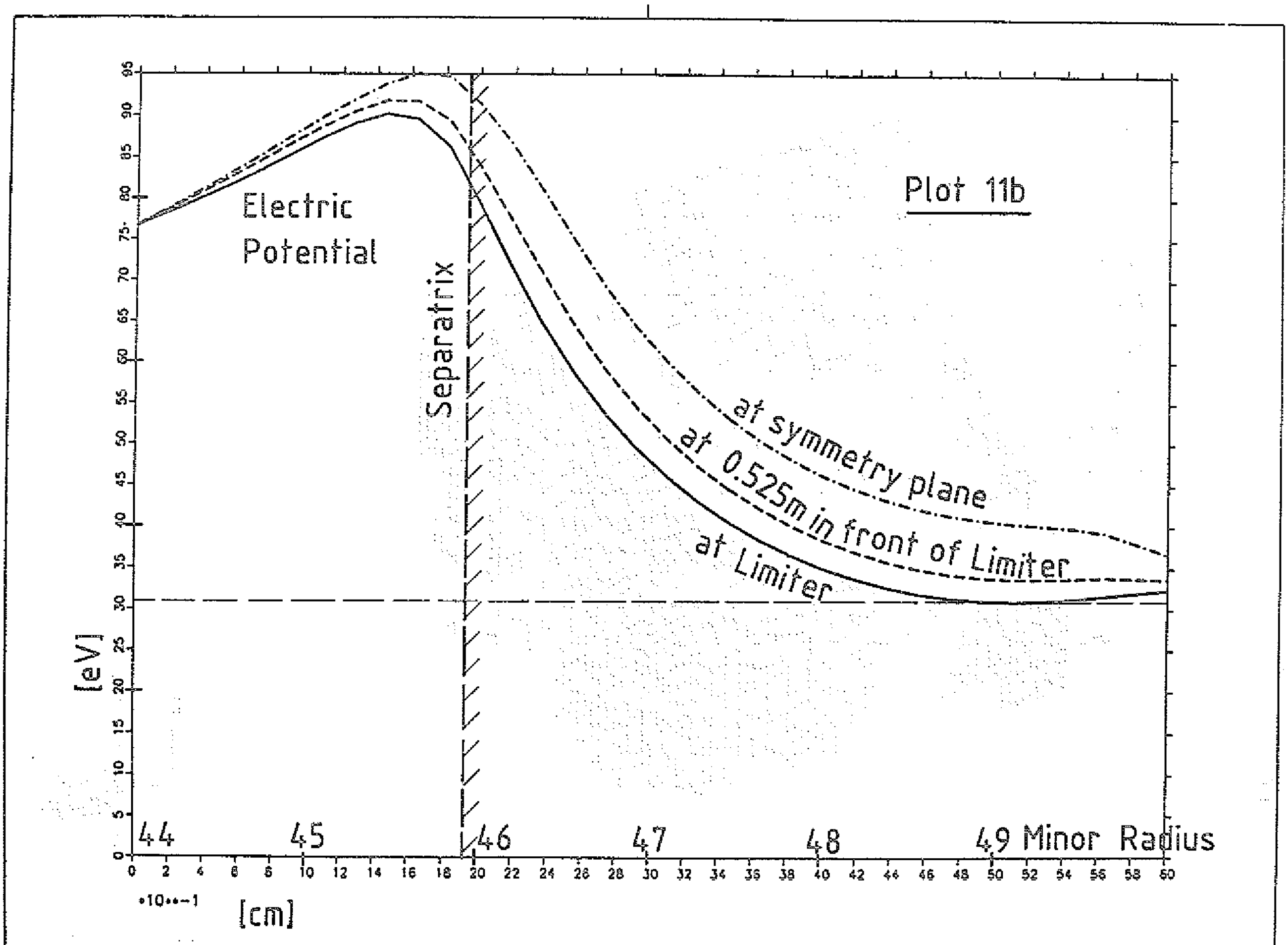
Plot 11b
Electric
Potential
Separatrix
at symmetry plane
at 0.525m in front of Limiter
at Limiter
[eV]
44
45
46
47
48
49 Minor Radius
*10**-1
[cm]

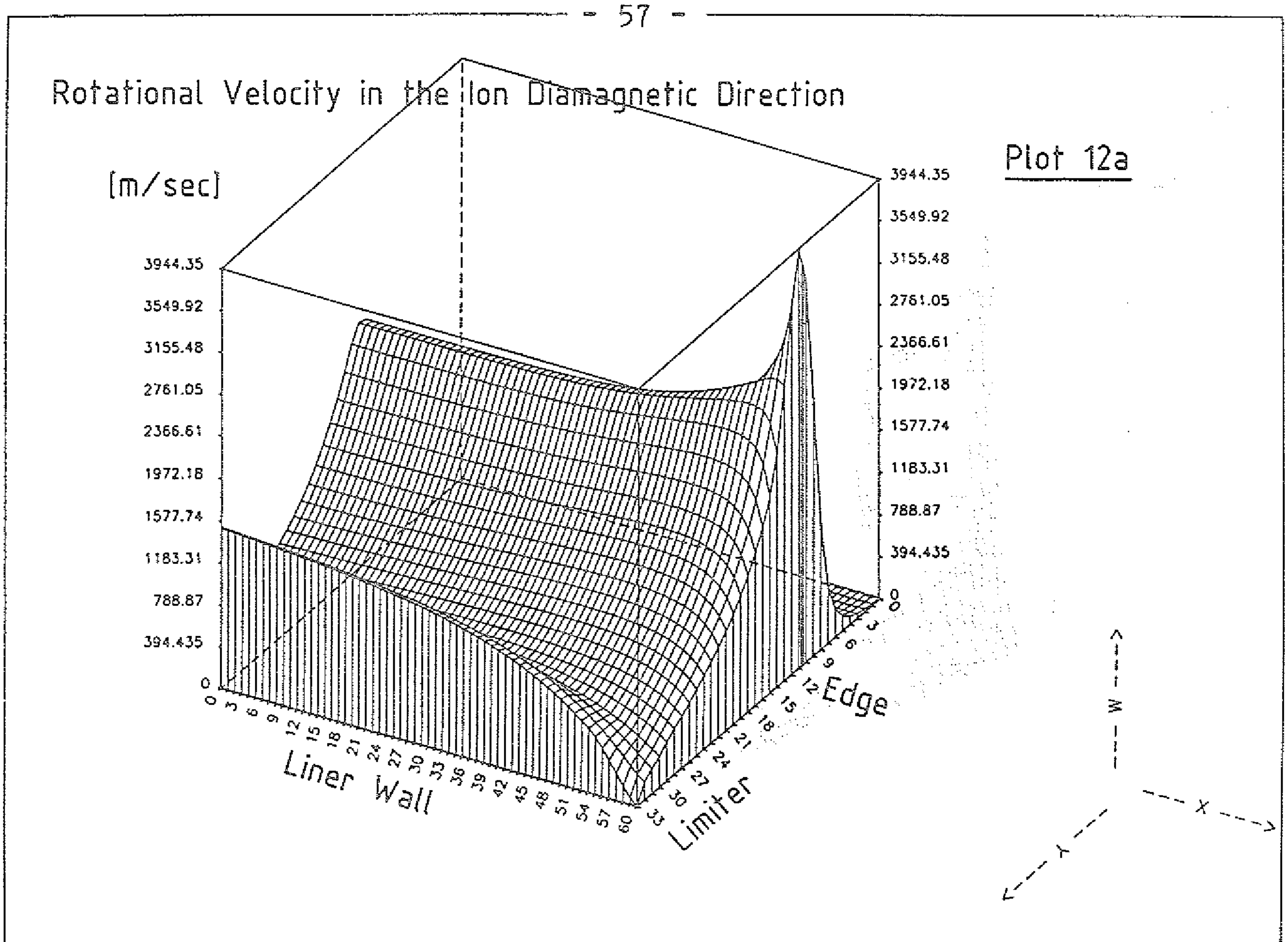
Rotational Velocity in the Ion Diamagnetic Direction
Plot 12a
[m/sec]
3944.35
3549.92
3155.48
2761.05
2366.61
1972.18
1577.74
1183.31
788.87
394.435
0
Liner Wall
Edge
Limiter
W
X
Y

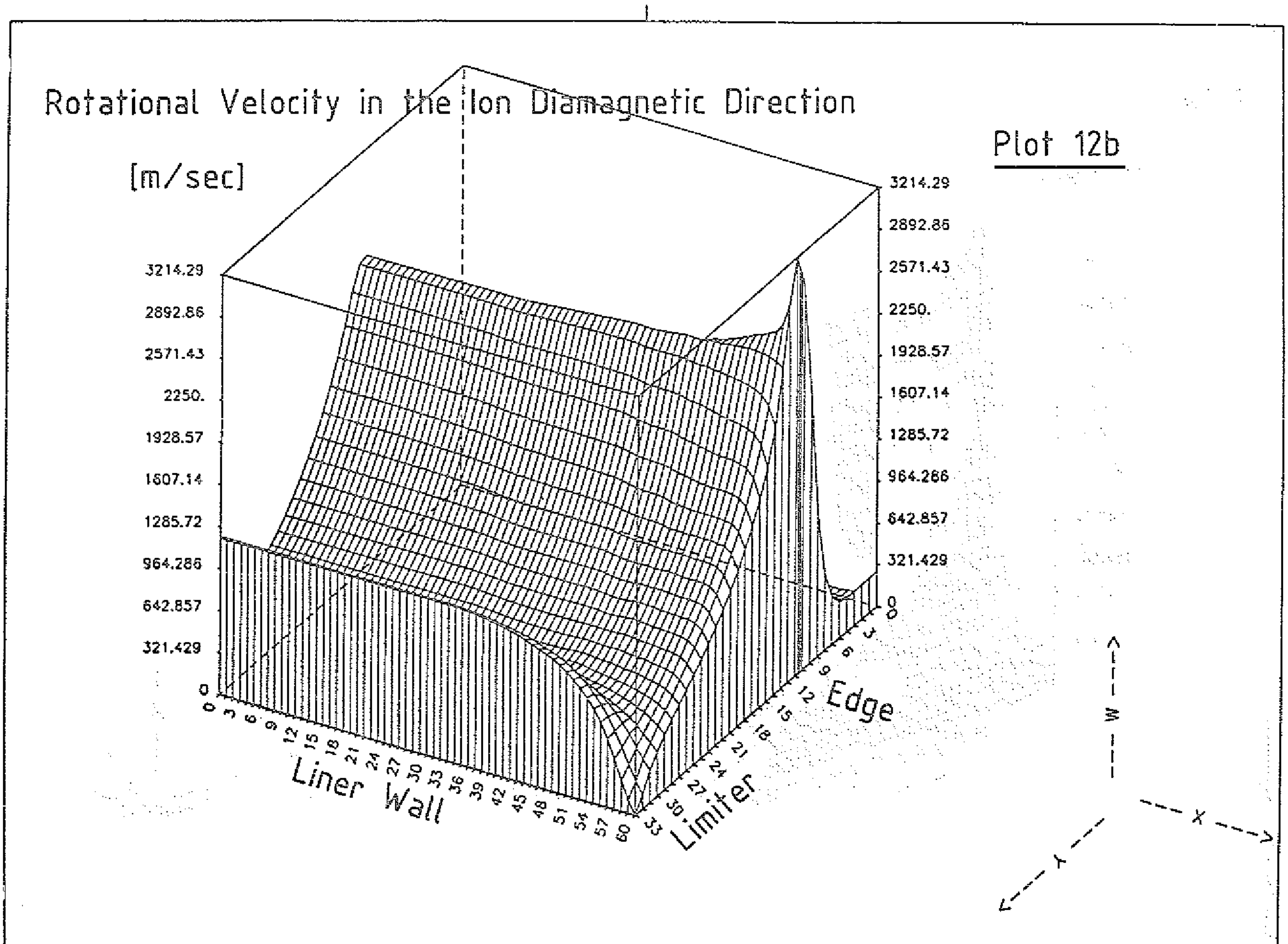
Rotational Velocity in the Ion Diamagnetic Direction
Plot 12b
[m/sec]
3214.29
2892.86
2571.43
2250.
1928.57
1607.14
1285.72
964.286
642.857
321.429
0
Liner Wall
Edge
Limiter
W
X
Y

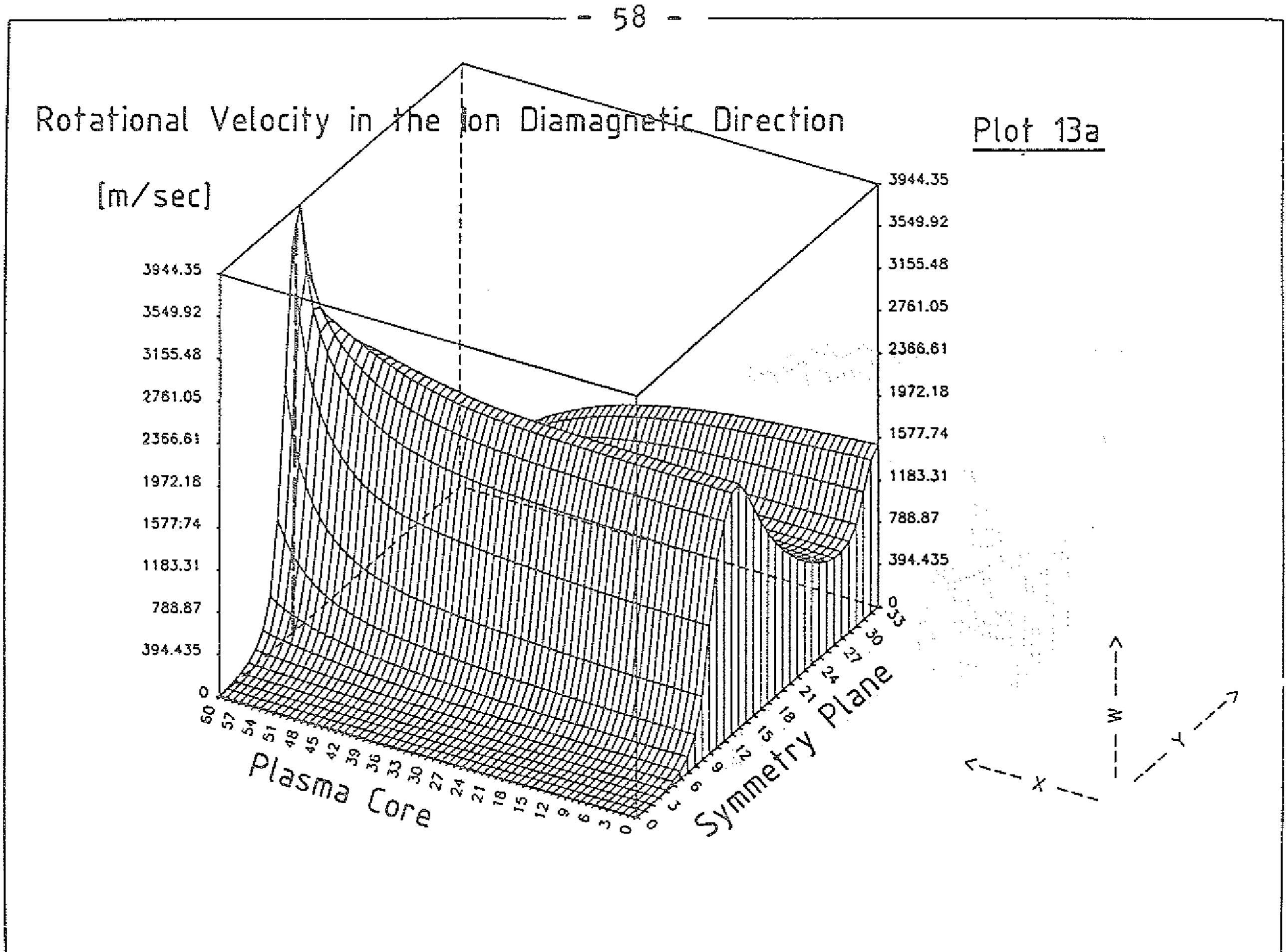
Rotational Velocity in the Ion Diamagnetic Direction
Plot 13a
[m/sec]
3944.35
3549.92
3155.48
2761.05
2366.61
1972.18
1577.74
1183.31
788.87
394.435
0
Plasma Core
Symmetry Plane
W
Y
X

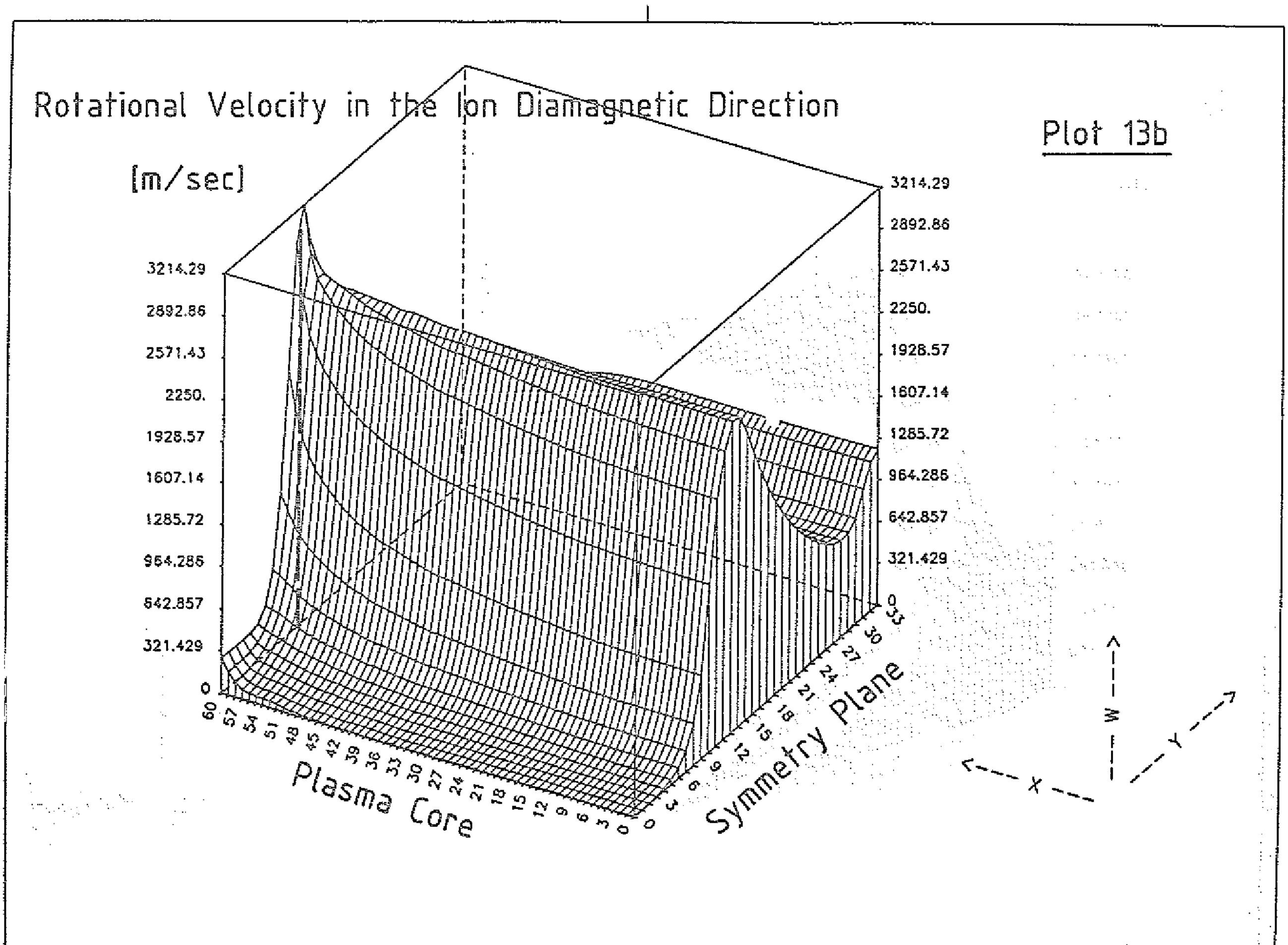
Rotational Velocity in the Ion Diamagnetic Direction
Plot 13b
[m/sec]
3214.29
2892.86
2571.43
2250.
1928.57
1607.14
1285.72
964.286
642.857
321.429
0
Plasma Core
Symmetry Plane
W
Y
X

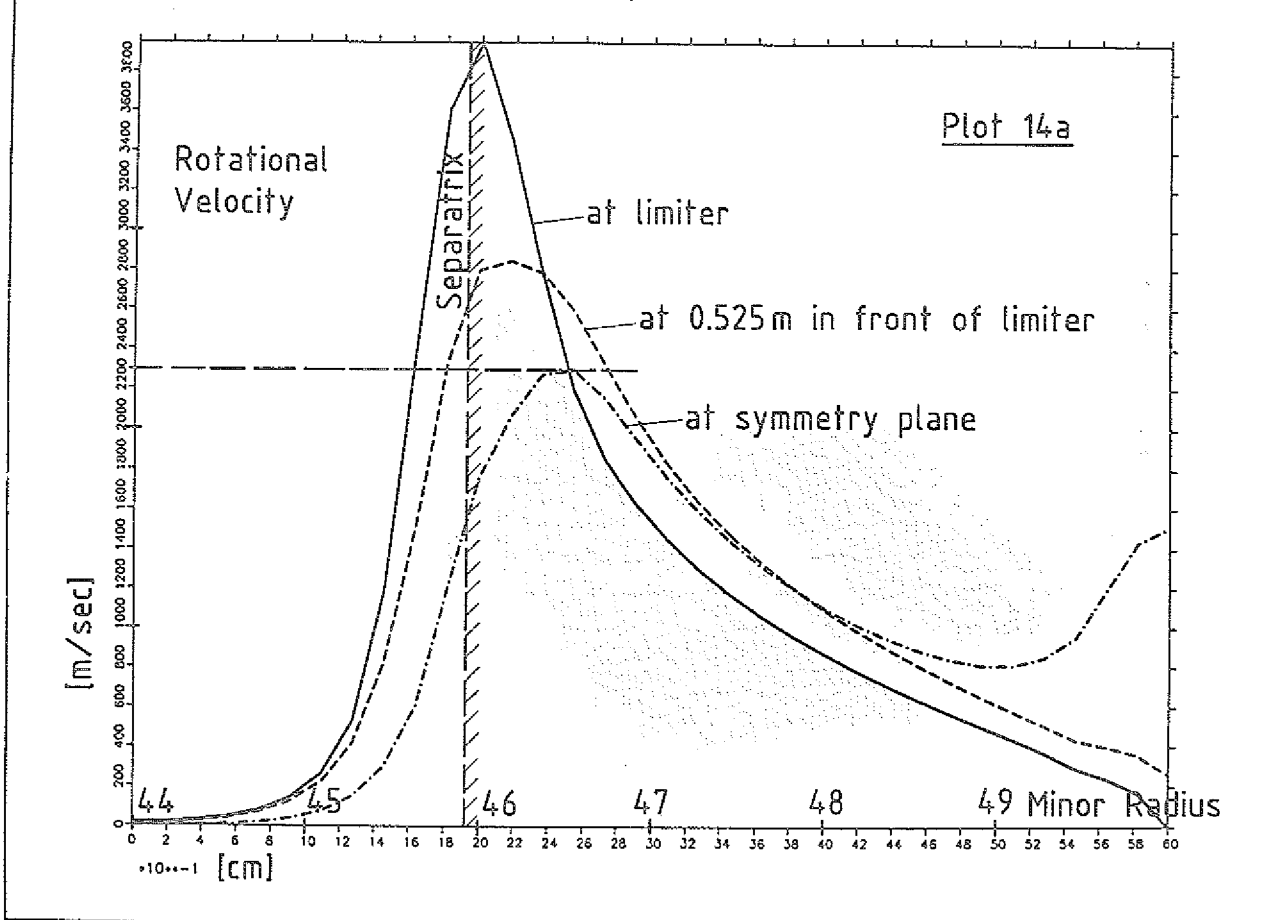
Plot 14a
Rotational Velocity
[m/sec]
at limiter
at 0.525m in front of limiter
at symmetry plane
Separatrix
44
45
46
47
48
49 Minor Radius
*10**-1 [cm]

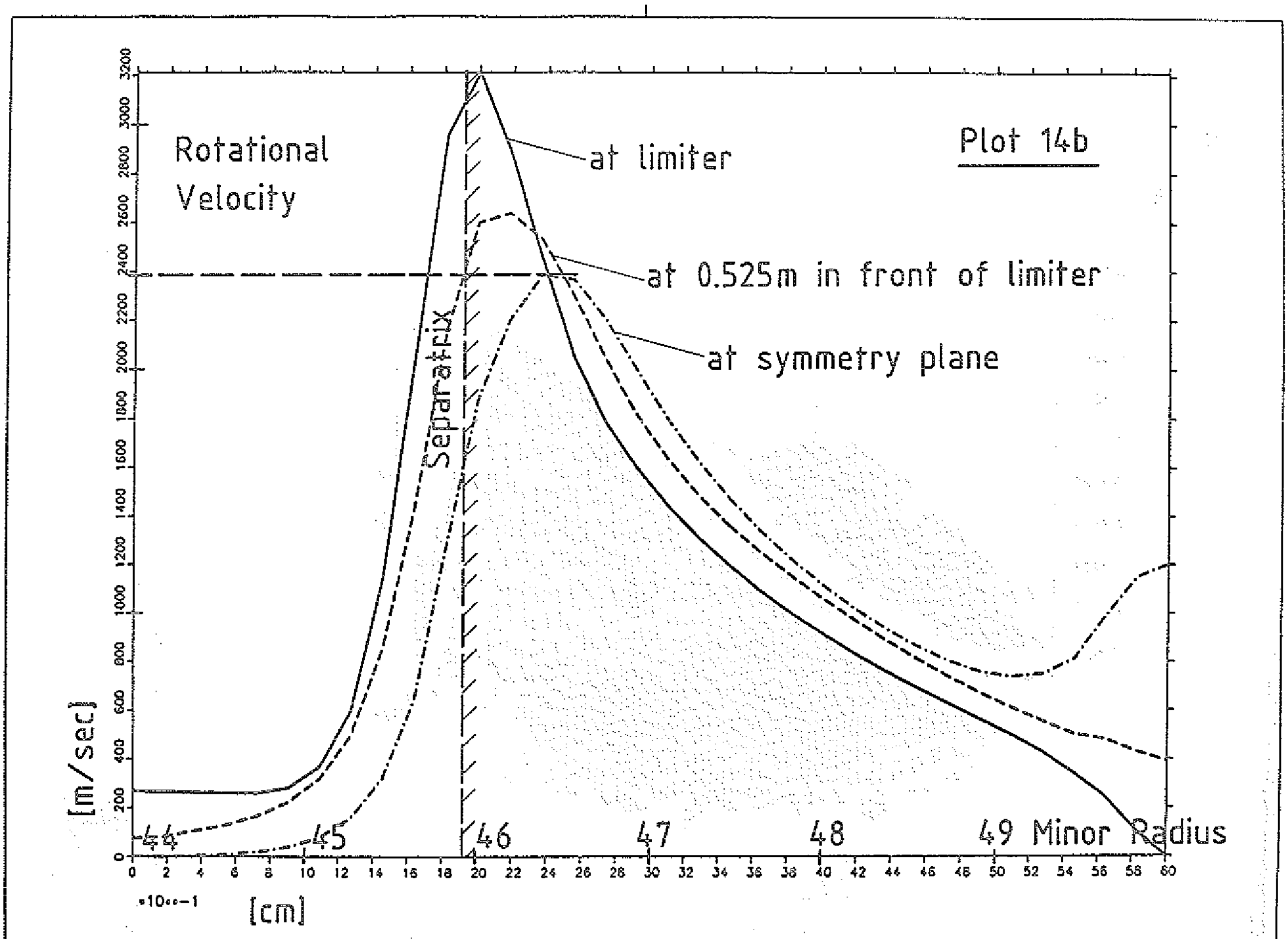
Plot 14b
Rotational Velocity
[m/sec]
at limiter
at 0.525m in front of limiter
at symmetry plane
Separatrix
44
45
46
47
48
49 Minor Radius
*10**-1 [cm]

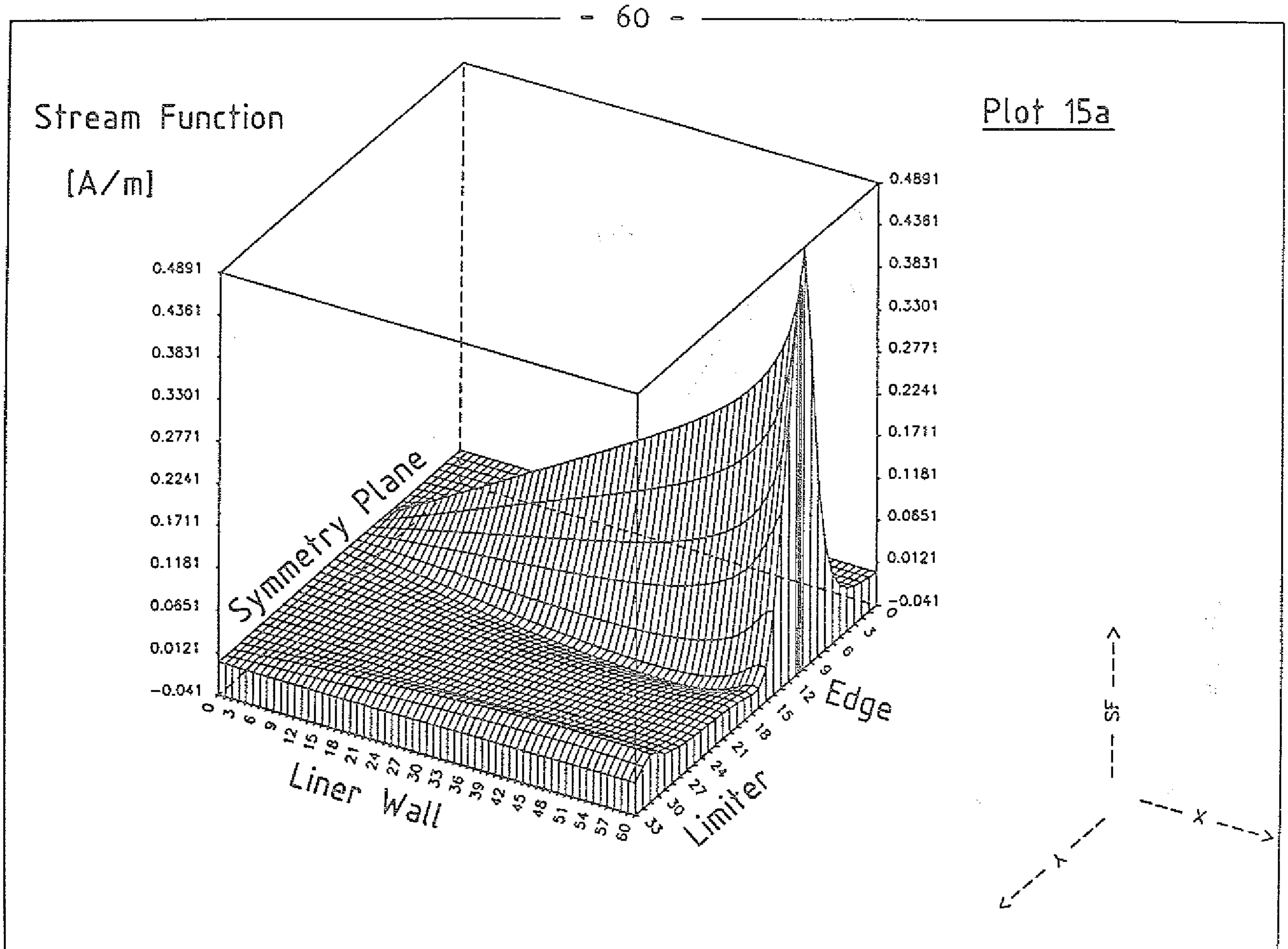
Stream Function
[A/m]
Plot 15a
Symmetry Plane
Liner Wall
Edge
Limiter
SF
X
Y

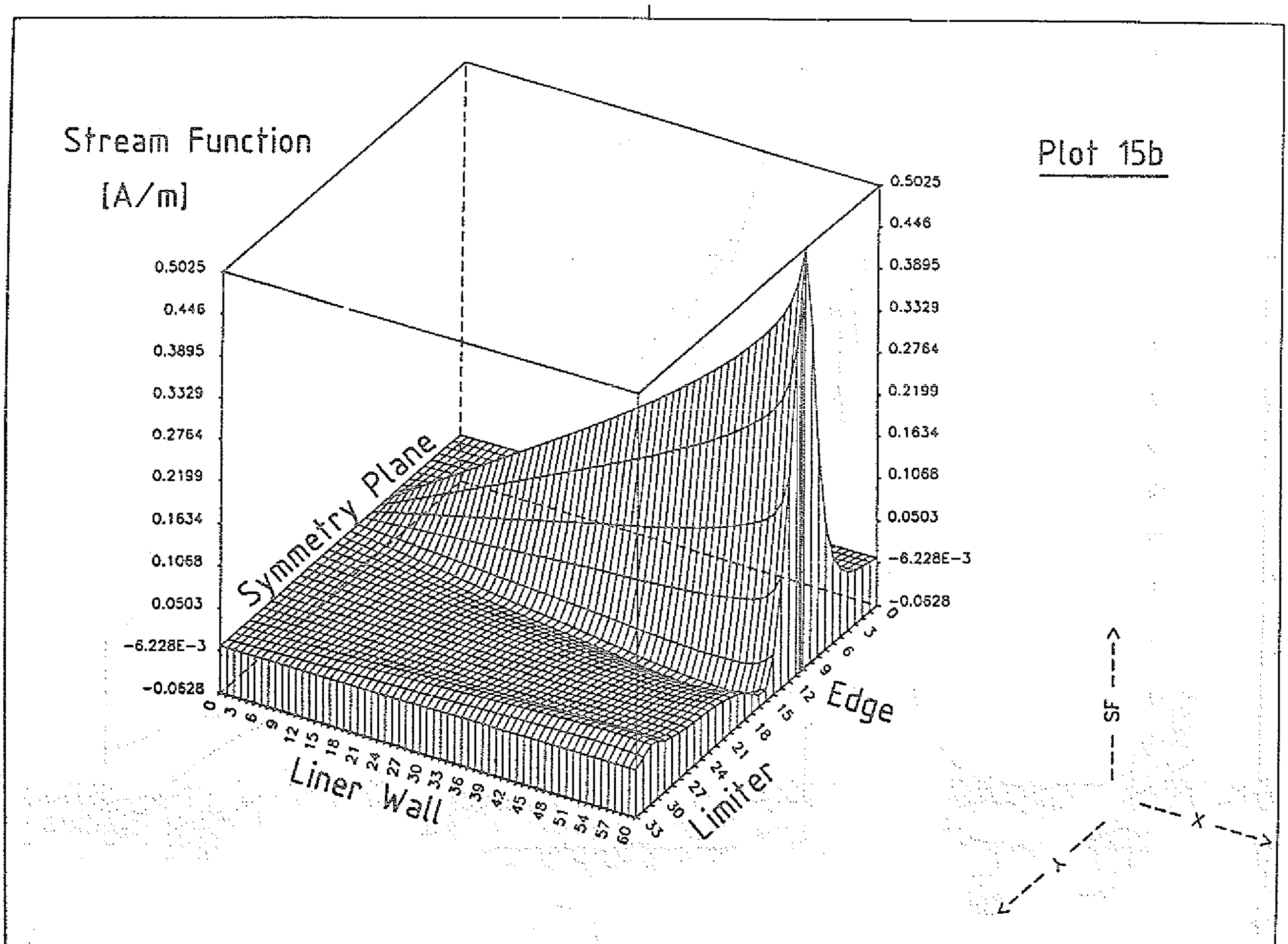
Stream Function
[A/m]
Plot 15b
Symmetry Plane
Liner Wall
Edge
Limiter
SF
X
Y

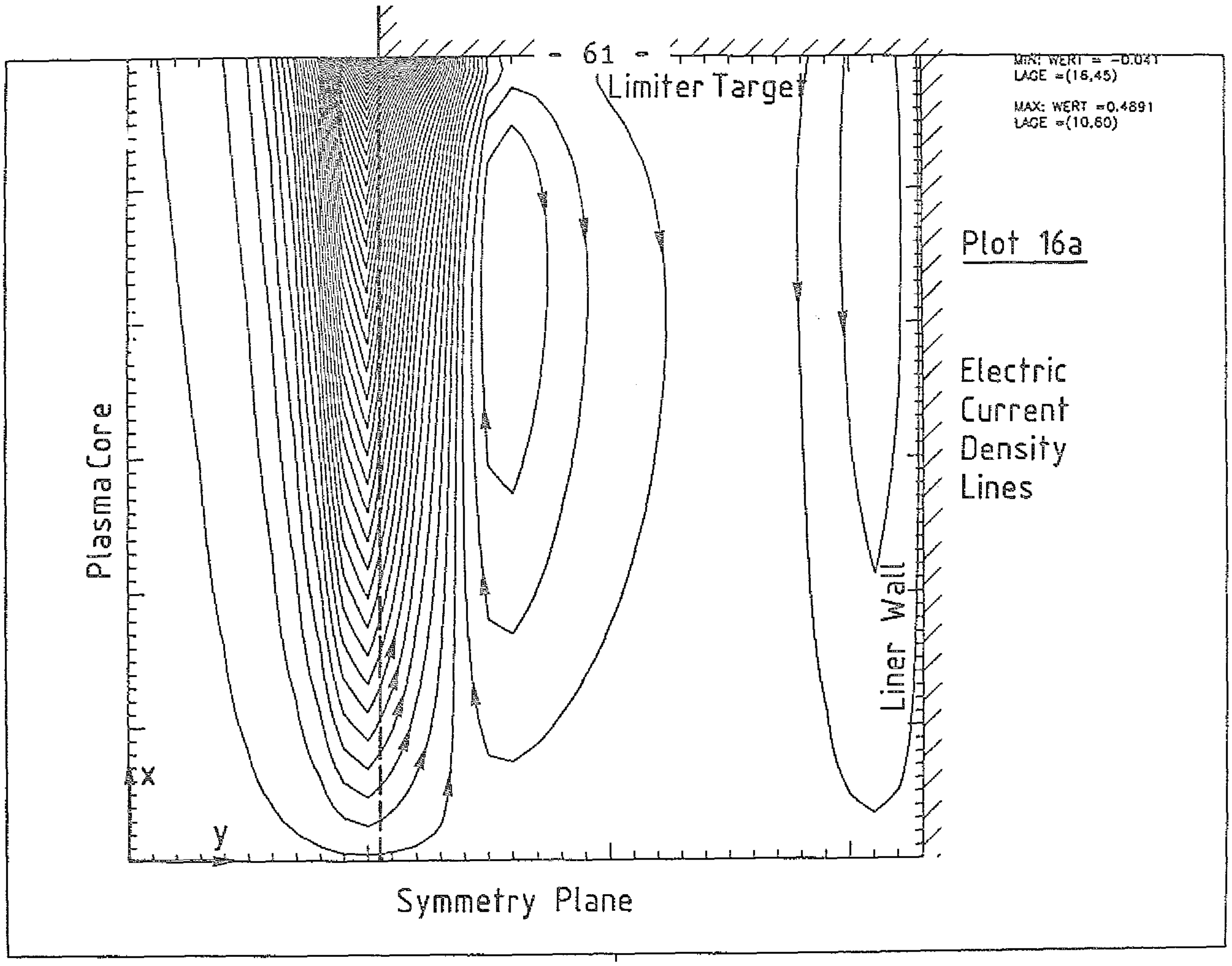
Limiter Target
MIN: WERT = -0.041
LAGE =(16,45)
MAX: WERT =0.4891
LAGE =(10,60)
Plot 16a
Electric
Current
Density
Lines
Plasma Core
Liner Wall
x
y
Symmetry Plane

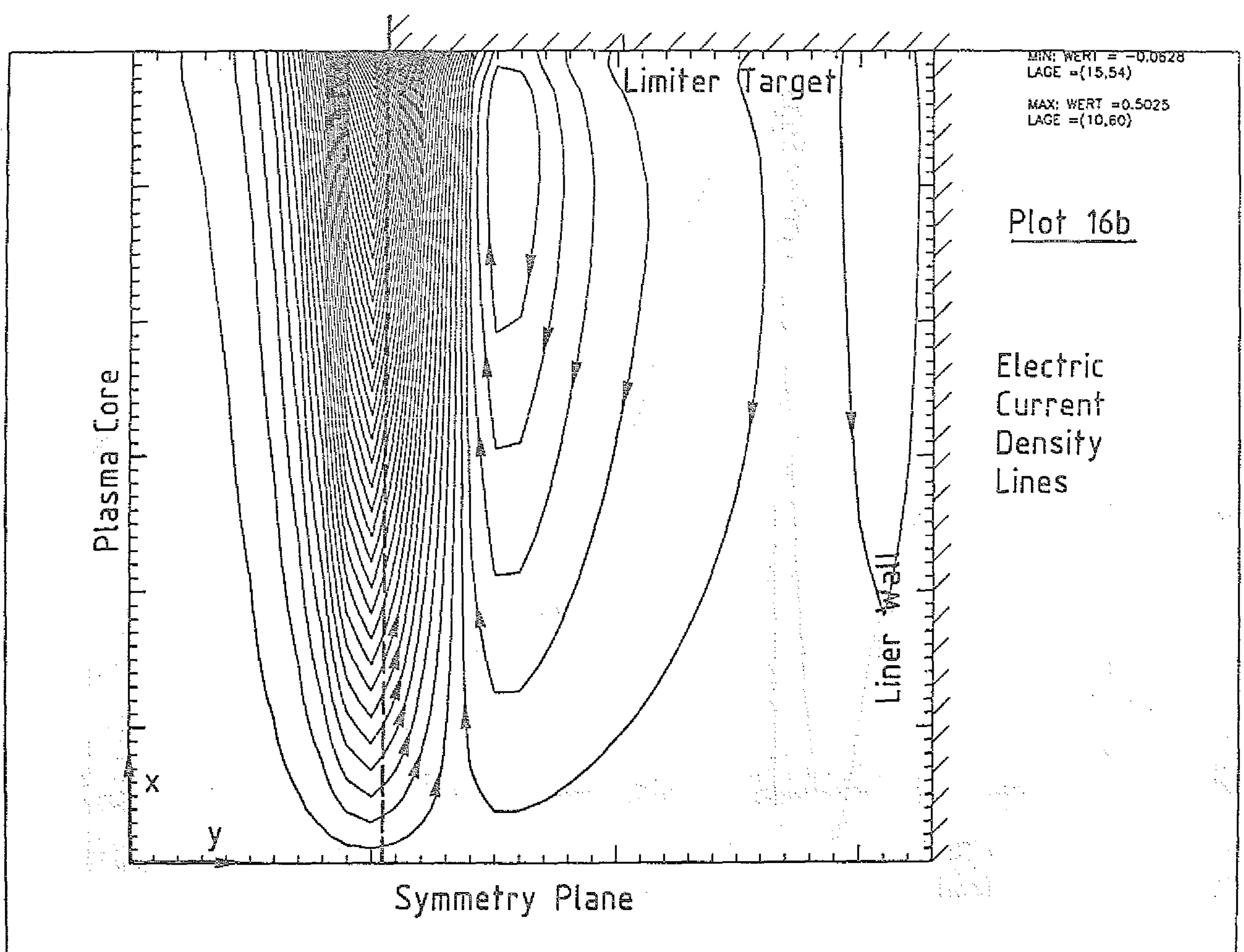
Limiter Target
MIN: WERT = -0.0628
LAGE =(15,54)
MAX: WERT =0.5025
LAGE =(10,60)
Plot 16b
Electric
Current
Density
Lines
Plasma Core
Liner Wall
x
y
Symmetry Plane

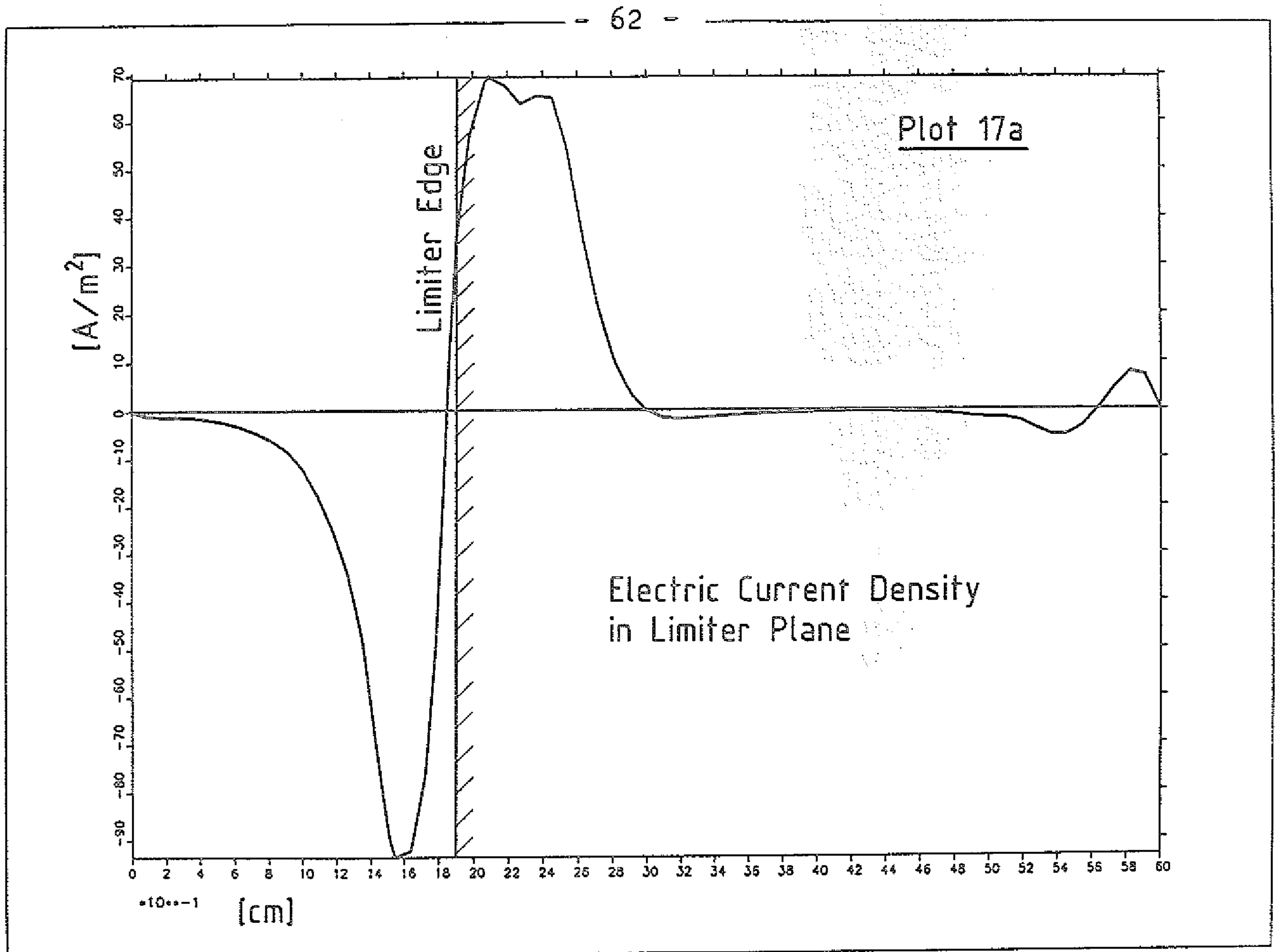
Plot 17a
Limiter Edge
[A/m²]
Electric Current Density
in Limiter Plane
*10**-1
[cm]

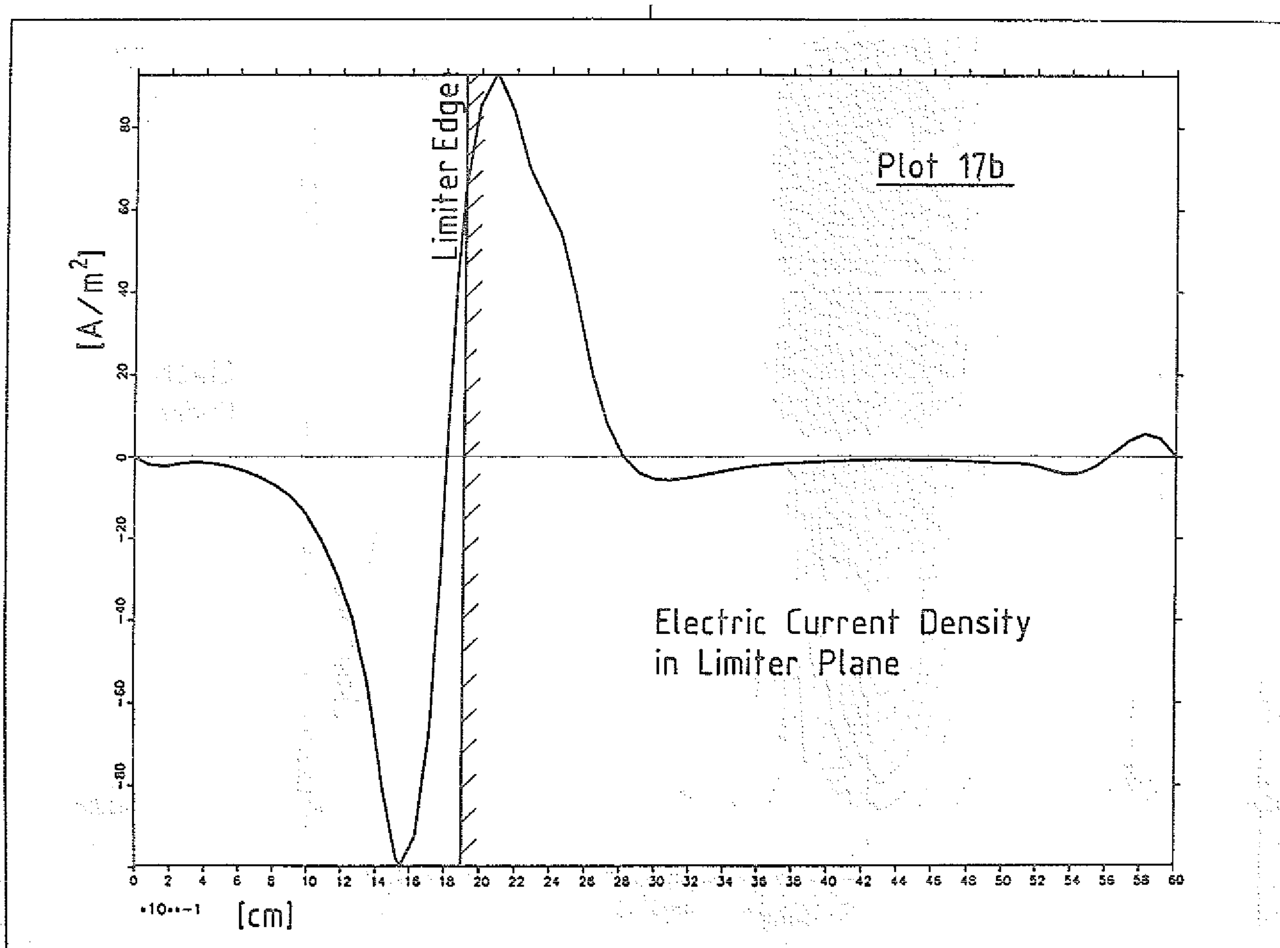
Plot 17b
Limiter Edge
[A/m²]
Electric Current Density
in Limiter Plane
*10**-1
[cm]

APPENDIX: Review of Boundary Conditions at Limiter

in the following we want to review our present knowledge on the origin of the boundary conditions (46), (47) and (48) at the limiter. We derive approximate formulae for the characteristic factors δ_s, δ_e, δ_i on the basis of certain simplifying assumptions for the electron and ion distribution functions at the transition from the presheath to the collisionfree Langmuir sheath. These distributions are commonly adopted, but the critical discussion will show that at least the ion distribution must be considerably modified in order to fulfill Bohm's criterion. The precise shape of the ion distribution could only result from a detailed self-consistent kinetic theory for the distribution functions and the electrostatic potential in the presheath, which is still lacking. We use the index p (= plasma) for denoting the left edge of the Langmuir sheath facing the scrape-off plasma, and the index w (= wall) for denoting the right edge facing the limiter surface. Hence for the sheath coordinate we have $x_p \leqslant x \leqslant x_w$, and the potential drop across the sheath is $\Delta\phi = \phi_p - \phi_w \geqslant 0$. Quasineutrality in the scape-off plasma means $n_{ep} = n_{ip} = n$.

1) Behaviour of the Electrons

The electron distribution function $f_{ep} = f_e(u_p)$ at the sheath entrance is assumed to be a Maxwellian with the tip of the negative tail cut off, corresponding to those electrons which moved fast enough to climb the potential hill and were absorbed at the limiter. With the electron thermal velocity $v_{Te} = \sqrt{2T_e/m_e}$ we have (fig. 9):

$$f_{ep} = \begin{cases} \dfrac{N_e}{\sqrt{\pi}\, v_{Te}}\, e^{-u_p^2/v_{Te}^2} & \text{for } u_p \geqslant -\sqrt{\dfrac{2e\Delta\phi}{m_e}} \\ 0 & \text{for } u_p < -\sqrt{\dfrac{2e\Delta\phi}{m_e}} \end{cases} \tag{A1}$$

From f_{ep} we obtain the electron density:

$$n_{ep} = \int_{-\sqrt{2e\Delta\phi/m_e}}^{\infty} f_{ep}\, du_p = \frac{N_e}{2}\left(1 + \operatorname{erf}\sqrt{\frac{e\Delta\phi}{T_e}}\right) \tag{A2}$$

Fig. 9: Assumed Electron Distribution Function on Entering the Langmuir Sheath

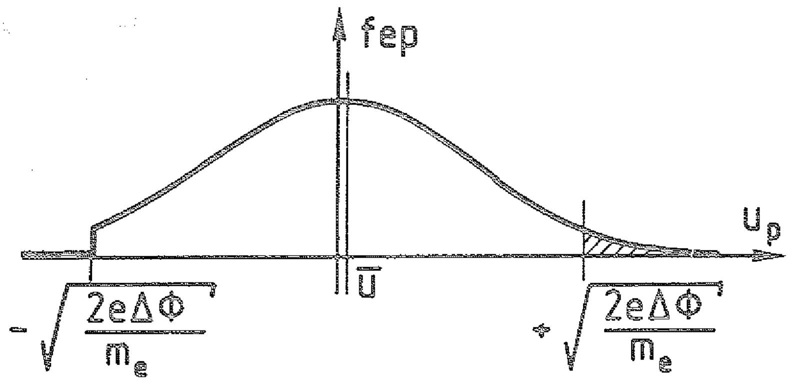

Anticipating $e\Delta\phi/T_e \approx 3$ we get $n_{ep} \approx 0.993\ N_e$, so that we may identify n_{ep} with N_e.
We use energy conservation $\frac{1}{2} m_e u_p^2 = \frac{1}{2} m_e u_w^2 + e\Delta\phi$ for transforming the electron flux density:

$$\Gamma_e^{\parallel} = \int_{-\sqrt{2e\Delta\phi/m_e}}^{\infty} f_{ep}\ u_p\ du_p = \int_{+\sqrt{2e\Delta\phi/m_e}}^{\infty} f_{ep}\ u_p\ du_p = \int_0^{\infty} f_{ew}\ u_w\ du_w$$

$$= \int_0^{\infty} \frac{N_e}{\sqrt{\pi}\ v_{Te}}\ e^{-\left(\frac{u_w^2}{v_{Te}^2} + \frac{e\Delta\phi}{T_e}\right)}\ u_w\ du_w$$

$$\Gamma_e^{\parallel} = \frac{N_e v_{Te}}{2\sqrt{\pi}}\ e^{-\frac{e\Delta\phi}{T_e}} \approx n_{ep}\bar{u} = nu_x \tag{A3}$$

The mean velocity $\bar{u}$ is if course identical with the electron fluid velocity u_x in front of the limiter, so that

$$u_x = \frac{v_{Te}}{2\sqrt{\pi}}\, e^{-\frac{e\Delta\phi}{T_e}} \tag{A4}$$

The perpendicular velocities $\vec{u}_\perp = u_2\ \vec{e}_y + u_3\ \vec{e}_z$ and the total distribution functions

$$F_{ep,w} = \frac{1}{\pi\, v_{Te}^2}\, e^{-\vec{u}_\perp^{\,2}/v_{Te}^2}\, f_{ep,w} \tag{A5}$$

must be taken into account for calculating the electron energy flux density:

$$Q_e^{\parallel} = \int_{-\sqrt{2e\Delta\phi/m_e}}^{\infty} du_p\, u_p \int\!\!\int_{-\infty}^{+\infty} d^2\,\vec{u}_\perp\, \frac{m_e}{2}\,(u_p^2 + \vec{u}_\perp^{\,2})\, F_{ep}$$

$$= \int_0^{\infty} du_w\, u_w \int\!\!\int_{-\infty}^{+\infty} d^2\,\vec{u}_\perp \left[\frac{m_e}{2}\,(u_w^2 + \vec{u}_\perp^{\,2}) + e\Delta\phi\right] F_{ew}$$

$$Q_e^{\parallel} = (2T_e + e\Delta\phi)\,\Gamma_e^{\parallel} = \left(2 + \frac{e\Delta\phi}{T_e}\right) T_e\, nu_x \tag{A6}$$

Hence the calculation of

$$\delta_e = 2 + \frac{e\Delta\phi}{T_e} \tag{A7}$$

requires first the knowledge of the potential drop.

2) Behaviour of the Ions

The ion distribution function $f_{ip} = f_i(v_p)$ is assumed to be a shifted Maxwellian with the whole negative tail cut off, because all ions are absorbed at the limiter. With the ion thermal velocity $v_{Ti} = \sqrt{2T_i/m_i}$ we have (fig. 10):

$$f_{ip} = \begin{cases} \dfrac{N_i}{\sqrt{\pi}\, v_{Ti}}\, e^{-(v_p - v_s)^2/v_{Ti}^2} & \text{for } v_p \geqslant 0 \\ 0 & \text{for } v_p < 0 \end{cases} \tag{A8}$$

Defining a dimensionless shift velocity by the Mach number $M_i = v_s/v_{Ti}$ we obtain for the ion density:

$$n_{ip} = \int_0^{\infty} f_{ip}\, dv_p = \frac{N_i}{2}\,(1 + \mathrm{erf}\, M_i) \tag{A9}$$

Fig. 10: Assumed Ion Distribution Function on Entering the Langmuir Sheath

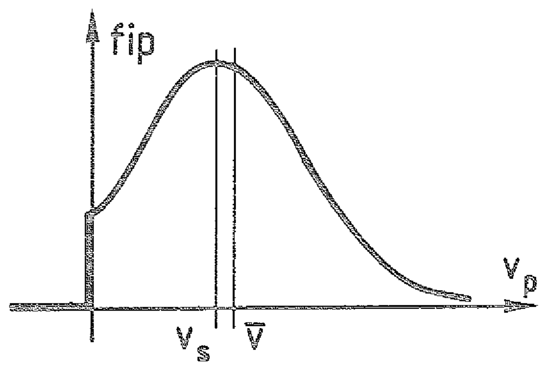

For $M_i = 1$ we get $n_{ip} = 0.92\ N_i$, so that n_{ip} may not be identified with N_i.

Integration of $f_{ip}\ v_p$ yields the ion flux density:

$$\Gamma_i^{\parallel} = \frac{N_i\ v_{Ti}}{2}\ [\ M_i\ (1 + \mathrm{erf}\ M_i) + \frac{e^{-M_i^2}}{\sqrt{\pi}}]$$

$$\Gamma_i^{\parallel} = n_{ip}\ v_s\ [1 + \frac{e^{-M_i^2}}{\sqrt{\pi}\ M_i\ (1+\mathrm{erf}\ M_i)}] = n_{ip}\ \bar{v} = nv_x \qquad \text{(A10)}$$

Hence the ion fluid velocity in front of the limiter reads

$$v_x = v_s\ [1 + \frac{e^{-M_i^2}}{\sqrt{\pi}\ M_i\ (1+\mathrm{erf}\ M_i)}] = v_{Ti}\ [M_i + \frac{e^{-M_i^2}}{\sqrt{\pi}\ (1+\mathrm{erf}\ M_i)}] \qquad \text{(A11)}$$

For $M_i = 1$ we get $v_x = 1.11\ v_s = 1.11\ v_{Ti}$. However, we don't know the value of M_i as yet. If $v_x = \delta_s\ c_s$ can be determined by Bohm's criterion, then it is possible to define M_i implicitly as a function of the temperature ratio T_i/T_e:

$$M_i + \frac{e^{-M_i^2}}{\sqrt{\pi}\ (1+\mathrm{erf}\ M_i)} = \delta_s \sqrt{\frac{1}{2}\ (1+\frac{T_e}{T_i})} \qquad \text{(A12)}$$

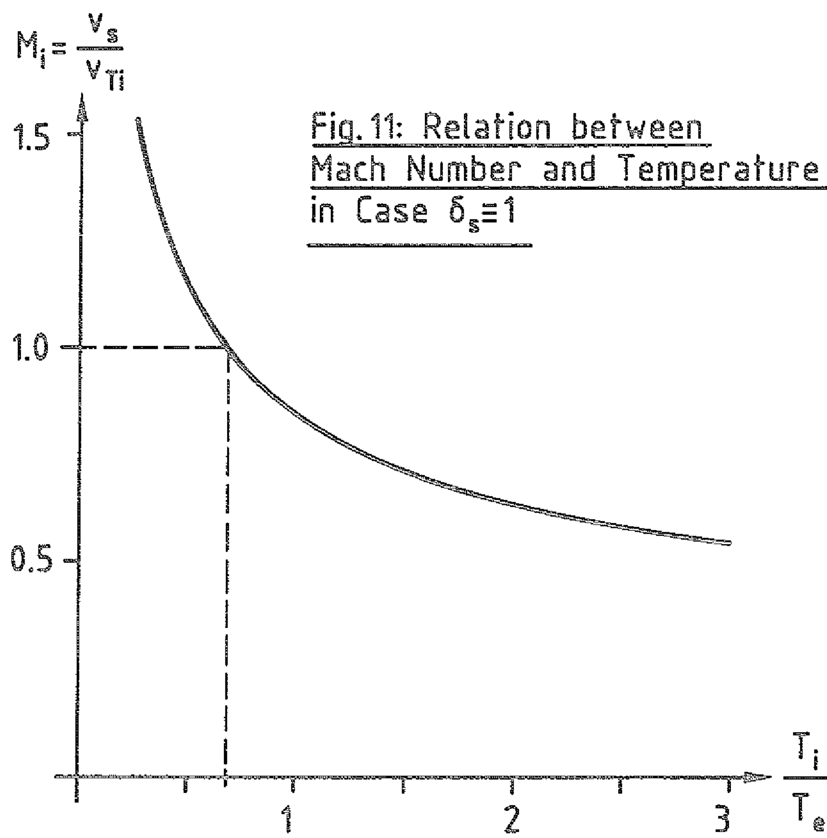

Fig. 11: Relation between Mach Number and Temperature Ratio in Case $\delta_s \equiv 1$

This relation is shown for the case $\delta_s \equiv 1$ in fig. 11. Now introducing a total distribution function F_{ip} similarly as for the electrons and performing the lengthy integrations we finally obtain the ion energy flux density:

$$Q_i^{\parallel} = \frac{m_i\ N_i\ v_{Ti}^3}{4}\left[(M_i^2 + \tfrac{5}{2})\ M_i\ (1+\mathrm{erf}\ M_i) + (M_i^2 + 2)\ \frac{e^{-M_i^2}}{\sqrt{\pi}}\right]$$

$$Q_i^{\parallel} = \frac{m_i\ v_{Ti}^2}{2}\ \Gamma_i^{\parallel}\ \frac{(M_i^2 + \frac{5}{2})\ M_i\ (1+\mathrm{erf}\ M_i) + (M_i^2 + 2)\ e^{-M_i^2}/\sqrt{\pi}}{M_i\ (1+\mathrm{erf}\ M_i) + e^{-M_i^2}\ \sqrt{\pi}} \qquad \text{(A13)}$$

$$Q_i^{\parallel} = T_i\ nv_x\ \delta_i$$

Hence δ_i is given by the formula

$$\delta_i = \frac{(M_i^2 + \frac{5}{2})\ M_i\ (1+\mathrm{erf}\ M_i) + (M_i^2 + 2)\ e^{-M_i^2}\ /\sqrt{\pi}}{M_i\ (1+\mathrm{erf}\ M_i) + e^{-M_i^2}\ /\sqrt{\pi}} \qquad \text{(A14)}$$

$$\delta_i \approx M_i^2 + \frac{5}{2} \qquad \text{(A15)}$$

For $M_i = 1$ we get $\delta_i = 3.45 \approx 3.5$.

3) Potential Drop across the Langmuir Sheath

We now combine the electron and the ion flux density to express the potential drop $\Delta\phi$ in terms of the electric current density:

$$j_x = e(\Gamma_i^{\parallel} - \Gamma_e^{\parallel}) = en\,(v_x - u_x)$$

$$\frac{j_x}{env_x} = 1 - \frac{v_{Te}}{2\sqrt{\pi}\,v_x}\, e^{-\frac{e\Delta\phi}{T_e}} \tag{A16}$$

$$-\frac{e\Delta\phi}{T_e} = \ln\left[\frac{2\sqrt{\pi}\,v_x}{v_{Te}}\left(1 - \frac{j_x}{en\,v_x}\right)\right] \tag{A17}$$

Using again $v_x = \delta_s\, c_s$ we finally arrive at

$$-\frac{e\Delta\phi}{T_e} = \ln\left[\sqrt{\frac{2\pi m_e}{m_i}\frac{T_e+T_i}{T_e}}\left(\delta_s - \frac{j_x}{enc_s}\right)\right] \tag{A18}$$

For $\delta_s = 1$, $m_i = m_D$, $T_i = 0$ and $j_x = 0$ we get $e\Delta\phi/T_e = 3.2$, which yields $\delta_e = 5.2$.

4) Compatibility with Bohm's Criterion

In the foregoing we have worked out the crucial role of the parameter δ_s. Given δ_s we are able to calculate M_i from (A12) and δ_i from (A14), as well as $\Delta\phi$ from (A18) and δ_e from (A7). However, it is an open question whether the distribution functions f_{ep} and f_{ip} are sufficiently well behaved to ensure the existence of a δ_s such that for $\bar{v} = v_x \geqslant \delta_s\, c_s$ Bohm's criterion is fulfilled:

$$\varepsilon_o \frac{dE_x}{dx} = -\varepsilon_o \frac{d^2\phi}{dx^2} = e(n_i - n_e) \geq 0 \quad \text{for} \quad x \geq x_p \text{ and } x \to x_p \tag{A19}$$

This means that when approaching the plasma edge of the Langmuir sheath there must be only positive space charges and a monotonically increasing electric field to ensure a continuous presheath-sheath transition of the electrical field. In the following we want to investigate if n_e and n_i have been assumed such as to be compatible with Bohm's criterion, and to derive δ_s.

We introduce the dimensionless potential $\chi = -e\phi/T_e \geq 0$ within the sheath $x_p \leq x \leq x_w$. We fix $\chi_p = 0$ so that $\chi_w = e\Delta\phi/T_e$. Considering the continuous transformation of the electron distribution function from f_{ep} to f_{ew} in the sheath potential gradient results in the following electron density:

$$n_e = N_e \, e^{-\chi} \, \frac{1}{2} \left(1+\text{erf}\sqrt{\frac{e\Delta\phi}{T_e} - \chi}\right) \tag{A20}$$

$$= \frac{N_e}{2} \left(1+\text{erf}\sqrt{\frac{e\Delta\phi}{T_e}}\right) e^{-\chi} \, (1-f(\chi))$$

$$n_e = n_{ep} \, e^{-\chi} \, (1-f(\chi)) \tag{A21}$$

Clearly
$$n_{ew} = \frac{N_e}{2} \, e^{-\chi_w} \approx \frac{n_{ep}}{2} \, e^{-\chi_w} \tag{A22}$$

so that the correction function $f(\chi)$ increases monotonically from zero to one half. Note that the Boltzmann factor $e^{-\chi}$ must be corrected because of the absorption at the wall. For small χ we have the expansion

$$f(\chi) = f_1\chi + f_2\chi^2 + \ldots = \frac{e^{-\chi_w}}{\sqrt{\pi\chi_w}\,(1+\text{erf}\,\sqrt{\chi_w})} \left[\chi + \frac{1}{2}\left(1+\frac{1}{2\chi_w}\right)\chi^2 + \ldots\right] \tag{A23}$$

With $\chi_w = \frac{e\Delta\phi}{T_e} = 3$ we get $f_1 \approx 0.008$, $f_2 \approx 0.005$.

Let us first investigate <u>the case $T_i = 0$</u>, that is a beam of monoenergetic ions. Continuity and energy conservation result in

$$n_i \, v_x = n_{ip} \, v_{xp} \tag{A24}$$

$$n_i = \frac{n_{ip} v_{xp}}{\sqrt{v_{xp}^2 + \frac{2T_e}{m_i} \chi}} = \frac{n_{ip}}{\sqrt{1 + \frac{2c_s^2}{v_{xp}^2} \chi}} \tag{A25}$$

Introducing the Mach number $M = v_{xp}/c_s$ and the dimensionless coordinate $\xi = x/\lambda_d$, where $\lambda_D = \sqrt{\varepsilon_o T_e/(n_{ip} e^2)}$ is the Debye length, the normalized Poisson equation (A19) becomes:

$$\chi'' = \frac{1}{\sqrt{1 + \frac{2\chi}{M^2}}} - e^{-\chi} (1 - f_1\chi - f_2\chi^2 - \ldots) \tag{A26}$$

Performing the operation $\int_{\xi_p}^{\xi} \chi' \ldots . d\xi$ yields

$$\frac{\chi'^2 - \chi_p'^2}{2} = M^2 \left(\sqrt{1 + \frac{2\chi}{M^2}} - 1\right) - \left[\chi - (1+f_1)\frac{\chi^2}{2} + \left(\frac{1}{2} + f_1 - f_2\right)\frac{\chi^3}{3} + \ldots\right] \tag{A27}$$

Expansion of the square root cancels the linear term:

$$\frac{\chi'^2 - \chi_p'^2}{2} = \left(1 + f_1 - \frac{1}{M^2}\right)\frac{\chi^2}{2} + \left(\frac{1}{M^4} - \frac{1+2f_1-2f_2}{3}\right)\frac{\chi^3}{2} + \ldots . \tag{A28}$$

To fulfil Bohm's criterion the right-hand side of equations (A26) through (A28) must be positive for all $\xi \geqslant \xi_p$ or equivalently for all $\chi \geqslant 0$. This requires a positive coefficient of the χ^2-term:

$$M^2 \geqslant \frac{1}{1+f_1} \quad \text{or} \quad v_{xp} \geqslant \delta_s \, c_s \quad \text{with} \quad \delta_s = \sqrt{\frac{1}{1+f_1}} \approx 0.996 \approx 1 \tag{A29}$$

If we want to have also a positive coefficient of the χ^3-term, M^2 must be in the interval

$$\frac{1}{1+f_1} < M^2 < \sqrt{\frac{3}{1+2f_1-2f_2}} \tag{A30}$$

$$\text{or} \quad 0.996 \lesssim M \lesssim 1.314$$

We conclude that for calculating δ_s the corrections by f_1 and f_2 may be neglected, and that for $T_i = 0$ we may indeed use $\delta_s = 1$.
In the case $T_i > 0$ we must start from our ion distribution function f_{ip} and generalize (A25) by the integral

$$n_i = \int_0^\infty \frac{dv_p \, f_{ip}}{\sqrt{1 + \frac{2T_e \chi}{m_i v_p^2}}} \tag{A31}$$

Proceeding again as above and neglecting f_1 and f_2 yields

$$\frac{\chi'^2 - \chi_p'^2}{2} = \frac{1}{n_{ip}} \int_0^\infty dv_p \, f_{ip} \frac{m_i v_p^2}{T_e} \left(\sqrt{1 + \frac{2T_e \chi}{m_i v_p^2}} - 1\right) + e^{-\chi} - 1 \tag{A32}$$

Since v_p may be arbitrarily small an expansion of the square root is not admitted and would lead to divergent integrals:

$$\frac{\chi'^2 - \chi_p'^2}{2} = \frac{1}{n_{ip}} \int_0^\infty dv_p \, f_{ip} \left[- \frac{T_e}{m_i v_p^2} \frac{\chi^2}{2} + \left(\frac{T_e}{m_i v_p^2}\right)^2 \frac{\chi^3}{2} + \ldots\right] + \frac{\chi^2}{2} - \frac{\chi^3}{6} + \ldots \tag{A33}$$

Thus we are forced to evaluate the integral in (A32) numerically. The question is whether we are able to choose $\bar{v} = v_x$ so large that

$$\lim_{\chi \to 0} \frac{\frac{1}{n_{ip}} \int_0^\infty \ldots dv_p + e^{-\chi} - 1}{\chi^2} > 0 \tag{A34}$$

Not very surprisingly we find that even for arbitrarily large $\bar{v}$ this limit is always negative, that is our f_{ip} cannot fulfil Bohm's criterion. However, if we smoothe out the discontinuity of f_{ip} at $v_p = 0$ such that $f_{ip} \sim v_p^2$ for $v_p \to 0$, then at least the first integral in (A33) is convergent, and we find a δ_s of the order of one, such that for $\bar{v} = v_x \geq \delta_s c_s = \delta_s \sqrt{(T_e + T_i)/m_i}$ the limit in (A34) is positive.
Fig. 12 shows that in the limit $\chi \to 0$

$$0.75 < \delta_s < 1.25 \quad \text{for} \quad 0 < \frac{T_i}{T_e} < 3 \tag{A35}$$

Of course $\delta_s \to 1$ for $T_i \to 0$. The slightly modified f_{ip} is sketched in the lower left part of the figure. We conclude that for $T_i \gg 0$ the usually assumed f_{ip} is not suitable, but with the modified f_{ip} we may again use $\delta_s = 1$ as a reasonable approximation. The exact dependency of δ_s on T_i/T_e is still unknown and would require the knowledge of the true shape of f_{ip}, which in turn presupposes a complete and self-consistent kinetic theory of the acceleration in the presheath under the influence of Coulomb collisions, interactions with neutrals, collective effects etc..
It is interesting to note that for one special case such a detailed theory does really exist. Riemann /16/ considered a weakly ionized plasma in contact with a negative absorbing wall and determined the potential and the ion distribution function in the quasineutral presheath selfconsistently under the assumption that the ion kinetics is dominated by charge exchange collisions with cold neutrals ($T_0 \ll T_e$). In this case the ions start with zero velocity after each charge exchange process and move only in the positive direction towards the absorbing wall. The distribution function of the ions arriving at the edge of the Langmuir sheath ($\chi = 0$) is for small v_p linear in the energy variable $\varepsilon = m_i v_p^2/2T_e$, so that indeed $f_{ip} \sim v_p^2$ for $v_p \to 0$. The mean velocity is

$$v_x = \bar{v} = 0.88161 \sqrt{\frac{2T_e}{m_i}} = 1.24678 \sqrt{\frac{T_e}{m_i}} \qquad \text{(A36)}$$

If, however, we define an effective ion temperature $T_{i\ eff}$ at the sheath edge by half the 1/e-width of the ion distribution function on the ε-energy scale (the maximum is at $\varepsilon \approx 1$), then we get $T_{i\ eff} \approx 0.55\ T_e$, so that

$$v_x = \bar{v} = \frac{1.24678}{\sqrt{1.55}} \sqrt{\frac{T_e + T_{i\ eff}}{m_i}} = 1.00144\ c_{s\ eff} \qquad \text{(A37)}$$

Thus taking a thermal broadening properly into account yields a $\delta_{s\ eff} = 1$ almost exactly. In fact Riemann shows that his f_{ip} fulfils Bohm's criterion just marginally, because the equivalent of eqs. (A32) and (A33) in his sheath theory results in the expansion ($\chi'_p = 0$):

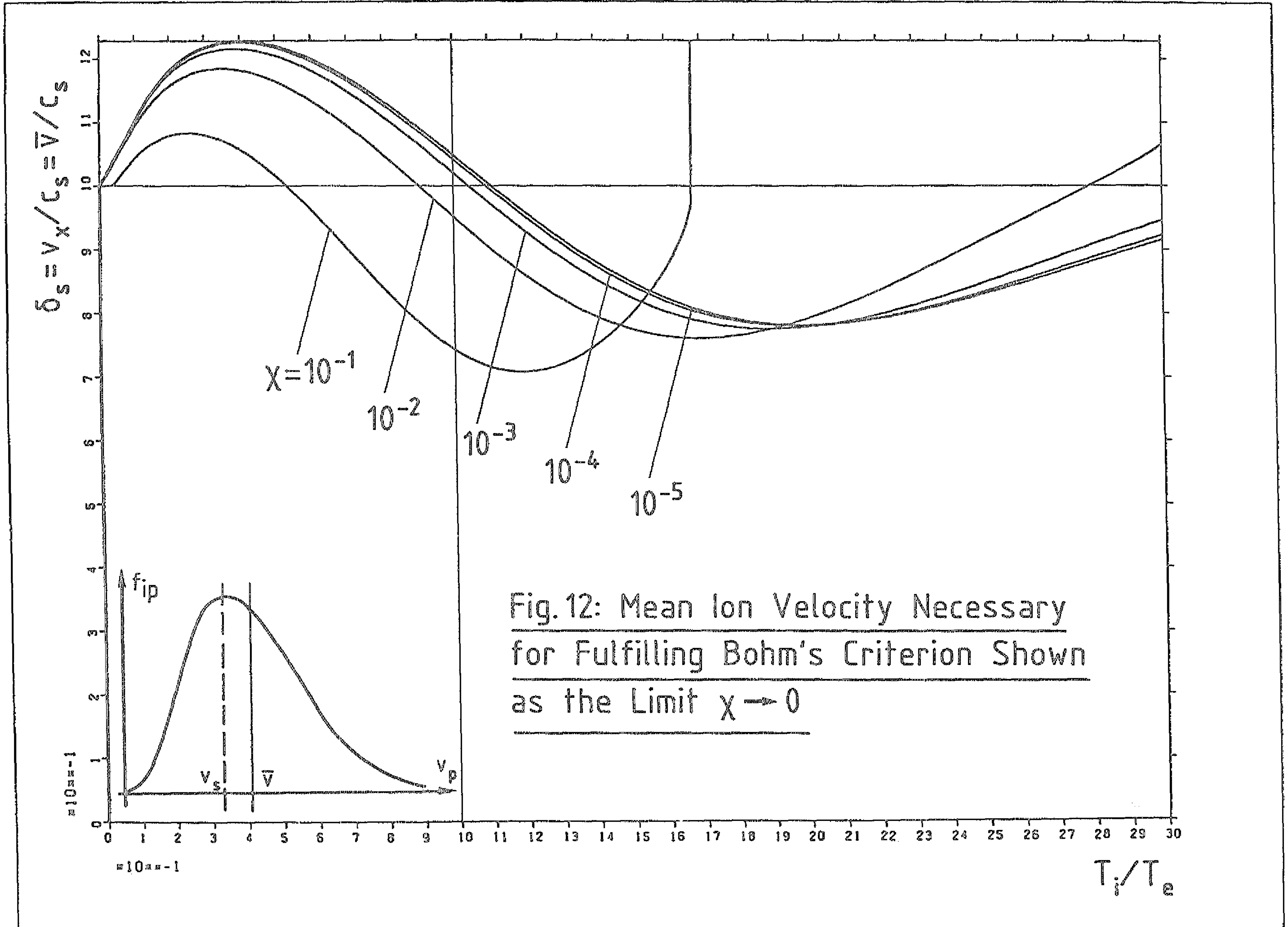

Fig. 12: Mean Ion Velocity Necessary for Fulfilling Bohm's Criterion Shown as the Limit $\chi \rightarrow 0$

$$\frac{1}{2}\chi'^2 = \chi \sum_{k=2}^{\infty} \beta_k \chi^{k/2} \tag{A38}$$

with $\beta_2 = 0$ and $\beta_3 = 0.3464$, that is the factor of χ^2 just vanishes, and the leading term is $\sim \chi^{5/2}$. He also claims that with Boltzmann--distributed electrons and completely absorbing walls $\beta_2 = 0$ is a consequence of <u>any</u> consistent presheath theory. Hence we conjecture that for our scrape-off plasma, too, the correctly modified f_{ip} must be such that $v_x = c_s$ is just reached at the sheath edge and just sufficient to fulfil Bohm's criterion marginally, which means that the boundary condition $\delta_s = 1$ is the best approximation presently available.